The Investigation of Plasma Membrane Localization of PCDH7 and CLIC4 During Cell Division

by

Beste Senem Degirmenci Alper

A Dissertation Submitted to the

Graduate School of Sciences and Engineering

in Partial Fulfillment of the Requirements for

the Degree of

Doctor of Philosophy

in

Molecular Biology and Genetics

KOÇ ÜNİVERSİTESİ

January 10, 2025

Investigating the Plasma Membrane Localization of PCDH7 and CLIC4 During Cell Division

Koç University

Graduate School of Sciences and Engineering

This is to certify that I have examined this copy of a doctoral dissertation by

Beste Senem Degirmenci Alper

and have found that it is complete and satisfactory in all respects, and that any and all revisions required by the final examining committee have been made.

Committee Members:

Prof. Dr. Nurhan Özlü (Advisor, Koç University)

Dr. Nazan Saner (Co-Advisor, Koç University)

Prof. Dr. Arzu Çelik (Boğaziçi University)

Assist. Prof. Ayşe Koca Çaydaşı (Koç University)

Assist. Prof. Serkan Kır (Koç University)

Assist. Prof. Erdinc Sezgin (Karolinska Institute)

Date: 10.01.2025

I dedicate my thesis to my lovely family
for their endless love, support and encouragement.

To my father, Salim, who made me the person I am today;
To my mother, Huriye, who knows my heart;
To my sweet trouble, my little brother, Utku;

And to my love,
my dearest husband, Altuğ, who fills my life with the purest love and joy.

ABSTRACT

Investigating the Plasma Membrane Localization of PCDH7 and CLIC4 During Cell Division

Beste Senem Degirmenci Alper

Doctor of Philosophy in Molecular Biology and Genetics

January 10, 2025

The regulation of the plasma membrane during cell division is essential for maintaining membrane dynamics and cortical stability, both of which are critical for the fidelity of cell division. This thesis investigates the underlying mechanism of two mitosis specific plasma membrane-enriched proteins, PCDH7 and CLIC4, and uncovers their importance in coordinating membrane-cytoskeleton interactions. PCDH7 is identified as a regulator of the actomyosin network during cytokinesis, where it facilitates proper cleavage furrow ingression and completion of cytokinesis. Palmitoylation emerges as an essential mechanism in the translocation of PCDH7 to the plasma membrane at the onset of mitosis through its interaction with a palmitoyl acyltransferase, ZDHHC5. Dynamic plasma membrane localization of PCDH7 promotes the activation of essential cytokinetic regulators, such as RhoA and myosin II, which facilitate actomyosin ring constriction and ensure successful cell division.

CLIC4 plays a dual role in stabilizing membrane dynamics and cortical tension during cytokinesis. My results suggest that CLIC4 may localize to the plasma membrane in a palmitoylation-dependent manner and bind phosphoinositols, such as $PI(3,5)P_2$ and $PI(4,5)P_2$, to regulate membrane-cytoskeleton interactions. Live-cell imaging using lattice light sheet microscopy reveals the rank of CLIC4's recruitment to the cortex during the bleb life cycle, where it supports membrane stabilization in the expansion phase and maintains cortical integrity. These findings highlight CLIC4's distinct role in coordinating membrane tension and bleb regulation, processes critical for cell shape maintenance during mitotic progression. Together, the work on PCDH7 and CLIC4 advances our understanding of how protein-membrane interactions contribute to cytokinesis and provides a framework for exploring their broader relevance to cellular architecture and function.

ÖZETÇE

Bölünme Sürecinde CLIC1 ve CLIC4'ün Moleküler Fonksiyonlarının ve Dinamiklerinin Araştırılması

Beste Senem Değirmenci Alper

Moleküler Biyoloji ve Genetik, Doktora

10 Ocak 2025

Hücre bölünmesi sırasında plazma membranının düzenlenmesi, hem membran dinamiklerinin hem de kortikal stabilitenin korunması açısından kritik bir öneme sahiptir ve bu süreçler, hücre bölünmesinin doğru bir şekilde tamamlanmasını sağlar. Bu çalışma, mitoz sırasında plazma membranında zenginleşen iki proteinin, PCDH7 ve CLIC4'ün mekanizmalarını incelemekte ve bu proteinlerin membran-iskelet etkileşimlerini düzenlemedeki önemini ortaya koymaktadır. PCDH7'nin, sitokinez sırasında ve kesim oyuğununa yerleşerek aktomiyozin ağının düzenlenmesinde ve bölünmenin tamamlanmasında rol oynadığı gösterilmiştir. Palmitolasyon, PCDH7'nin mitoz başlangıcında plazma membranına yerleşimini sağlayan önemli bir mekanizma olarak öne çıkmaktadır ve bu süreç, palmitol transferaz ZDHHC5 ile etkileşimiyle gerçekleşmektedir. PCDH7'nin dinamik plazma membran lokalizasyonu, aktomiyozin halkasının daralmasını sağlayan RhoA ve miyozin II gibi kritik sitokinetik düzenleyicilerin aktivasyonunu destekleyerek hücre bölünmesinin başarılı bir şekilde gerçekleşmesini sağlamaktadır.

CLIC4, sitokinez sırasında membran dinamiklerinin ve kortikal gerilimin stabilizasyonunda çift yönlü bir rol oynamaktadır. Bulgularımız, CLIC4'ün plazma membranına palmitolasyona bağlı bir şekilde yerleşebileceği ve $PI(3,5)P_2$ ile $PI(4,5)P_2$ gibi fosfoinositollere bağlayarak membran-iskelet etkileşimlerini düzenlediğini göstermektedir. Canlı hücre görüntülemesi, CLIC4'ün kutup membran kabarcıklarının yaşam döngüsü boyunca zamansal dinamiğine bağlı olarak yer alındığını ortaya koymuş, genişleme fazında membranı stabilize ettiği ve kortikal bütünlüğü koruduğu gözlemlenmiştir. Bu bulgular, CLIC4'ün mitoz sırasında hücre şeklinin korunmasında ve membran dinamiklerinin düzenlenmesinde oynadığı ayırt edici rolü vurgulamaktadır. PCDH7 ve CLIC4 üzerine yapılan bu çalışma, protein-membran etkileşimlerinin sitokineze katkısını anlamamıza katkı sağlamakta ve hücresel mimarinin ve fonksiyonun daha geniş kapsamlı araştırılması için bir çerçeve sunmaktadır.

ACKNOWLEDGEMENT

I would like to express my sincere gratitude to my advisor, Prof. Dr. Nurhan Özlü, for accepting me as an MS-integrated PhD student and for her guidance and support during my doctoral studies. Her expertise and insights have been invaluable throughout this journey. Additionally, I would like to sincerely thank my co-advisor, Dr. Nazan Saner, for her constant support and encouragement throughout this project. Her guidance, innovative ideas, and dedication have been crucial in navigating experimental challenges and driving the progress of this work. I am deeply grateful for her mentorship and the inspiration she has provided during my doctoral studies. I thank my thesis committee members, Ayşe Koca Çaydaşı and Arzu Çelik, for following my project over the past two years and helping me improve this project with their valuable discussions and guidance.

I extend my heartfelt thanks to Dr. Erdinc Sezgin for welcoming me as an EMBO scientific fellow in his lab for three months, just an important period for both my scientific journey and personal growth. During this time, I not only learned invaluable lessons about research and science, but also about life, friendship, and leadership. Your guidance as an advisor helped shape me into a better scientist, while your wisdom and our deep conversations made me a better person. I will always cherish our conversations and the unforgettable memories shared at Ramazan Abi's table with Yağmur, Cenk, and Tuğçe. I also express my gratitude to Jan Schlegel, an exceptional supervisor whose intelligence, humor, and relaxed yet encouraging approach made my time in the lab unforgettable. Your constant encouragement, even during late-night hours, and the lessons you taught me will remain with me always. As I've often said, you're among the top ten favorite people in my life—thank you for everything.

I sincerely thank all the members of our lab. Nazlı, you have been an incredible teammate, teaching me so much about science, manuscripts, and publications. Witnessing the positive changes in your life has been inspiring, and I truly hope you find great happiness in Sweden. I will miss you and Deniz dearly. Büşra Akarlar, I feel incredibly fortunate to have learned everything about proteomics from you. Your depth of knowledge is unmatched, and your exceptional teaching skills, combined with your kind, positive, and patient attitude, have been a source of encouragement and motivation for me. Hale, you were an amazing housemate

and continue to be a fantastic labmate. Gamze, you are my hero. You encouraged me in my weakest times, and I felt confident with your words. Asiye and Dilaray, you have been wonderful friends, and sharing life's challenges while trying to grow together as a lab has been truly invaluable. Helin and Selin, my two incredible interns, made my life so much easier with hard work and dedication. I am proud of your courage and determination, and I have no doubt you will achieve great success in whatever path you choose.

I want to express my heartfelt gratitude to all my friends from Koç University, especially A. Tuğçe Şahin (former Nozlu member) and Cansu Dilege. Tuğçe, my best friend forever, my soulmate, my "can yoldaşım." You already know how much you mean to me. Cansu, my dearest "baby," you both made my life so much better during my time at this school. You stood by me, even in the darkest times, and I cannot imagine this journey without you. I love you both so much. Büşra Harmanda (former Nozlu member) you have been such a great friend to me, bringing so much fun and joy to my time in the lab! "Limonlu Coronalar" Ezgi Memiş and Altuğ Kamacıoğlu (former Nozlu members), I will always cherish your warm friendship and the wonderful moments we shared. I feel fortunate to have met the "Koçtaşlar" team: Hüseyin, İdil, Cansu, and Tuğçe. Hüseyin, your joyful personality always brings fun to every moment. İdil, you've been a wonderful friend to me since our METU days. I love you all! I want to thank Rana (former Nozlu member) for her friendship and support. You've helped me become a brave person, and I've learned so much from you about life and friendship. Thank you for our meaningful conversations and for always being there. Tuğçe Ünlü, my dear office buddy, I wish we had met earlier because spending time with you has improved both my personal growth and my outlook on life. You are the most open-minded, self-reflective, and sweetest person I have ever met. I will always cherish our deep conversations, our shared journey of understanding our emotions and life, and the new meaning "Coco" holds for me because of you.

I would like to thank my dearest friends, İlayda and Dilem. Knowing that you'll always be there for me, no matter what, is truly priceless. I'll always stand by your side, through both dark and bright times. Love you all from the bottom of my heart.

As mentioned in the dedication, I extend my heartfelt thanks to my lovely family. I owe who I am today to my father, Salim. His principles and memories continue to guide me and will always live with me. Love you and miss you dearly, babacım. My mother, Huriye, has been my anchor during my most challenging times, always supporting me to find my light. Your guidance is incredibly special to me, and I am deeply proud to be your daughter. My

little brother, Utku, who isn’t so little anymore—it's incredible to see how you’ve grown into such a smart, patient, and hardworking person as it feels like you were born just yesterday. I’m so lucky to have you as my brother, someone I can always trust, no matter what. It’s truly special to realize that you have taught me how to embrace and become my true self. I want you to know that I will always be by your side throughout your life and I know you will be there for me always.

And my dearest husband, my best friend, and my greatest love—you and your support have made me stronger, happier, and brighter. With you, I’ve become the best version of myself. Your love has brought meaning to my life, and everything you touch turns extraordinary. I feel incredibly lucky to walk this path with you, to share my days, my dreams, and even my smallest thoughts. Even the most ordinary days feel special with you by my side, and a simple conversation with you can brighten my entire day. You are my home, where I feel safe, loved, and truly myself. I can’t wait to share this beautiful journey of life with you. I love you beyond words.

TABLE OF CONTENT

LIST OF FIGURES

LIST OF TABLES

ABBREVIATIONS

17-ODYA	17-Octadecynoic Acid
2BP	2-Bromopalmitate
BioID	Proximity dependent biotin identification
Cdk	Cyclin dependent kinase
CLIC1	Chloride intracellular channel protein 1
CLIC4	Chloride intracellular channel protein 4
DKO	Double knockout
CRISPR	Clustered Regularly Interspaced Short Palindromic Repeats
DAPI	4',6-diamidino-2-phenylindole
DMEM	Dulbecco's Modified Eagle Medium
DNA	Deoxyribonucleic acid
DTT	Dithiothreitol
ECL	Enhanced chemiluminescence
EDTA	Ethylenediaminetetraacetic acid
eGFP	Enhanced Green Fluorescence Protein
ECT2	Epithelial cell transforming 2
ESCRT	Endosomal sorting complex required for transport
ERM	Ezrin-Radixin-Moesin proteins
FBS	Fatal Bovine Serum
GFP	Green Fluorescence Protein
GPMV	Giant Plasma Membrane Vesicle
HEK293	Human Embryonic Kidney Cells
HeLa	Human cervical cancer cell line S3
HRP	Horseradish Peroxidase
mDia2	Protein diaphanous homolog 2
KO	Knockout
NEM	N-ethylmaleimide
NP40	Nonyl phenoxypolyethoxylethanol
PALM	Palmitate
PBS	Phosphate buffered saline
PCDH1	Protocadherin 1
PCDH7	Protocadherin 7
PCDH7-BAC-GFP	Protocadherin 7-Bacterial Artificial Chromosome GFP
Pcdhs	Protocadherins
Pen-Strep	Penicilin-Streptomycin
PFA	Paraformaldehyde
PLA	Proximity ligation assay
RFP	Red fluorescent protein
RhoA	Ras homolog family member A
RNA	Ribonucleic acid
ROCK	Rho-associated protein kinase
ROI	Region of Interest
SDS-PAGE	Sodium dodecyl sulfate - polyacrylamide gel electrophoresis
sgNT	Non targeting sgRNA
SLK kinase	STE20-like serine/threonine-protein kinase

STC	S-trityl-L-cysteine
TCA	Trichloroacetic Acid
TCEP	(tris(2-carboxyethyl)phosphine)
Tx	Triton X
Ub	Unbound
WCL	Whole cell lysate
WT	Wild type
ZDHHC	Zinc fingers DHHC-type palmitoyltransferase

CHAPTER 1

1. INTRODUCTION

The regulation of protein localization to the plasma membrane during cell division is crucial for maintaining membrane dynamics, cortical tension, and cytoskeletal organization. Among the proteins implicated in these critical events, PCDH7 and CLIC4 have emerged as two players, as identified in our previous study, which demonstrated their specific enrichment at the mitotic cell surface during cell division [1]. Understanding the mechanisms that regulate these proteins' dynamic localization and function is important for addressing fundamental questions about membrane stability, actomyosin regulation, and processes like blebbing.

The first part of this thesis investigates PCDH7, a member of the protocadherin family, known for its roles in cell adhesion and recognition [2]. Our findings demonstrate that PCDH7 dynamically localizes throughout cell division, with a specific transition to the cleavage furrow during cytokinesis. Analysis of PCDH7-deficient cells showed cytokinetic defects, including furrow regression and multinucleation, emphasizing its essential role in mitotic progression. Moreover, we showed that PCDH7 facilitates actomyosin ring constriction by promoting active RhoA and phosphorylated myosin II at the cleavage furrow, both essential regulators of cortical stability and furrow ingression. Furthermore, we identified ZDHHC5 as the palmitoyltransferase responsible for PCDH7 palmitoylation, a lipid modification that facilitates PCDH7 localization to the plasma membrane. These findings provide critical insights into how PCDH7 contributes to the spatial regulation of the actomyosin network, maintaining cortical integrity and cytokinetic fidelity.

The second part focuses on CLIC4, a member of the chloride intracellular channel family, known for its ability to transition between soluble and membrane-bound states [3]. We demonstrated that CLIC4 localizes to the plasma membrane in a palmitoylation-

dependent manner, with its surface enrichment significantly reduced following inhibition of this modification. Moreover, our results suggested that CLIC4 binds to $PI(3,5)P_2$, which regulate endosomal homeostasis [4], and colocalizes with $PI(4,5)P_2$ at the cleavage furrow, where it might stabilize membrane-cytoskeleton interactions during cytokinesis. Live-cell imaging revealed the sequential recruitment of CLIC4 to polar membrane blebs, arriving shortly after actin and preceding ezrin and myosin. This temporal hierarchy suggests a role for CLIC4 in stabilizing the expansion phase of blebbing by maintaining cortical tension and preventing excessive membrane protrusions. Despite its essential role in membrane stabilization, the absence of CLIC4 did not affect the localization or phosphorylation of canonical regulators such as profilin-1, mDia2, or non-muscle myosin II, suggesting it operates through distinct pathways to regulate membrane-cytoskeleton interactions.

In summary, this thesis demonstrates the essential roles of PCDH7 and CLIC4 in regulating membrane dynamics and cortical stability during cell division. This work deepens our understanding of the molecular processes that drive cytokinesis by revealing new mechanisms for PCDH7 and CLIC4 involving palmitoylation and lipid binding. These findings highlight the importance of protein-membrane interactions in cell division and provide a basis for exploring their wider role in maintaining cellular structure and function.

CHAPTER 2

2. Palmitoylation-Dependent Membrane Localization of PCDH7 during Cell Division

2.1. LITERATURE REVIEW

2.1.1. Cell Division

Cell division is a fundamental biological process critical for growth, tissue repair, and reproduction in living organisms. This process involves a series of highly regulated events that lead to the division of a parent cell into two or more daughter cells [5, 6].

In eukaryotic cells, there are two primary types of cell division: mitosis and meiosis. Mitosis generates daughter cells that are genetically identical to the parent cell, ensuring the maintenance of genetic material necessary for growth and tissue regeneration. Meiosis produces genetically diverse daughter cells, a process vital for sexual reproduction and genetic variability [5, 7].

2.1.1.1.Mitotic Cell Cycle

The mitotic cell cycle is composed of two main stages: interphase and mitosis. During interphase, the cell grows and prepares for division through a series of phases: G1, S, and G2 [8].

The G1 phase, or Gap 1 phase, is the initial stage of interphase in the cell cycle. In this phase, the cell undergoes significant growth, synthesizing proteins and RNA necessary for DNA replication and subsequent cell division. This period is characterized by intense metabolic activity and cellular growth. The duration of the G1 phase varies between cell types and organisms, with some cells spending extended periods in G1, while others progress quickly [9].

The S phase, also known as the Synthesis phase, is a crucial stage in which DNA replication occurs. In this phase, the cell duplicates its entire genome, ensuring that two identical copies of genetic information are available for the daughter cells. DNA replication begins with the unwinding of the double helix, creating two single strands, each serving as a template for synthesizing a new complementary strand. Key enzymes, such as DNA polymerases, facilitate precisely adding nucleotides to the growing DNA strand. The result is the formation of two identical sister chromatids connected by a centromere. The fidelity of DNA replication during the S phase is essential for maintaining genetic stability. Errors or mutations during this process can have significant consequences for both the cell and the organism. Various proofreading and repair mechanisms operate to minimize such errors and ensure the integrity of genetic information [10].

The G2 phase, or Gap 2 phase, is the final stage of the interphase before the cell transitions into mitosis. During this phase, the cell grows, synthesizing proteins required for mitosis, such as tubulin for microtubule formation. Additionally, organelles like mitochondria and chloroplasts are duplicated, ensuring their distribution to daughter cells. The G2 phase also acts as a critical checkpoint, verifying the accuracy of DNA replication and ensuring optimal conditions for cell division [7, 11].

The transition from the G2 phase to mitosis represents a critical shift as the cell moves from preparation to active division. Mitosis itself consists of four sub-stages: prophase, metaphase, anaphase, and telophase [5, 6].

Prophase marks the onset of mitosis, characterized by significant cellular changes. Chromatin condenses into tightly coiled chromosomes. The nuclear envelope disintegrates, enabling the mitotic spindle to interact with the chromosomes. Centrosomes organize microtubules into the mitotic spindle which is essential for chromosome separation. As prophase advances, chromosomes become increasingly compact, facilitating their efficient segregation in later stages.

Metaphase is defined by the alignment of chromosomes along the equatorial plane of the cell, forming the metaphase plate. Mitotic spindle fibers attach to the kinetochores which are specialized protein complexes at each chromosome's centromere. Equal tension applied by spindle fibers ensures proper chromosome alignment. This is a critical step for the accurate separation of sister chromatids in anaphase [12, 13].

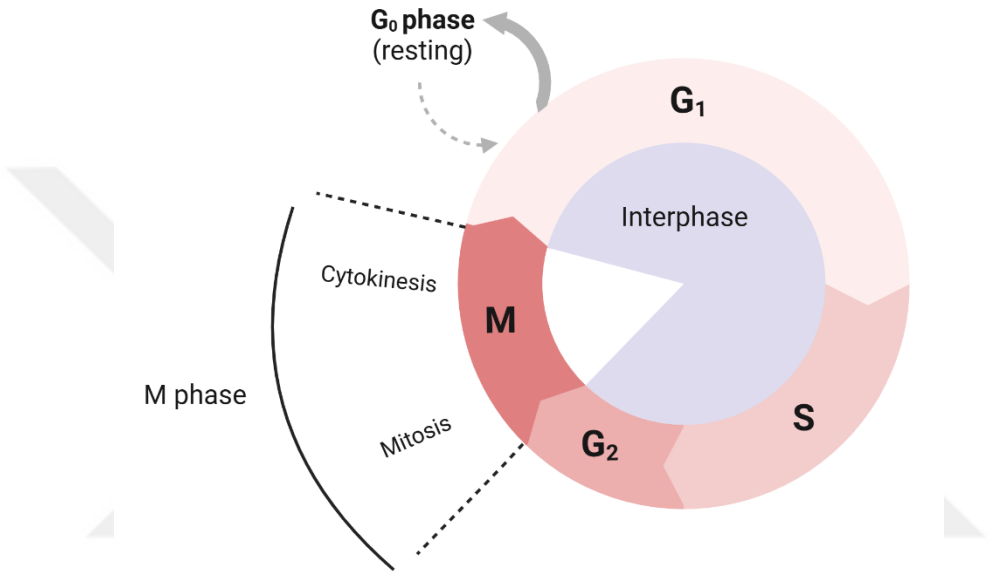

Figure 1. The overview of the cell cycle (BioRender.com).

During anaphase, the sister chromatids are held together by a centromere, separate from each other. The mitotic spindle fibers shorten, pulling the chromatids toward opposite cell poles. This separation ensures that each daughter cell receives a complete set of chromosomes.

In telophase, the cell begins to reverse the changes that occurred during prophase. The mitotic spindle disassembles, and new nuclear envelopes form around each set of chromosomes. The chromosomes begin to uncoil and return to their chromatin form. Nucleoli, reappear within the newly formed nuclei [11, 12].

Cytokinesis is the final stage of cell division, where the cytoplasm divides to form two separate daughter cells. In animal cells, a contractile ring composed of actin and myosin filaments constricts the cell membrane, creating a cleavage furrow that gradually deepens until the cell is divided into two. In plant cells, a cell plate develops at the midline

of the dividing cell, eventually fusing with the cell wall to generate two distinct daughter cells, each surrounded by its own cell wall [14].

2.1.2. Reorganization of the cell shape during cell division

Cell division involves dynamic changes in cell shape alongside cytosolic and nuclear material reorganization. During interphase, adherent cells maintain canonical focal adhesion complexes, which include proteins such as focal adhesion kinase (FAK), paxillin, talin, and integrins. These complexes form a critical signaling interface with the extracellular matrix [12]. However, during the onset of mitosis, the increased activity of CDK1-cyclin B and mitotic kinases, such as Aurora B and Polo-like kinase, drives the phosphorylation of key mitotic proteins. This phosphorylation triggers the disassembly of adhesion complexes and stress fibers, facilitating mitotic rounding through actin cytoskeleton reorganization [15, 16].

During mitosis, the actomyosin network undergoes significant reorganization to facilitate mitotic rounding. Actin nucleation shifts from Arp2/3-mediated branched actin assembly to formin-mediated linear actin polymerization. This transition, driven primarily by Diaphanous (DIA) formins, leads to the loss of lamellipodia and promotes the formation of a robust cortical actin network [16, 17]. This cortical network provides an optimal substrate for non-muscle myosin II filaments, which generate cortical tension necessary for mitotic rounding [17, 18].

The assembly of the cortical actin network is tightly regulated by ECT2, a guanine nucleotide exchange factor (GEF) released from the nucleus by the CDK1-cyclin B complex. ECT2 activates RhoA at the plasma membrane, initiating a signaling cascade that stimulates DIA and ROCK (Rho-associated protein kinase). ROCK enhances actomyosin contractility by phosphorylating myosin II, further reinforcing cortical tension and maintaining the structural integrity of the mitotic cell [19, 20].

ERM proteins (Ezrin, Radixin, and Moesin) also play a crucial role during mitosis by linking the cortical actin network to the plasma membrane. These proteins bind to $PI(4,5)P_2$ and are phosphorylated by SLK kinase, enabling them to stabilize the cortical structure and ensure the mechanical integrity required for mitotic rounding [21-23].

Together, these mechanisms allow the mitotic cell to establish the physical framework necessary for subsequent stages of division.

As mitosis progresses into cytokinesis, the cortical actomyosin network reorganizes to form the contractile ring at the cell's equator. This highly dynamic structure is composed of key proteins, including ECT2, RhoA, DIA, non-muscle myosin II, ezrin and anillin, which collectively drive the formation of the cleavage furrow [14, 24, 25]. ECT2, recruited to the spindle midzone by the centralspindlin complex, polarizes the cortex and coordinates cytokinesis through central constriction and peripheral relaxation [20, 26].

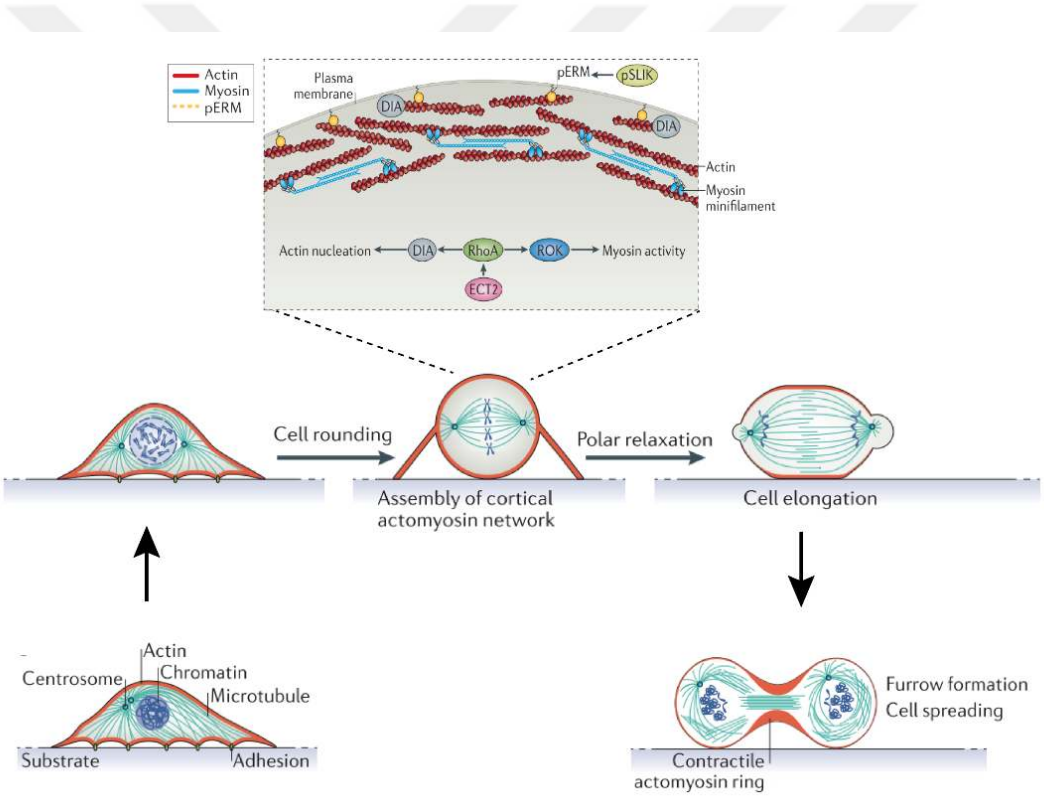

Figure 2. Dynamic organization of cell shape (Adapted from [16]).

Anillin is one of the main organizers of the cytokinetic machinery, functioning as an actomyosin crosslinker. It bundles F-actin, interacts with non-muscle myosin II to stabilize the contractile ring, and binds to Rho-GTP, Citron kinase, septins, and PI(4,5)P_2 [27-29]. These interactions position anillin as a key player in anchoring the actomyosin network to the plasma membrane, ensuring the stability and functionality of the cleavage

furrow. PI(4,5)P_2 binding plays a crucial role in targeting anillin to the furrow early in cytokinesis by linking the actomyosin and anillin-septin sub-networks to ensure successful cytokinesis. [30].

Following the contraction and disassembly of the actomyosin ring, the final steps of cytoplasmic division involve the formation of the midbody, a structure essential for the physical separation of daughter cells. The disassembly of the actomyosin ring and the microtubule-rich central spindle is facilitated by the degradation of ECT2 and the depletion of RhoA, PI(4,5)P_2, and actin [16, 20]. These changes mark the transition from the contractile phase of cytokinesis to midbody formation, which serves as a platform for the abscission process.

In the final stage of cytokinesis, midbody abscission, the ESCRT (endosomal sorting complexes required for transport) machinery has crucial roles. CEP55, a key midbody protein, recruits TSG101 and ALIX, which guide the assembly of the ESCRT III complex at the abscission site. This complex drives the membrane scission events required to cut the intercellular bridge. Syndecan-4, along with the ALIX-syntenin complex, stabilizes ESCRT III polymers at the abscission site, ensuring the precise and timely separation of the daughter cells [31-33].

These tightly regulated processes involve cytoskeletal remodeling and membrane dynamics, collectively enabling the successful completion of mitosis and cell division.

2.1.3. Protocadherins and Role of PCDH7 in Cellular Adhesion, Development, and Division

Protocadherins (Pcdhs) are a diverse family of cell adhesion proteins that form the largest subgroup of the cadherin superfamily, comprising more than 70 genes. They are primarily expressed in the nervous system and play crucial roles in cell-cell adhesion, neuronal connectivity, and cell recognition [34, 35]. Structurally, they are type-I transmembrane proteins with extracellular cadherin (EC) repeats, resembling classical cadherins but differing in key domains. Protocadherins lack the tryptophan residues and hydrophobic pockets required for homophilic interaction in classical cadherins, instead featuring unique disulfide-bonded loops [36]. They also do not contain catenin-binding

sites but they have distinct cytoplasmic domains, which contribute to their diverse cellular functions [37]. Based on genomic organization, protocadherins are classified into clustered and non-clustered groups, with the clustered Pcdhs further subdivided into Pcdhα, Pcdhβ, and Pcdhγ families. Clustered Pcdhs exhibit combinatory and monoallelic expression patterns, enabling extensive molecular diversity and functioning as neuronal self-recognition codes. Non-clustered protocadherins, in contrast, are dispersed across the genome and divided into Pcdhδ and solitary protocadherins [38].

PCDH7, a member of the δ1-Pcdh subgroup of non-clustered protocadherins, is a type-I transmembrane protein characterized by seven EC repeats in its extracellular domain. It exists in three isoforms (PCDH7a, b, and c) produced by alternative splicing, differing mainly in their cytoplasmic domains [39]. PCDH7 mediates weak homophilic cell adhesion and participates in cell sorting, morphogenesis, and ectodermal integrity during embryonic development [40]. Furthermore, it has been implicated in neuronal development, where its activity influences axon and dendrite growth. In addition to its developmental roles, PCDH7 may also play a role in cancer progression. Dysregulation of PCDH7 expression has been observed in various cancer types, including lung, bladder, and breast cancers, as well as melanomas [41]. PCDH7 has been linked to tumor growth, chemoresistance, and metastatic behavior by modulating signaling pathways such as MAPK and forming gap junctions in carcinoma-astrocyte interactions [42].

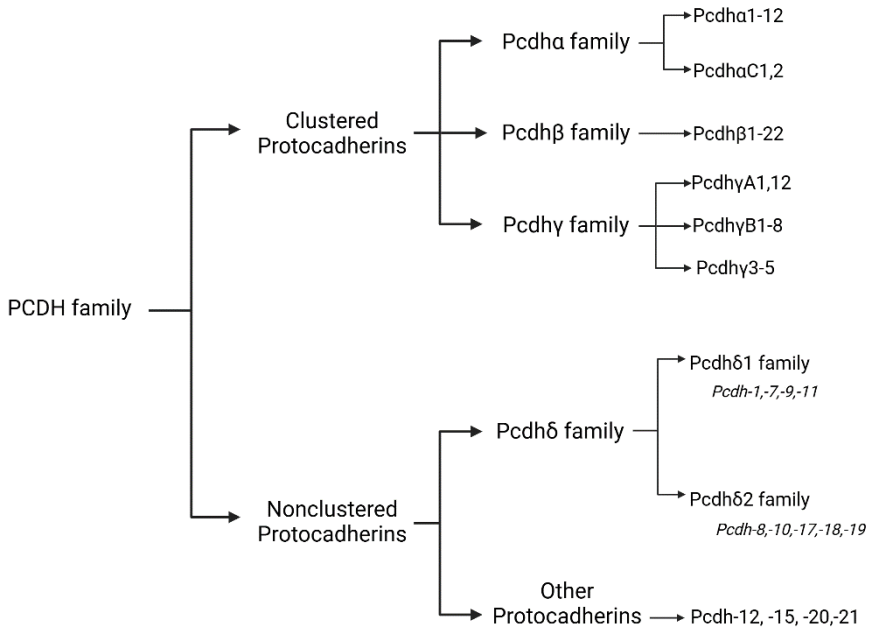

Figure 3. Classification of Protocadherin family.

Quantitative proteomic analysis from our laboratory identified PCDH7 as a mitosis-selective surface protein, with its localization to the plasma membrane and retraction fibers during mitotic rounding [1]. These finding suggested that PCDH7 contributes to proper cell rounding, which is critical for ensuring accurate chromosome segregation. While these observations underscore the potential importance of PCDH7 in cell division, its molecular role remains largely unexplored. Understanding the function of PCDH7 in this context could provide valuable insights into its broader roles in cellular physiology and pathology.

The interactome of PCDH7 during mitosis and interphase was mapped using a proteomic approach based on proximity-dependent biotinylation (BioID) [43]. PCDH7 was fused with the promiscuous biotin ligase BirA*, allowing biotinylation of proteins in close proximity, which were subsequently isolated with streptavidin beads and identified through liquid chromatography-tandem mass spectrometry (LC-MS/MS). Comparative analysis with non-transfected, biotin-supplemented control cells led to the identification of 78 PCDH7 interactors specific to mitosis and 129 to interphase, with 47 proteins common to both stages. Interactors were analyzed using the STRING database, and enrichment analysis for Gene Ontology (GO) and KEGG pathways resulted in their clustering into functional groups, including actomyosin network components, cell adhesion and cadherin-binding proteins, vesicular transport proteins, and ERM family proteins. These findings reveal the involvement of PCDH7 in cytoskeletal organization and membrane dynamics throughout the cell cycle [44].

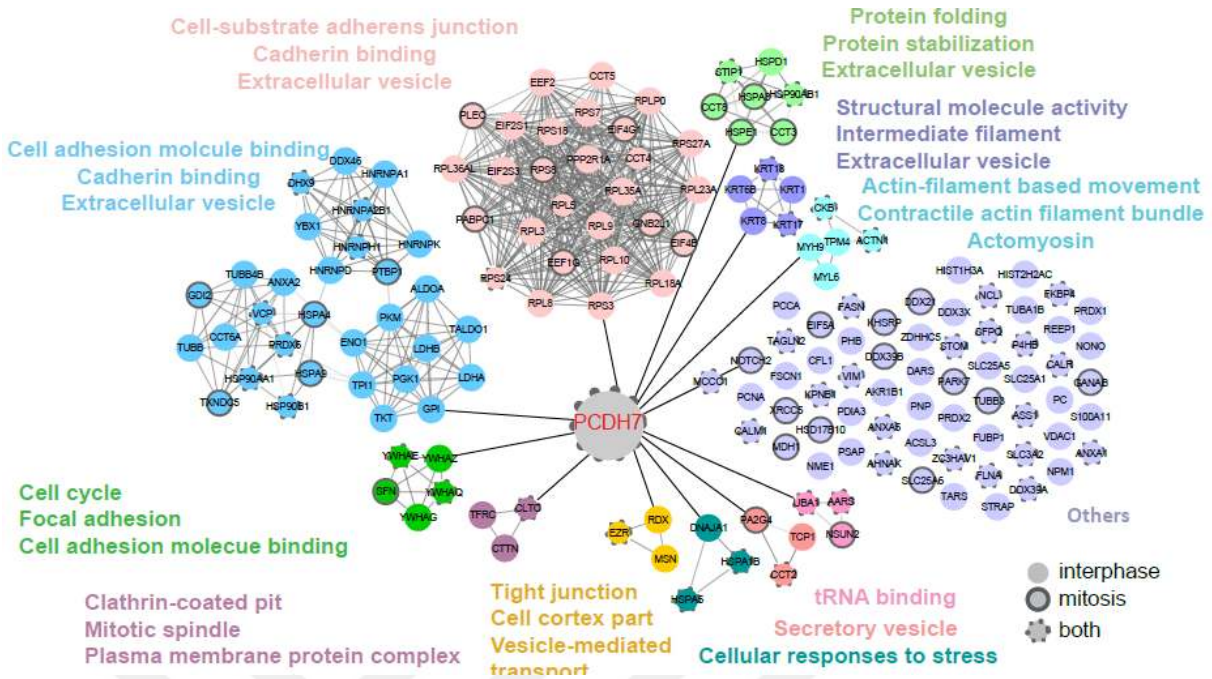

Figure 4. The interactome map of PCDH7 in cell cycle dependent manner.

2.1.4. Importance of Protein Palmitoylation

Palmitoylation, also referred to as S-acylation, is a widespread and dynamic post-translational lipid modification in which fatty acids, predominantly 16-carbon palmitic acid, are covalently attached to cysteine residues via a thioester bond. Unlike other lipid modifications such as myristoylation or prenylation, palmitoylation is fully reversible, allowing proteins to cycle between palmitoylated and depalmitoylated states. This reversibility is critical for regulating protein activity, localization, and interactions in response to cellular stimuli [45].

The regulation of palmitoylation is mediated by two key enzymatic players: protein acyltransferases (PATs), which catalyze the addition of palmitate, and acylprotein thioesterases (APTs), which remove the modification. Among PATs, the zinc finger DHHC-domain containing (ZDHHC) protein family plays a central role, characterized by the conserved Asp-His-His-Cys (DHHC) motif in their cysteine-rich domains [46]. The ZDHHC family comprises 23 members in mammals, with each exhibiting distinct subcellular localizations and substrate specificities. Notably, ZDHHC5 is a unique PAT predominantly localized to the plasma membrane, although it also resides in endosomal

compartments. The extended C-terminal tail of ZDHHC5 is rich in post-translational modification sites, including phosphorylation and palmitoylation, which regulate its interactions with PDZ domain-containing substrates and cellular signaling pathways [47].

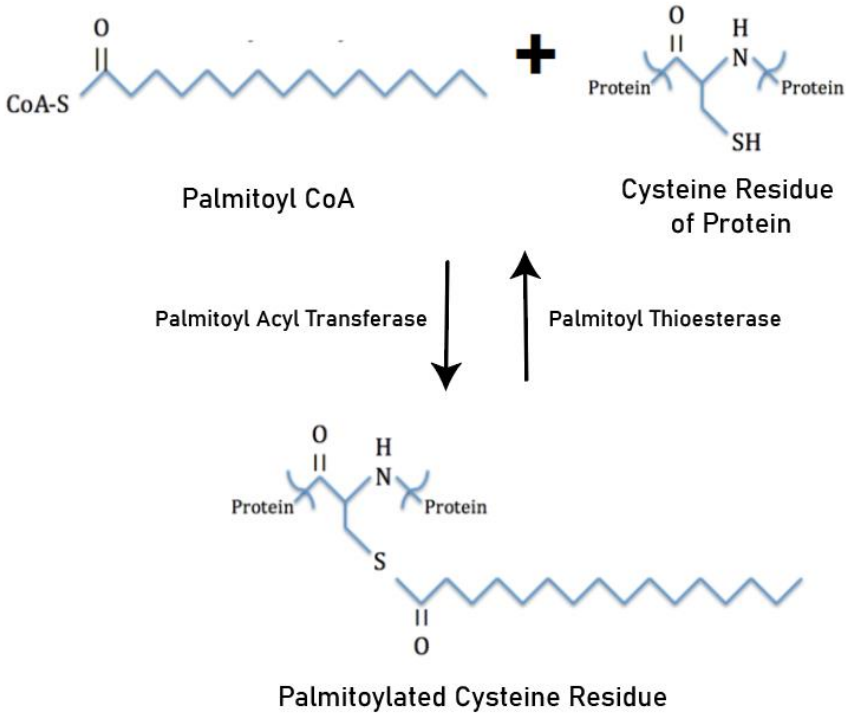

Figure 5. Addition of palmitoyl group to cysteine residue.

Palmitoylation serves as a versatile regulator of protein stability, subcellular localization, membrane trafficking, and protein-protein interactions. By increasing the hydrophobicity of proteins, palmitoylation facilitates their anchoring to cellular membranes, a process critical for their spatial and functional regulation of protein [48]. This lipid modification is especially significant in targeting proteins to specific membrane compartments, including lipid rafts, which are specialized microdomains involved in clustering and signaling. For instance, Palmitoylation of RAS GTPases, which is ZDHHC9-mediated palmitoylation at the Golgi enables their trafficking to the plasma membrane, highlighting the importance of palmitoylation in spatially orchestrating protein signaling [46].

In the context of cell division, palmitoylation might be a potential mechanism for translocating proteins to the plasma membrane during cytokinesis. Dynamic palmitoylation allows proteins to alternate between intracellular compartments and the cell cortex, ensuring precise membrane localization that is essential for maintaining cellular integrity and function [49]. Understanding the interplay between palmitoylation and plasma membrane localization provides critical insights into the spatial regulation of proteins involved in cell division and other fundamental cellular processes.

2.2. MATERIALS AND METHODS

2.2.1. Cell Culture and Synchronization

Cells were cultured in Dulbecco's modified Eagle medium (DMEM; Sigma-Aldrich, D6429) supplemented with 10% fetal bovine serum (FBS; Gibco, 10270106) and 1% penicillin-streptomycin (P/S; Capricorn Scientific, PS-B). The PCDH7-GFP-BAC transgenic cell line, generously provided by Dr. Ina Poser (Max Planck Institute of Molecular Cell Biology and Genetics, Dresden, Germany), was maintained in DMEM containing 10% FBS, 1% P/S, and 400 µg/ml G418 (Santa Cruz Biotechnology, sc-29065A).

Stable HeLa S3 cell lines expressing PCDH7::GFP were generated using lentiviral transduction. The PCDH7 sequence was cloned into the pLenti CMV GFP Puro vector (Addgene, 17448), and the resulting construct was introduced into cells. These cells were cultured in DMEM supplemented with 10% FBS, 1% P/S, and 2 µg/ml puromycin.

For interphase synchronization, the cells were treated with 2.5 mM thymidine (296542, Santa Cruz) containing media for 16 hours and pelleted. During bipolar synchronization, thymidine treatment followed the release for 8 hours, then the cells were treated with 30 ng/ml nocodazole (487928, Calbiochem) for 5 hours to arrest them in mitosis. To arrest the cells into cytokinesis, the cells were released for 1 hour after nocodazole treatment. During monopolar synchronization, following thymidine treatment, the cells were treated with 10 uM STC (164739, Sigma-Aldrich) for 16 hours to arrest the cell in mitosis. The cells were treated with 100 uM purvalanol A (1580, Tocris Bioscience) treatment for 15 minutes for cytokinesis arrest.

**HeLa S3 SgNT and PCDH7KO cells were prepared as mentioned in Nazlı Ezgi Ozkan's PhD thesis*

**HeLa S3 emptyGFP and PCDH7::GFP cells were prepared as mentioned in Nazlı Ezgi Ozkan's PhD thesis*

2.2.2. The proximity ligation assay (PLA)

For Proximity Ligation Assay, Duolink PLA Kit (Sigma-Aldrich, 92101) was used following the manufacturer's instructions [50]. HeLa S3 PCDH7-GFP-BAC cells were seeded onto glass coverslips and synchronized to cytokinesis using bipolar synchronization. Cells were fixed with 3.2% paraformaldehyde (PFA) in PBS and permeabilized with 0.1% Triton X-100 in TBS. Blocking was performed using Duolink blocking solution, with cells incubated in a humidified chamber at 37°C for 30 minutes.

After blocking, the coverslips were incubated overnight at 4°C with anti-GFP antibody (Invitrogen, A11120) for PCDH7 and anti-ZDHHC5 antibody (Sigma-Aldrich, HPA014670) as a pair (target) or with a single antibody (control) in Duolink antibody diluent. Following incubation, cells were washed with Wash Buffer A for 10 minutes at room temperature, then incubated with Plus and Minus PLA probes diluted in Duolink antibody diluent for 1 hour at 37°C. After another wash with Wash Buffer A, the cells were treated with ligase in ligation buffer for 30 minutes at 37°C. The washing step was repeated with Wash Buffer A, and the cells were incubated with polymerase in amplification buffer for 100 minutes at 37°C. Final washes included a 20-minute wash with 1x Wash Buffer B and a 1-minute wash with 0.01x Wash Buffer B.

Slides were mounted with coverslips using Duolink Mounting Medium with DAPI and incubated for 15 minutes before sealing.

2.2.3. Acyl-Biotin Exchange Assay (ABE)

ABE procedure was performed as previously described [51]. HeLa S3 cells overexpressing PCDH7-GFP were collected from culture plates, and the cell pellets were lysed in ice-cold lysis buffer (LB; 150 mM NaCl, 50 mM Tris, 5 mM EDTA, pH 7.4) supplemented with 10 mM N-ethylmaleimide (NEM), 2x protease inhibitor cocktail (PI), and 2x phenylmethylsulfonyl fluoride (PMSF). The lysates were homogenized using sonication at 4°C, followed by membrane protein enrichment via ultracentrifugation at 200,000 × g for 30 minutes (Optima MAX-XP Ultracentrifuge, TLA-120.2 rotor). After centrifugation, the supernatant was discarded, and the pellet was resuspended in LB supplemented with 10 mM NEM, 1x PI, and 1x PMSF. Triton X-100 was added to a final concentration of 1.7%, and the mixture was incubated at 4°C with

end-over-end rotation for 2 hours. Insoluble particulates were removed by centrifugation at 250 × g for 5 minutes at 4°C.

To purify the proteins, methanol-chloroform precipitation was performed. Methanol, chloroform, and ddH_2O were sequentially added to the sample in a 4:1.5:3 ratio of the initial sample volume, with vortexing after each addition. Following centrifugation at 4470 × g for 35 minutes at 4°C, the upper aqueous phase was carefully removed without disturbing the intermediate protein layer. Ice-cold methanol was added to the remaining protein layer, and the sample was gently mixed until the protein phase dissolved completely. After a second centrifugation at 4470 × g for 35 minutes at 4°C, the supernatant was discarded, and the protein pellet was air-dried for 2–3 minutes. The pellet was dissolved in 4% SDS buffer (4SB; 4% SDS, 50 mM Tris, 5 mM EDTA, pH 7.4) with 10 mM NEM and incubated at 37°C for 20 minutes to ensure complete dissolution. The sample was further diluted with LB containing 1 mM NEM, 1x PI, 1 mM PMSF, and 0.2% Triton X-100, and incubated overnight at 4°C with gentle rocking.

To remove residual NEM, three sequential methanol-chloroform precipitation steps were performed. The final protein pellet was resuspended in 4SB and divided equally into two tubes for hydroxylamine (HA) treatment. HA- buffer (50 mM Tris, 1 mM HPDP–biotin, 0.2% Triton X-100, 1 mM PMSF, 1x PI, pH 7.4) was added to one sample, while HA+ buffer (0.7 M hydroxylamine, 1 mM HPDP–biotin, 0.2% Triton X-100, 1 mM PMSF, 1x PI, pH 7.4) was added to the other. Both samples were incubated at room temperature for 1 hour with end-over-end rotation. Following incubation, methanol-chloroform precipitation was repeated for both samples to remove unreacted biotin, and the protein pellets were dissolved in 4SB.

To label biotinylated proteins, the samples were treated with low HPDP–biotin buffer (150 mM NaCl, 50 mM Tris, 5 mM EDTA, 0.2 mM HPDP–biotin, 0.2% Triton X-100, 1 mM PMSF, 1x PI, pH 7.4) and incubated at room temperature for 1 hour with rotation. Another three rounds of methanol-chloroform precipitation were performed to remove excess biotin. The final protein pellets were dissolved in 4SB, and SDS was diluted to 0.1% by adding LB containing 0.2% Triton X-100, 1x PI, and 1 mM PMSF. After a 30-minute incubation at room temperature, the samples were transferred to tubes

containing pre-conditioned Streptavidin Plus UltraLink Resin (Pierce, 53117) and incubated at room temperature for 90 minutes with end-over-end rotation. Unbound fractions were collected, and the resins were washed three times with LB containing 0.1% SDS and 0.2% Triton X-100.

To elute bound proteins, 2x Laemmli buffer with 1% β-mercaptoethanol was added to the resins, and the samples were boiled for 10 minutes at 95°C (Figure 6).

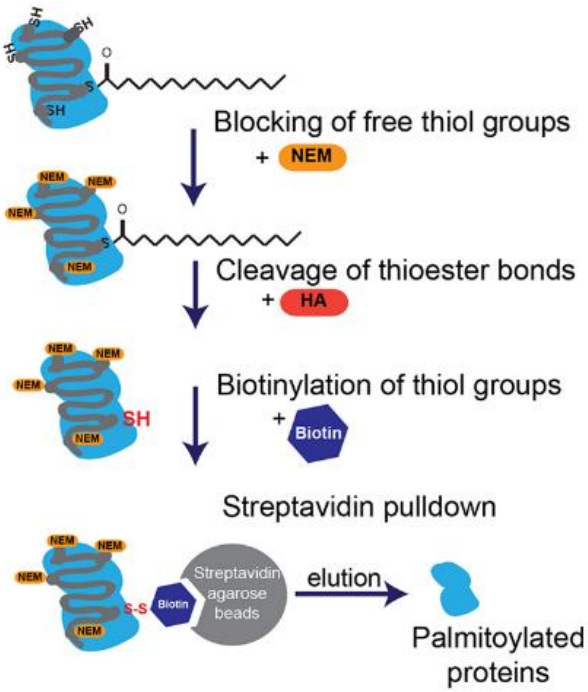

Figure 6. Schematic illustration of the acyl-biotin exchange assay [44].

2.2.4. GFP-Trap Pull-Down Assay for Protein Interactions

HeLa S3 cells expressing either empty GFP or PCDH7-GFP were synchronized to mitosis using thymidine and STC treatments. Mitotic cells were collected and pelleted by centrifugation. The pellets were resuspended in PBS containing 1% Triton X-100, EDTA-free protease inhibitor cocktail (Thermo Pierce, 88666), and PhosSTOP phosphatase inhibitor (Roche, 4906845001). Cell lysates were homogenized using a syringe and incubated at 4°C with rotation for 20 minutes to ensure effective lysis.

Following homogenization, the lysates were clarified by centrifugation at 14,000 rpm for 10 minutes at 4°C. Supernatants were transferred to fresh tubes, and a small volume was set aside for protein quantification using the BCA protein assay (Pierce, 23225). Protein concentrations were determined, and input samples (I) were saved for downstream analysis. Equal amounts of total protein from each lysate were then incubated with pre-conditioned GFP-Trap A beads for 3 hours at 4°C with gentle rotation to facilitate protein binding.

After the incubation, unbound fractions (Ub) were collected by centrifugation at 2,500 × g for 2 minutes at 4°C. The GFP-Trap A beads were washed three times with ice-cold PBS to remove nonspecifically bound proteins. Bound proteins were eluted by resuspending the beads in 2x Laemmli buffer supplemented with 100 mM DTT and boiling the samples for 10 minutes at 95°C. The eluted proteins were subsequently analyzed for protein-protein interactions.

2.2.5. Knockdown of PCDH7 Using siRNA and esiRNA

PCDH7 expression was silenced using a range of siRNA and esiRNA pools, including FlexiTube GeneSolution for PCDH7 (QIAGEN, GS5099), FlexiTube siRNA PCDH7 6 (QIAGEN, SI03080469), FlexiTube siRNA PCDH7 5 (QIAGEN, SI03040261), and esiPCDH7 (Sigma-Aldrich, EHU077631). For negative controls, AllStars Negative Control siRNA (QIAGEN, 1027280) was employed. Transfections were performed using Lipofectamine RNAiMAX transfection reagent (Thermo Fisher Scientific) following the manufacturer's guidelines.

Cells were seeded and subsequently transfected with 15 pmol of siRNA on two occasions: 24 hours and 48 hours post-seeding. At 72 hours post-seeding, cells were either collected as pellets for western blot analysis or fixed for immunofluorescence studies to assess the efficiency of PCDH7 knockdown and its effects on cellular processes.

2.2.6. Immunofluorescence Staining and Live-cell Imaging

Cells grown on coverslips were washed with 1× PBS and fixed using either 4% paraformaldehyde (PFA) at room temperature or 10% trichloroacetic acid (TCA) at 4°C

for 10 minutes. Following fixation, the cells were washed three times with 1× PBS containing 0.1% Triton X-100 (PBS-Tx), with each wash incubating for 5 minutes.

For blocking, the coverslips were incubated with a blocking solution (2% BSA in PBS-Tx) at room temperature for 1 hour. After blocking, the solution was replaced with primary antibodies diluted in the same blocking buffer. The cells were incubated with the primary antibodies for 3 hours at room temperature or overnight at 4°C. Subsequently, the cells were washed three times with PBS-Tx before being treated with fluorescent secondary antibodies, diluted in PBS-Tx, and incubated for 1 hour at room temperature.

After secondary antibody incubation, the coverslips were washed three more times with PBS-Tx and counterstained with Hoechst stain for 5 minutes to label nuclei. Finally, after three additional washes, the coverslips were mounted onto microscope slides for imaging. Images of siRNA- and shRNA-treated cells were captured and quantified by Nazlı Ezgi Özkan using Leica DMi8/SP8 TCS-DLS confocal microscopy.

For live-cell imaging, HeLa S3 PCDH7KO-LifeAct-RFP and HeLa S3 PCDH7KO-eGFP-RhoA cells were seeded into ibiTreat µ-Slide 4-well plates and visualized using a Leica DMi8/SP8 TCS-DLS confocal microscopy equipped with HC PL APO 63×/1.40 Oil CS2 objective and a temperature-controlled chamber set to 37°C and 5% CO_2. Three z-stacks were captured every 3 minutes.

2.2.7. Protein Extraction and Western Blot

HeLa S3 cells were lysed in 1× PBS containing 0.1% Triton X-100, a complete EDTA-free protease inhibitor cocktail (Roche), and PhosSTOP phosphatase inhibitor mixture (Roche). The inhibitor cocktail tablets were prepared at a ratio of 1 tablet per 10 ml of lysis buffer. Cell homogenization was achieved by passing the suspension through a thin syringe. Protein extracts were separated by centrifugation at 14,000 rpm for 20 minutes at 4°C, and the supernatant was collected. Protein concentration was determined using a BCA protein assay kit (Pierce, 23227). Protein samples were prepared in 2× Laemmli sample buffer containing 4% (w/v) SDS, 20% glycerol, 120 mM Tris-Cl (pH 6.8), 0.02% (w/v) bromophenol blue, and 100 mM dithiothreitol (DTT) at a 1:1 (v/v) protein-to-buffer ratio. The samples were heated at 95°C for 5 minutes to denature

proteins and cooled before loading onto SDS-PAGE gels. Electrophoresis was conducted at 120 V for 100 minutes to separate proteins by molecular weight.

Proteins were transferred onto nitrocellulose membranes (Whatman Protran, Ba85) using the Trans-Blot Turbo transfer system (Bio-Rad). Membranes were blocked for 45 minutes at room temperature with 4% milk in 1× TBS containing 0.1% Tween-20 (TBS-T) to prevent non-specific binding. Primary antibody incubation was performed overnight at 4°C or for 3 hours at room temperature, depending on the antibody. Following incubation, membranes were washed three times in TBS-T for 5 minutes each to remove unbound primary antibodies.

Secondary antibody incubation was carried out at room temperature for 1.5 hours, followed by three additional washes in TBS-T for 5 minutes each. Protein bands were visualized using the ECL Western Blotting Substrate system (Pierce, 32106) and imaged with the ChemiDoc system (Bio-Rad).

Quantification of Western blot results was performed using ImageLab software (Bio-Rad). Protein band intensities were measured, and values were normalized to the corresponding tubulin intensities to account for loading variability. This quantification ensured reliable and reproducible analysis of protein expression across experiments.

Table 1. The list of antibodies used for Western Blot (WB) and Immunofluorescence Staining (IF) in Chapter 2 with their host, brand, lot number and dilution information.

Antibody	**Host**	**Brand**	**Lot**	**Dilution**	**Applications**
Anti-GFP	Goat	Non-commercial		1:5000, 1:2000	WB and IF
Alpha-Tubulin	mouse	Cell Signaling Technology	3873S	1:2000, 1:1000	WB and IF
PCDH7	mouse	Abcam	ab139274	1:400	WB
phospho-myosin light chain (S19)	mouse	Cell Signaling Technology	CS3675	1:500	IF

Phalloidin iFluor 555		Abcam	ab176756	1:1000	IF
DAPI		Sigma-Aldrich	D8417	1:1000	IF
ZDHHC5	Rabbit	Sigma - Atlas Antibodies	HPA014670	1:2000, 1:500	WB and IF
anti-phospho-histone H3	rabbit	Upstate	06-570,	1:500	IF
EGFR	rabbit	Santa Cruz Biotechnology	SC-03	1:100	WB
Calnexin	rabbit	Abcam	ab22595	1:1000	WB
Alexa Fluor 488	mouse	Invitrogen	A21202	1:1000	IF
Alexa Fluor 488	rabbit	Invitrogen	A21206	1:1000	IF
HRP-conjugated secondary antibody	rabbit	Cell Signaling Technology	7074S	1:2000	WB
HRP-conjugated secondary antibody	mouse	Cell Signaling Technology	70765	1:2000	WB

2.3. RESULTS

2.3.1. PCDH7 Localization and Functional Role in Cytokinesis

PCDH7 was observed to localize dynamically throughout the cell cycle. Immunostaining of PCDH7-GFP-BAC cells showed that it is present at cell-cell contacts during interphase, enriched at the cell surface and retraction fibers at mitotic onset, and ultimately concentrated at the cleavage furrow during cytokinesis. Notably, PCDH7 accumulation at the cleavage furrow has a slight asymmetry [44] (Figure 7).

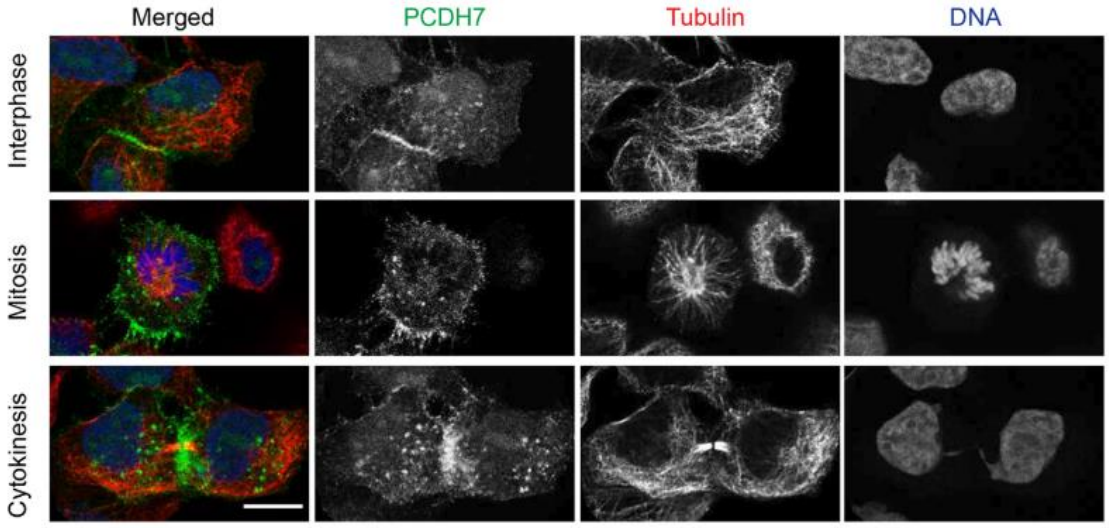

Figure 7. PCDH7 is enriched at the mitotic cell surface and accumulated at the cleavage furrow during cell division.

Subcellular localization of PCDH7 (green, anti-GFP), microtubules (red, anti-tubulin), and DNA (blue, DAPI) in PCDH7-GFP-BAC cells in interphase, mitosis, and cytokinesis. Scale bar: 10 μm.

To investigate the role of PCDH7 in cell division, we utilized CRISPR-Cas9 genome editing to achieve PCDH7 knockout in HeLa S3 cells [1]. We analyzed the multinucleation rate in fixed cells to examine the effects of PCDH7 loss on cell division. There is a significant increase in multinucleation in PCDH7KO cells compared to the control group (Figure 8A and B). Expression of PCDH7::GFP in the KO cells

successfully decreased the multinucleation rate, bringing it back to levels similar to the control and rescuing the observed defect [44].

The weak yet statistically significant increase in multinucleation observed in PCDH7 KO cells may result from cellular adaptations, as HeLa S3 cells can proliferate even in suspension conditions [52]. To further investigate, we depleted PCDH7 using siRNA and esiRNA in adherent HeLa Kyoto which resulted in an approximately twofold increase in multinucleation rate (7.7%) compared to control siRNA-treated cells (4.3%) (Figure 8C). HeLa Kyoto cells were treated with either control siRNA or a PCDH7-specific siRNA mix, and successful PCDH7 protein depletion was verified by western blotting (Figure 9).

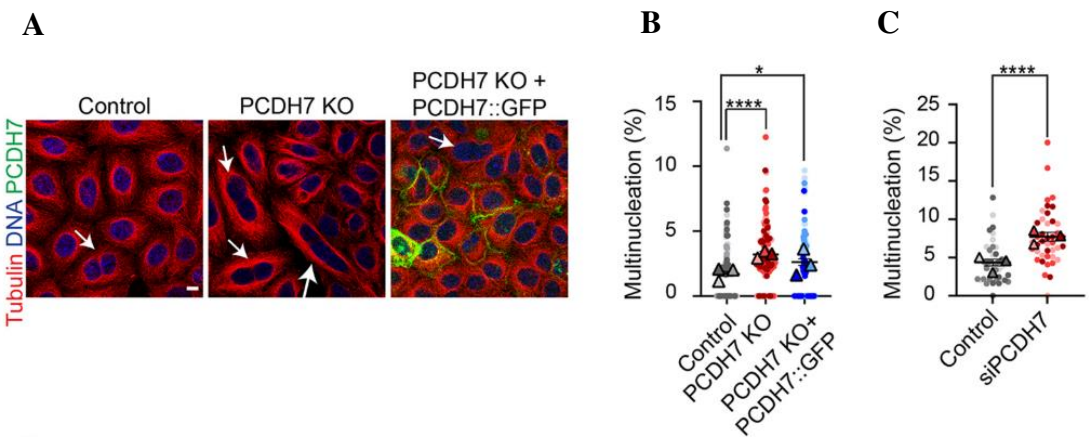

Figure 8. The multinucleation percentage is increased in PCDH7-depleted cells.

A. Representative images show the multinucleated cells in control (left), PCDH7KO (middle), and PCDH7KO+PCDH7::GFP (rescue) conditions (left). **B.** Percentages of multinucleation of control (gray; mean 1.7% n=4337 cell), PCDH7 KO (red; mean 3.2%, n=4582 cells) and rescued (PCDH7 KO+PCDH7:: GFP) (blue; mean 2.6%, n=4591 cells) HeLa S3 cells. **C.** Quantification of multinucleation in control siRNA (gray; mean 4.3%, n=1988 cells) and PCDH7 siRNA (siPCDH7) (red; mean 7.7%, n=2156 cells)-treated HeLa Kyoto cells.

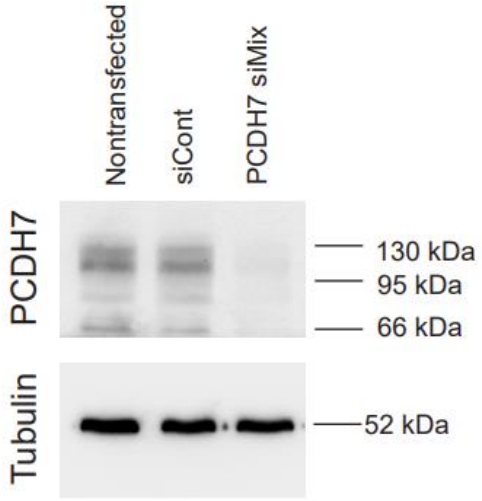

Figure 9. The depletion of PCDH7 using siMix was confirmed by Western Blot.

PCDH7 is 116 kDa. Tubulin was used as loading control**.**

To investigate the multinucleation phenotype associated with PCDH7, live-cell imaging was performed using LifeAct::RFP-expressing cells. While control cells successfully completed cytokinesis, PCDH7 KO cells started to initiate the cleavage furrow ingression but failed to complete cytokinesis, resulting in multinucleated cells (Figure 10). Additionally, the timing of cleavage furrow initiation (27 min in control vs. 36 min in PCDH7 KO) and furrow completion (33 min in control vs. 42 min in PCDH7 KO) was delayed in PCDH7 KO cells (Figure 10). Similar delays in mitotic progression and cleavage furrow ingression were observed in siRNA-treated HeLa Kyoto cells (Figure 11). (Quantification was done by Gamze Yapıcı)

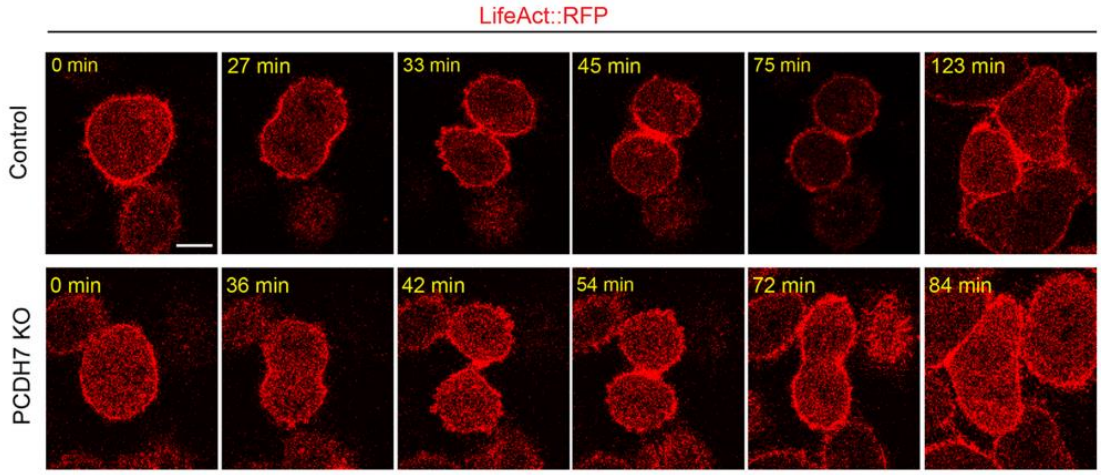

Figure 10. The absence of PCDH7 results in cell division failure.

Representative images from live-cell imaging of control cells (top) and PCDH7 knockout cells (bottom), both stably expressing LifeAct::RFP**.** The time points are indicated in minutes relative to mitotic rounding. Scale bar: 10 µm.

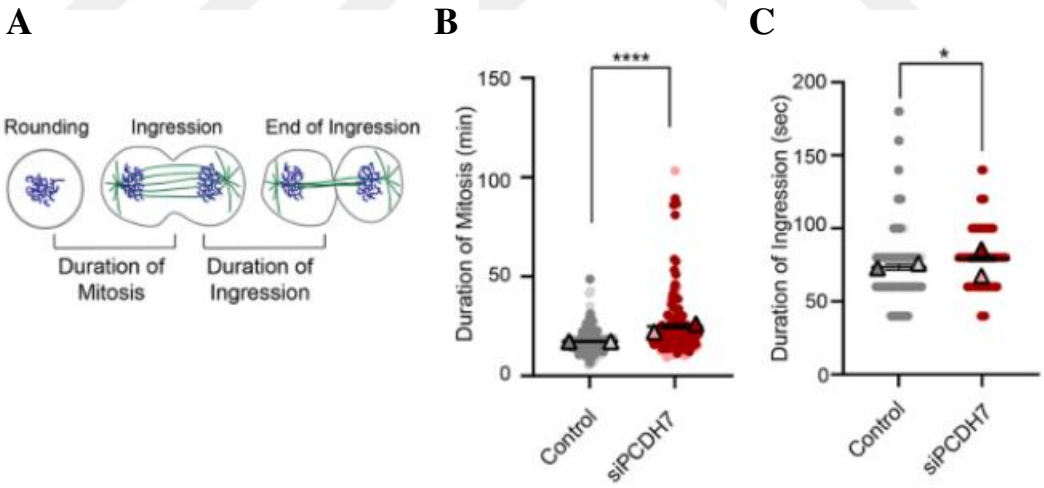

Figure 11.Mitotic progression and cleavage furrow ingression are prolonged in the absence of PCDH7

A. Schematic representation of timing in live-cell analysis. The "Duration of mitosis" denotes the time interval from cell rounding onset to the initiation of furrow ingression,

while the "Duration of ingression" measures the time from the onset to completion of furrow ingression. **B.** Quantification of mitosis duration in control (gray; mean 17.42 min) and PCDH7 knockdown (siPCDH7) (red; mean 25.00 min) HeLa Kyoto cells. Data represents two independent biological replicates (colored circles) [control, n=64 cells (BR1), n=88 cells (BR2); siPCDH7, n=46 cells (BR1), n=95 cells (BR2)], with average values shown as colored triangles. **C.** Quantification of ingression duration in control (gray; mean 73.55 s) and PCDH7 knockdown (siPCDH7) (red; mean 79.15 s) HeLa Kyoto cells. Data represents two independent biological replicates (colored circles) [control, n=65 cells (BR1), n=90 cells (BR2); siPCDH7, n=46 cells (BR1), n=85 cells (BR2)], with average values shown as colored triangles. For (F) and (G), means with s.e.m. are indicated with black lines, and statistical significance was determined using a two-tailed unpaired t-test (*P<0.05; ****P<0.0001).

To further investigate the cytokinesis defect in PCDH7-depleted cells, we analyzed active RhoA and myosin levels at the cleavage furrow. Control and PCDH7 KO cells were transfected with an eGFP–RhoA biosensor, which specifically detects active RhoA [53]. Live-cell imaging revealed reduced RhoA activity at the cleavage furrow in PCDH7 KO cells compared to control cells (Figure 12A and B). Despite impaired RhoA activity, furrow ingression was initiated in PCDH7 KO cells.

We next analyzed active myosin levels in PCDH7-depleted cells using an anti-phospho-myosin II (S19) antibody (Figure 13). In control cells, phosphorylated myosin was strongly enriched at the cleavage furrow (Figure 13A). However, PCDH7 KO cells exhibited a notable reduction in phospho-myosin intensity at this site (Figure 13B). Reintroducing PCDH7 into the KO cells restored phospho-myosin levels at the cleavage furrow, comparable to control cells (Figure 13B and C).

These findings underscore the critical role of PCDH7 in ensuring successful cytokinesis. By dynamically localizing to the cleavage furrow and regulating key components such as active RhoA and phosphorylated myosin II, PCDH7 facilitates proper furrow ingression and completion. Loss of PCDH7 disrupts these processes, leading to cytokinesis failure and multinucleation, highlighting its essential function in maintaining mitotic integrity and cell division fidelity.

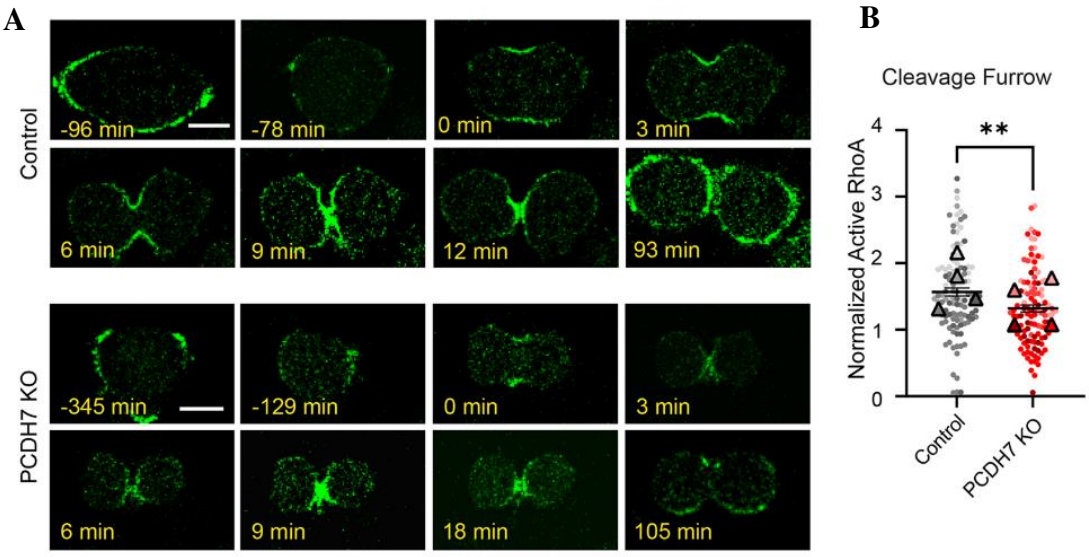

Figure 12. Active RhoA level at cleavage furrow is reduced in PCDH7KO cells.

A. Live-imaging imaging of control and PCDH7 knockout (KO) cells that were transfected with a pEGFP–RhoA biosensor vector to track active RhoA. The relative timing to cleavage furrow ingression is shown in minutes. Scale bars: 10 μm. B. Statistical analyses used unpaired two-tailed t-test. Error bars show the s.d. ns, not significant; **P<0.01

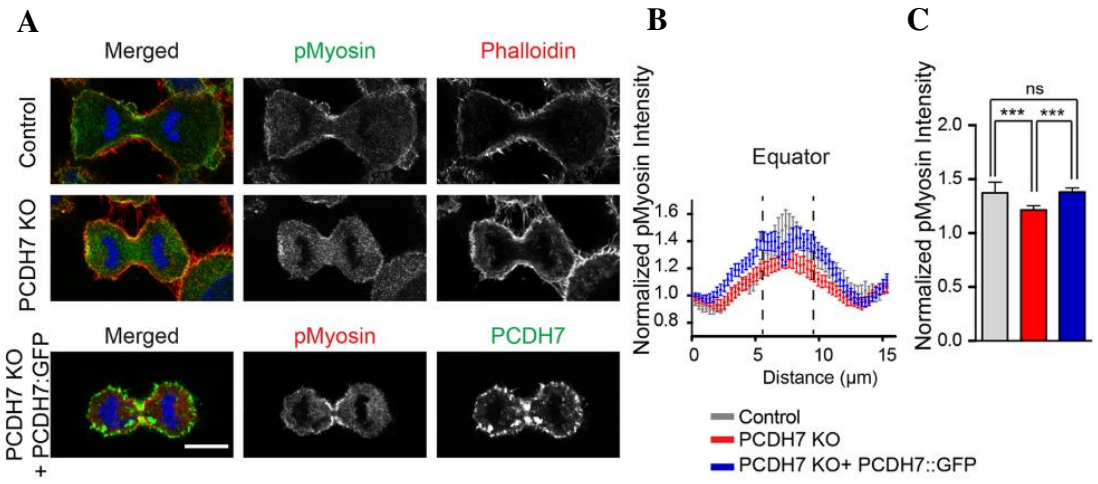

Figure 13. The absence of PCDH7 results in the reduced pMyosin (Ser19) at the cleavage furrow.

A. Representative fluorescence images displaying phospho-myosin II (S19) (pMyosin, green), actin filaments (red, phalloidin), and DNA (blue, DAPI) localization in control (top) and PCDH7 KO (middle) cells. Representative images of a rescued cell (PCDH7 KO+PCDH7::GFP, bottom) show PCDH7::GFP (green), phospho-myosin II (S19) (red) and DNA (blue, DAPI). Scale bar: 10 μm. **B.** Intensity profiles of pMyosin levels at the equatorial zone during cytokinesis in the control (gray) (n=24), PCDH7 KO (red) (n=24), and rescued (PCDH7 KO+PCDH7::GFP) (blue) (n=41) cells (left). The sum of pMyosin intensities between the dashed lines covering the ±15% distance around the middle zone was quantified (right). **C.** Statistical analyses used one-way ANOVA with Bonferonni's multiple comparison test. Error bars show the s.d. Statistical analyses used unpaired two-tailed t-test. Error bars show the s.d. ns, not significant; ***P<0.001.

2.3.2. PCDH7 Interaction with ZDHHC5 and Its Localization During Cell Division

Among several notable candidates, a striking interaction partner of PCDH7 was identified as the palmitoyl transferase ZDHHC5, an enzyme that catalyzes the addition of palmitoyl groups to target proteins. Palmitoylation, a reversible post-translational modification, regulates the hydrophobicity, membrane domain interactions, and conformation of transmembrane proteins [45].

To investigate potential cooperation between PCDH7 and ZDHHC5 during cell division, we examined their subcellular localization in PCDH7-GFP-BAC cells using anti-GFP and anti-ZDHHC5 antibodies. During interphase, both proteins localized to cell–cell contact regions (Figure 14, top). As cells entered mitosis, PCDH7 and ZDHHC5 decorated the cell surface and retraction fibers (Figure 14, middle), and further accumulated at the cleavage furrow during cytokinesis (Figure 14, bottom).

To confirm the colocalization of PCDH7 and ZDHHC5, we performed a proximity ligation assay (PLA) [54] using fixed PCDH7-GFP-BAC cells with anti-GFP and anti-ZDHHC5 antibodies. As expected, cells treated with both primary antibodies displayed a significantly higher PLA signal compared to control cells treated with only one primary antibody (Figure 15). The PLA signals were predominantly concentrated at the equatorial zone between segregating chromosomes during cytokinesis, consistent with the immunofluorescence results (Figure 15).

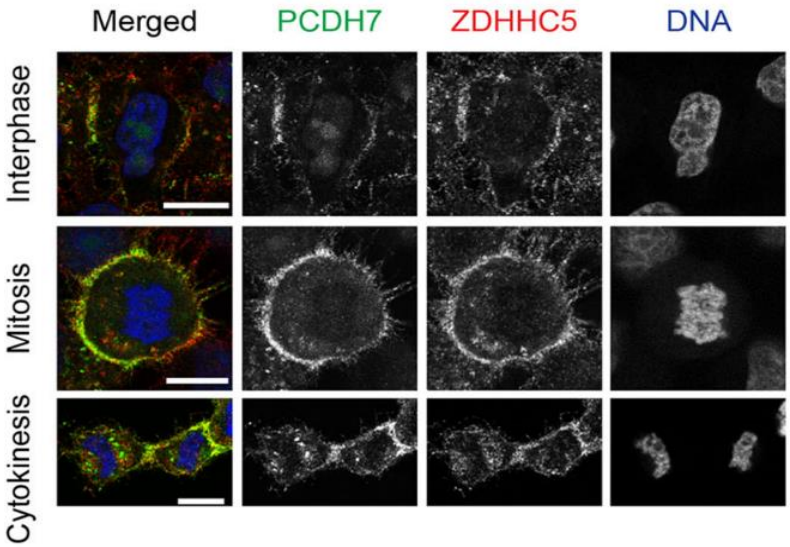

Figure 14. ZDHHC5 colocalized with PCDH/ during cell division.

Localization of PCDH7 (green, anti-GFP), ZDHHC5 (red, anti-ZDHHC5), and DNA (blue, DAPI) within PCDH7-GFP-BAC cells during interphase (top), mitosis (middle), and cytokinesis (bottom). Scale bars: 10 μm.

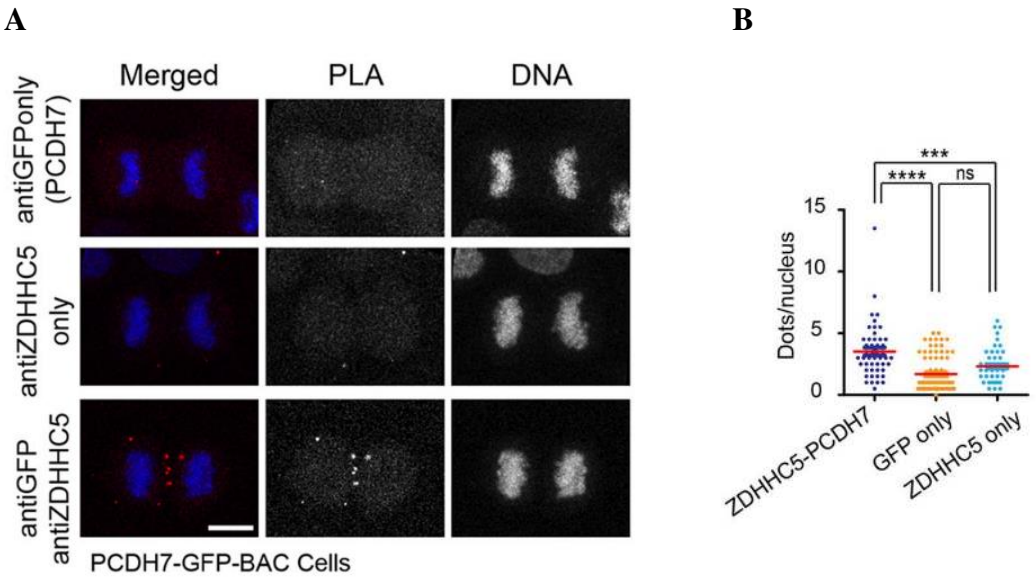

Figure 15. Spatial interaction of PCDH7 and ZDHHC5 during cytokinesis was analyzed using an in-situ proximity ligation assay (PLA).

A. Representative images display interactions as red fluorescent PLA puncta, with DNA labeled in blue (DAPI). Controls included separate treatments with anti-GFP and anti-

ZDHHC5 antibodies. Scale bar: 10 μm. **B.** Quantification of PLA puncta in cells treated with anti-GFP (PCDH7) antibody alone (n=77), anti-ZDHHC5 antibody alone (n=59), and both antibodies together (n=49). Images are maximum-intensity projections of z-stacks, with statistical analysis performed using one-way ANOVA with Sidak's multiple comparisons test. ns, non-significant; ***P<0.001; ****P<0.0001.

To determine whether PCDH7 interacts with ZDHHC5 during mitosis, we performed GFP-trap coimmunoprecipitation in mitotic PCDH7::GFP-expressing cells. The results confirmed a physical interaction between PCDH7 and ZDHHC5 (Figure 16).

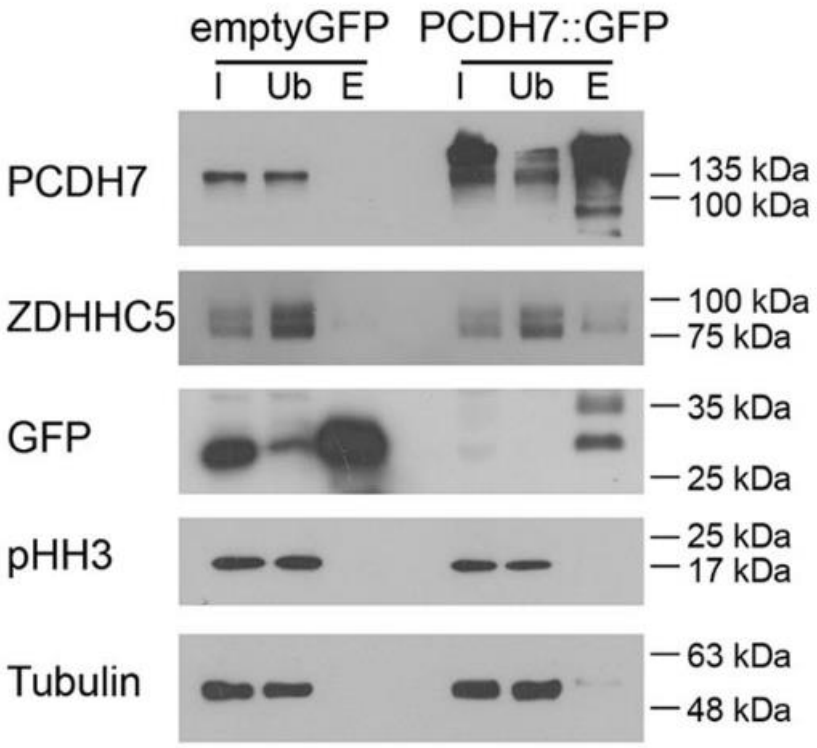

Figure 16. The interaction between PCDH7 and ZDHHC5 was confirmed using GFP-trap method.

HeLa S3 cells stably expressing PCDH7::GFP or GFP alone (control) were synchronized in mitosis. Western blot analysis of whole-cell lysates (input, I), unbound fractions (Ub), and elutes (E) were performed using antibodies against PCDH7, GFP, and

ZDHHC5. Phospho-histone H3 (pHH3) served as a mitotic marker, and α-tubulin was used as the loading control.

The interaction between PCDH7 and ZDHHC5 highlights a critical regulatory mechanism for cytokinesis. Palmitoylation by ZDHHC5 may facilitate PCDH7's dynamic localization to the cleavage furrow, ensuring proper membrane organization and protein interactions required for successful cell division. These findings underscore the functional cooperation between PCDH7 and ZDHHC5, providing insight into how palmitoylation-driven processes contribute to cytokinetic progression and cellular integrity.

2.3.3. PCDH7 Palmitoylation Confirmed by Acyl-Biotin Exchange Assay

The interaction between PCDH7 and ZDHHC5 led us to investigate whether PCDH7 undergoes direct palmitoylation. To test this, we performed a palmitoylation assay using acyl-biotin exchange (ABE) chemistry [51] in PCDH7::GFP-expressing HeLa S3 cells to enrich PCDH7 protein. Membrane proteins were isolated via high-speed centrifugation, and free cysteine thiol groups were blocked with N-ethylmaleimide (NEM). Samples were then split into two: one was treated with hydroxylamine (HA) to cleave thioester-linked palmitate groups, enabling biotinylation of exposed cysteines, while the other (HA−) served as a negative control. Biotinylated proteins were pulled down using streptavidin beads and analyzed by western blotting. Palmitoylated PCDH7 was detected in the hydroxylamine-treated (HA+) eluates, but not in the untreated (HA−) samples. EGFR and calnexin, known palmitoylated proteins, were used as positive controls and confirmed the assay's validity. These results demonstrate that PCDH7 is palmitoylated (Figure 17).

Palmitoylation may serve as a key mechanism for targeting PCDH7 to the plasma membrane during cytokinesis, ensuring its proper spatial distribution and activity. These findings provide critical insight into how post-translational modifications like palmitoylation contribute to the dynamic behavior of PCDH7 during cell division.

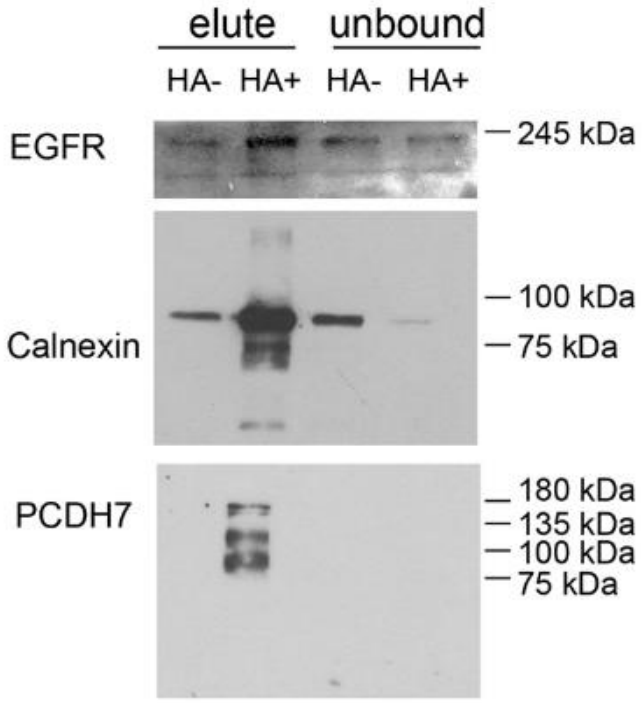

Figure 17. The palmitoylated proteins were confirmed using the ABE assay.

HA+ indicates hydroxylamine-treated samples, while HA− represents untreated controls. HeLa S3 cells expressing PCDH7::GFP were analyzed, with PCDH7 detected using anti-PCDH7 antibodies (116 kDa for PCDH7 and 143 kDa for PCDH7::GFP). EGFR and calnexin, known palmitoylated proteins, were included as positive controls.

2.4. DISCUSSION AND CONCLUSION

In this study, we explored the functional significance of PCDH7 during cell division and investigated its regulation through palmitoylation, a reversible lipid modification. Our findings demonstrate that PCDH7 dynamically localizes throughout the cell cycle, transitioning from cell-cell contacts during interphase to the cell surface and retraction fibers at mitotic onset, and ultimately accumulating asymmetrically at the cleavage furrow during cytokinesis. This dynamic localization suggests a role for PCDH7 in processes that are essential for mitotic progression, particularly cytokinesis.

Functional analysis using PCDH7 knockout (KO) cells revealed a cytokinetic defect characterized by increased multinucleation and delays in cleavage furrow formation and ingression. Live-cell imaging showed that, while PCDH7-depleted cells could initiate furrow ingression, they often failed to complete cytokinesis, leading to furrow regression and the formation of multinucleated cells. These phenotypic outcomes highlight the essential role of PCDH7 in maintaining cytokinetic fidelity. Importantly, reintroducing PCDH7 rescued the multinucleation phenotype and restored normal mitotic progression, emphasizing its functional relevance.

The mechanism underlying PCDH7's role in cytokinesis appears to involve the regulation of the actomyosin network. We observed a significant reduction in active RhoA and phosphorylated myosin II levels at the cleavage furrow in PCDH7 KO cells. These observations align with previous studies showing that RhoA and myosin II are critical regulators of the actomyosin ring, driving furrow ingression during cytokinesis [19]. Given that PCDH7 depletion compromises RhoA activity and myosin II phosphorylation, PCDH7 likely facilitates proper actomyosin ring constriction and cortical stability during cytokinesis.

We further identified ZDHHC5 as a key palmitoyltransferase interacting with PCDH7. Both proteins colocalized dynamically at the cell surface, retraction fibers, and cleavage furrow during mitosis, suggesting their cooperation in regulating membrane dynamics. Palmitoylation of PCDH7 was confirmed using the acyl-biotin exchange assay, demonstrating that this lipid modification is crucial for PCDH7's localization and

function during cytokinesis. As ZDHHC5 is predominantly localized at the plasma membrane, it likely mediates the palmitoylation of PCDH7, enabling its targeted recruitment to the cleavage furrow.

Palmitoylation enhances PCDH7's hydrophobicity and membrane association, playing a critical role in the spatial regulation of key proteins. However, identifying the specific palmitoylated cysteine is essential to deepen our understanding of how this modification alters PCDH7's structure for effective membrane binding.

In summary, our results uncover a critical role for PCDH7 in cytokinesis, where it facilitates proper actomyosin ring regulation and cleavage furrow ingression. We further demonstrate that PCDH7 localization and function are regulated through palmitoylation, mediated by ZDHHC5. These findings highlight the importance of PCDH7 in maintaining mitotic fidelity and reveal a previously unappreciated role for palmitoylation in cytokinesis. Future studies will be needed to explore the broader implications of palmitoylation in cell division and identify additional substrates that contribute to this essential process.

CHAPTER 3

3. The Investigation of Molecular Function and Dynamics of CLIC4 During Cell Division

3.1 LITERATURE REVIEW

3.1.1. The Chloride Intracellular Channel (CLIC) Protein Family

The chloride intracellular channel (CLIC) protein family in mammalian cells comprises seven members: p64 and CLIC1–6. Despite differences in the length and amino acid composition of their N-terminal regions, all CLIC proteins share a conserved CLIC homology domain in the C-terminal region, spanning approximately 220 amino acids. These proteins also feature two putative transmembrane domains, nuclear localization signals (NLS), and phosphorylation sites, reflecting their structural and functional diversity [55-57].

CLIC proteins are metamorphic, meaning they can adopt multiple stable three-dimensional conformations rather than a single defined structure [58]. This unique property enables CLIC proteins to transition between soluble cytoplasmic and membrane-bound states, allowing them to adapt to diverse cellular environments and perform various functions. While some studies have demonstrated that CLIC proteins can act as chloride ion channels in artificial systems such as lipid bilayers, this function remains unconfirmed in living cells [59, 60].

CLIC proteins perform diverse organelle-specific functions, including ion channel activity, membrane trafficking, cytoskeletal regulation, and apoptosis (Figure 18). CLIC1 regulates cell volume in neurons and contributes to oxidative stress responses, while CLIC4 is involved in mitochondrial apoptosis, cell division, and endosomal regulations [61-63]. Other members, such as CLIC2, CLIC3, CLIC5, and CLIC6, play tissue-specific roles, modulating ryanodine receptors, supporting cytoskeletal structures, and regulating hormone secretion, highlighting their specialized and therapeutic potential [64].

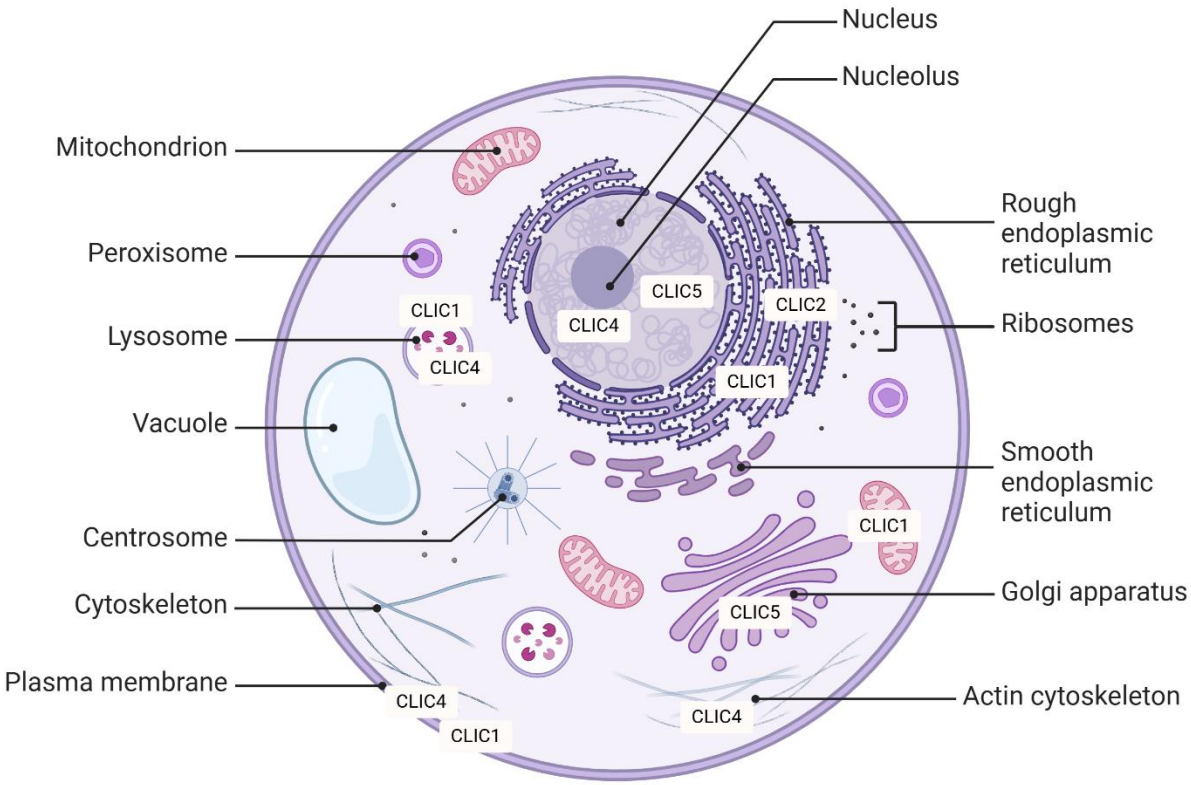

Figure 18. Schematic illustration showing the distribution of CLIC proteins in intracellular organelles (BioRender.com).

Recent evidence suggests that CLIC proteins may function as fusogens, facilitating membrane fusion through dynamic conformational changes [65]. Under basal conditions, CLIC proteins predominantly exist in a globular conformation, which conceals their hydrophobic inter-domain interface and limits their interaction with membranes. Environmental triggers, such as acidic pH or reactive oxygen species (ROS), induce a conformational shift to an elongated structure, exposing the hydrophobic interface to enable membrane association. Upon membrane binding, CLIC subunits assemble into oligomeric complexes [66], destabilizing adjacent membranes and lowering the energetic barrier for fusion. This fusogenic activity underscores the significance of CLIC proteins'

structural flexibility and inter-domain interactions in mediating their transition from soluble to membrane-bound forms [65].

Structural studies have established a close relationship between soluble CLIC proteins and the omega class of glutathione S-transferase (GST) enzymes [67]. Similar to GST proteins, which are involved in redox signaling and detoxification, CLIC proteins possess a reactive cysteine residue at their glutathione-binding site—a feature conserved across the family [68] . This reactive cysteine confers potential redox activity and enables regulation through glutathione-dependent reactions. Alternatively, the glutathione-binding site may facilitate the targeting of CLIC proteins to specific cellular compartments or mediate interactions with other proteins, highlighting its importance in cellular function [67, 69].

The metamorphic nature of CLIC proteins, coupled with their conserved glutathione-binding site, positions them as versatile regulators of cellular processes. Their ability to undergo dynamic conformational changes and interact with various cellular components underscores their functional significance in maintaining cellular homeostasis and responding to environmental cues.

3.1.2. CLIC4: Structure, Function, and Role in Cell Division

CLIC4, also referred to as mtCLIC, p64H1, RS43, or HuH1, is a 253-amino-acid protein consisting of an N-terminal thioredoxin-like domain and a C-terminal domain primarily composed of α-helices. The N-terminal domain contains a putative transmembrane region, while the C-terminal domain includes a nuclear localization signal (NLS). This dual-domain structure reflects CLIC4's versatility in adopting various functional roles within the cell [55, 67].

Among the CLIC protein family, CLIC4 is the most extensively studied and has been implicated in several actin-based processes, including cell differentiation, adhesion, migration, integrin signaling, spreading, and protein trafficking [55]. Despite its established roles, the molecular mechanisms regulating CLIC4’s transition between soluble and membrane-bound states remain poorly understood.

It was demonstrated that CLIC4 translocated to the plasma membrane in N1E-115 neuroblastoma cells in response to Gα13-mediated RhoA activation by lysophosphatidic acid (LPA). This translocation requires intact F-actin and is mediated by specific residues homologous to GST omega-1. Mutations in the reactive cysteine (C35A) or glutathione-binding site residues (F37D, D87A, P76A) disrupt CLIC4's translocation to the membrane. Interestingly, CLIC4 colocalizes with NHERF2, an ERM protein-binding partner, suggesting that ERM proteins may facilitate its membrane association [3, 56].

In addition to its membrane-associated roles, CLIC4 contributes to actin cytoskeleton regulation. It regulates branched actin networks on early endosomes [70] and interacts with profilin-1 in the RhoA-mDia2 signaling pathway, promoting actin polymerization. Moreover, depletion of CLIC4 promotes integrin-regulated filopodia formation, further supporting its involvement in membrane trafficking and actin dynamics [58, 71]. Additionally, the expression of CLIC4 has been implicated in cancer progression, with varying expression levels observed across different carcinoma types, highlighting its broader biological relevance [55, 65].

Recent findings have revealed a conserved GXXXG motif in the transmembrane domains of CLIC proteins, indicating potential cholesterol-binding activity critical for their membrane interactions [66]. These interactions may underpin CLIC4's ability to transition between soluble and membrane-bound states dynamically during cellular processes.

Proteomics studies by Özlü et al. demonstrated significant changes in protein composition at the plasma membrane during mitotic progression compared to interphase, with CLIC1 and CLIC4 showing notable enrichment at the plasma membrane during mitosis [1]. This dynamic regulation of CLIC proteins throughout the cell cycle highlights their crucial roles in mitotic processes, particularly cytokinesis. During cytokinesis, CLIC4 localizes to the cleavage furrow and midbody in a RhoA-dependent manner, which is disrupted by mutations in its glutathione S-transferase activity–related residues (C35A and F37D) [62].

Furthermore, CLIC4 interacts with key components of the cytokinetic machinery, including ezrin, anillin, and ALIX, at the cleavage furrow and midbody. Notably, CLIC4 is involved in ezrin activation, with mutual interdependence, as inhibition of ezrin activation impairs CLIC4 translocation. The loss of CLIC4, along with CLIC1, leads to polar membrane blebbing, cleavage furrow regression, and multinucleated cells, underscoring their essential role in maintaining cortical stability and supporting successful cell division [62].

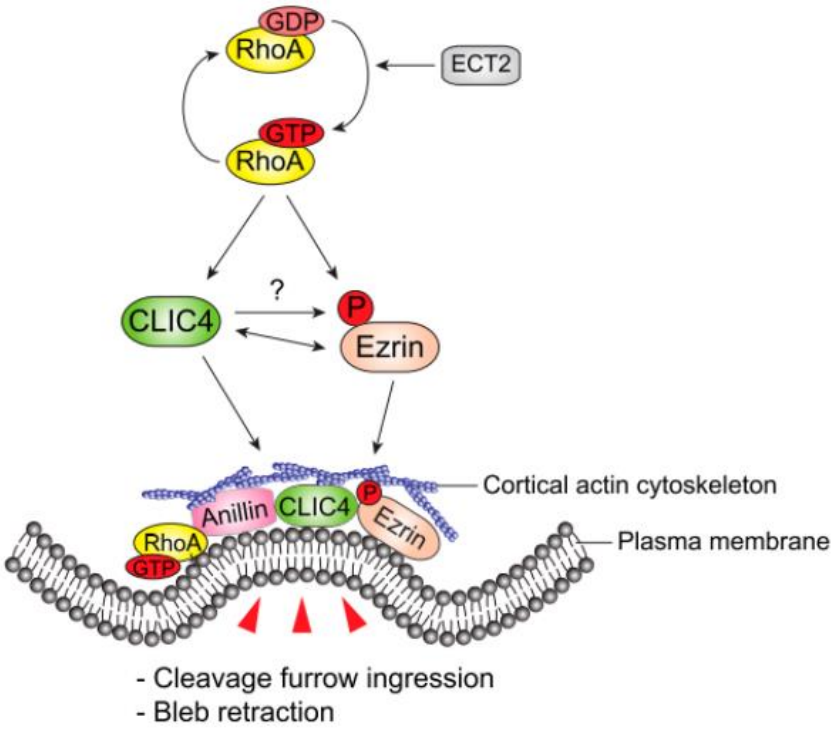

Figure 19. Schematic illustration of the potential role of CLIC4 in the cortical actin network [62].

CLIC4 translocated to the plasma membrane during cytokinesis, driven by RhoA activation via RhoGEF ECT2, and enhances ezrin activation through phosphorylation. Activated ezrin, in turn, promotes CLIC4 accumulation at the cleavage furrow, ensuring cortical stability by linking the actin cytoskeleton to the plasma membrane during cleavage furrow ingression and bleb retraction.

Although the role of CLIC4 during cell division has been extensively explored, the exact mechanisms governing its translocation to the membrane remain unclear. Elucidating these mechanisms could reveal new insights into the regulation of cytokinesis and the functional versatility of CLIC proteins.

3.1.3. Dynamics of Membrane Blebbing

Blebs are plasma membrane protrusions that form at the cortex-membrane boundary due to Laplace pressure, often arising at sites where the F-actin cortex is ruptured [72, 73]. Blebbing is a dynamic and physiological process observed during cytokinesis [74], cell migration [75], and apoptosis [76]. It has been identified in various cell types, including HeLa cells [77], L929 cells, and BHK21 cells [78].

Blebbing occurs in three distinct stages: nucleation, expansion, and retraction. During nucleation, the plasma membrane detaches from the underlying actin cortex due to localized increases in intracellular hydrostatic pressure, which exceed the forces maintaining membrane-cortex attachment. This process is driven by myosin II motor activity, which generates the intracellular pressure necessary for bleb initiation. Studies have shown that inhibiting myosin II activity prevents bleb formation [76], while laser ablation of the actin cortex induces blebbing [79], emphasizing the importance of cortical tension in regulating bleb nucleation. Membrane-cortex coupling strength also influences blebbing, as demonstrated in migrating A375 melanoma cells: ezrin knockdown weakens this coupling and increases blebbing, whereas ezrin overexpression strengthens the attachment and reduces bleb formation [80].

During expansion, cytosolic pressure generated by actomyosin contraction forces fluid into the newly formed bleb, causing it to increase in size. The size of blebs is tightly regulated during this stage, as proper bleb size is critical for maintaining membrane stability and cellular integrity. Laplace pressure, the difference between intracellular and extracellular pressures, plays a significant role in determining bleb size. Higher Laplace pressure results in fewer, larger blebs and faster completion of blebbing activity during cytokinesis [81]. Conversely, reducing intracellular pressure, such as through

electroporation, leads to smaller blebs [79, 82]. Additionally, actomyosin contractility helps sustain optimal Laplace pressure, preventing excessive bleb enlargement and ensuring cell shape and stability during critical processes like cytokinesis. Unregulated bleb expansion can destabilize the cell, creating a tension imbalance between cellular poles and disrupting the buffering role of blebs in relieving intracellular tension [77] . Mechanisms proposed for increasing the bleb surface area during expansion include membrane tearing from the actin cortex and the unfolding of pre-existing membrane folds [83].

The structural transition of the bleb during expansion involves the recruitment of membrane-actin linker proteins to the bleb rim, together with actin network assembly. This process is regulated by RhoA signaling, where the concentration of Rnd3, a RhoA inhibitor, decreases on the membrane, leading to RhoA activation. Active RhoA triggers actin cortex reassembly, forming a cage-like actin network with a mesh size of approximately 200 nm that provides structural integrity for the bleb [72, 84].

Retraction typically begins within 30 seconds of bleb initiation and is completed in approximately 90 seconds (Figure 20) [85]. During retraction, the reassembled actin cortex is stabilized by proteins such as ezrin and actin-bundling factors, including α-actinin, while myosin II-driven contractility pulls the membrane back toward the cell body [72]. Recent imaging studies in HeLa cells have shown that ezrin is recruited to the bleb prior to retraction, and filamentous actin continues to accumulate even after retraction begins. Inhibition of Arp2/3, a nucleator of cortical actin, reduces the speed of retraction, decreases myosin II recruitment, and stabilizes filamentous actin, indicating that both actin flux and myosin-driven contraction are essential for efficient retraction [85].

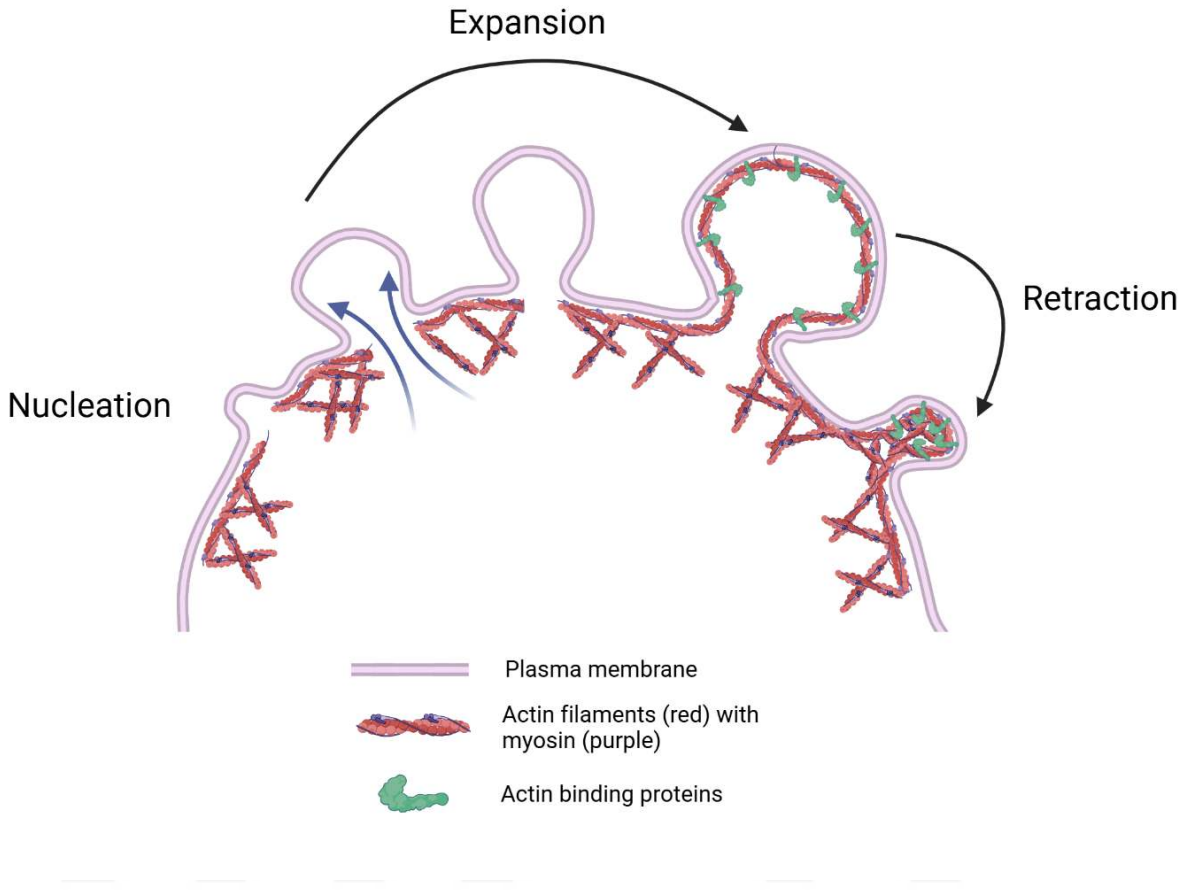

Figure 20. Schematic illustration of blebbing life cycle; nucleation, expansion and retraction (BioRender.com).

Blebbing also contributes to maintaining cell morphology during cytokinesis by relieving intracellular tension generated by actomyosin ring constriction. However, excessive or unregulated blebs can destabilize cell shape, underscoring the importance of tight size regulation to maintain cell boundary uniformity and ensure symmetric division [86]. In our previous study, we demonstrated that CLIC4 localizes to polar membrane blebs during cytokinesis, and the absence of CLIC1 and CLIC4 results in the formation of unstable and abnormally large blebs [62]. Given that CLIC proteins localize to both the actomyosin ring and polar blebs, and their absence leads to destabilized bleb dynamics, CLIC proteins might tether the plasma membrane to the actin cortex. This tethering likely stabilizes blebs and ensures proper cell division, highlighting the

importance of CLIC proteins in regulating bleb formation and dynamics during cytokinesis.

3.1.4. Regulation of the Actomyosin Cytoskeleton and Role of CLIC Proteins

The actin cytoskeleton undergoes extensive reorganization during cell division, a process regulated by actin-binding proteins and motor proteins like non-muscle myosin II (NMII). NMII, a key driver of cortical contractility, is composed of heavy and light chains and functions similarly to myosin in muscle contraction. Its activity is regulated by phosphorylation of its regulatory light chain (MLC) at Ser19/Thr18, mediated by ROCK downstream of RhoA signaling [19]. This phosphorylation enhances NMII's ability to bind antiparallel F-actin filaments, facilitating the assembly of actomyosin complexes that generate cortical tension [87]. During cytokinesis, RhoA-activated ROCK also inhibits myosin phosphatase, maintaining NMII in its active state and ensuring its rapid accumulation at the equatorial cortex [88]. These mechanisms are crucial for the contraction of the actomyosin ring and the formation of the cleavage furrow.

CLIC4 plays an important role in regulating the actomyosin network during cytokinesis. It translocates to the mitotic cell surface and becomes enriched at sites of cortical actin assembly, including the cleavage furrow. Depletion of CLIC proteins, including CLIC1 and CLIC4, disrupts cytokinesis, leading to defects such as abnormal polar blebs and cleavage furrow regression [62]. These observations suggest that CLIC4 might contribute to the organization and stability of the actomyosin ring by coordinating interactions between NMII and actin filaments. Furthermore, CLIC4 directly interacts with profilin-1, a G-actin-binding protein that facilitates the formation of ATP-actin dimers and promotes F-actin polymerization and elongation. Profilin-1 is also a component of the RhoA-mDia2 signaling pathway, which regulates cortical actin assembly during cytokinesis [89]. mDia2, a formin protein, nucleates linear actin filaments and plays a critical role in actomyosin ring formation [90].

In addition to its role in cytokinesis, CLIC4 is involved in broader aspects of actin cytoskeleton regulation. It translocates to membranes in an F-actin-dependent manner

upon RhoA activation by serum or lysophosphatidic acid (LPA) [3] and regulates branched actin formation on early endosomes [70]. Depletion of CLIC4 disrupts vesicular trafficking and cargo transport, causing an accumulation of branched actin on endosomal surfaces [70]. These findings highlight the versatility of CLIC4 in modulating actin cytoskeleton dynamics across multiple cellular contexts.

The interplay between NMII, formins such as mDia2, and actin-binding proteins like profilin-1 underscores the complexity of actomyosin regulation during cell division. Investigating NMII levels and localization in cells lacking CLIC proteins may further elucidate the regulatory role of CLIC proteins in maintaining actomyosin organization and promoting successful cytokinesis.

3.2. MATERIALS AND METHODS

3.2.1. Cell Culture

HeLa S3 cells were grown in 10% fetal bovine serum (FBS) and 1% penicillin/streptomycin (P/S) containing Dulbecco's modified Eagle's medium at 37 °C and 5% CO in a humidified incubator.

**CLIC4-GFP expressing stable cells, CLIC4-GFP LifeAct-RFP expressing stable cells and CLIC4-GFP and Ezrin-RFP expressing stable cells were generated by Cansu Üretmen..*

**CLIC1/CLIC4 DKO cells were generated in the previous study [62].*

3.2.2. Cloning of the Plasmids

For generation of P449_pLVX_PH_PLCdelta1-RFP, the vector containing the pleckstrin homology (PH) domain of PLCδ (Addgene #36075) was obtained from Addgene. The PH PLCδ sequence was cloned into the pLenti vector and tagged with RFP. The resulting construct was validated through restriction enzyme digestion and DNA sequencing.

P373_pLVX_MLC2-RFP vector is a gift from Michael Way.

GFP-tagged phosphomimetic and phosphomutant constructs (CLIC4 S108E-GFP and CLIC4 S108A-GFP) were generated using Gateway cloning and site-directed mutagenesis. The p342_pENTRY_CLIC4 WT_GFP vector available in our laboratory was used as a template for PCR, along with primers carrying the desired point mutations, to generate p486_pENTRY_CLIC4 S108A_GFP and p487_pENTRY_CLIC4 S108E_GFP constructs. The presence of the intended mutations in the newly generated vectors was confirmed by DNA sequencing. Subsequently, an LR recombination reaction was performed between these entry vectors and the pLenti CMV Hygro DEST destination vector, yielding p488_pLenti_CLIC4 S108A_GFP and p489_pLenti_CLIC4 S108E_GFP constructs.

**Cloning of the plasmids were performed by Nazan Saner.*

Table 2. The list of plasmids generated and utilized in Chapter 3.

Plasmid No	Plasmid Name	Backbone	Gene
449	pLVX_PH PLCdelta1-RFP	pLVX	PH PLCdelta1-RFP
373	pLVX_MLC2-RFP	pLVX	Myosin Light Chain C2 RFP
342	CLIC4 WT-GFP (Entry vector)	pDONR221	CLIC4 WT-GFP
486	CLIC4 S108A-GFP (Entry vector)	P342	Site-directed mutagenesis of CLIC4; Serine108 to Alanine
487	CLIC4 S108E-GFP (Entry vector)	P342	Site-directed mutagenesis of CLIC4; Serine108 to Glutamic Acid
488	CLIC4 S108A-GFP (Destination vector)	pLenti CMV Hygro DEST	CLIC4 S108A-GFP
489	CLIC4 S108E-GFP (Destination vector)	pLenti CMV Hygro DEST	CLIC4 S108E-GFP

3.2.3. Lentiviral transduction

Stable cell lines expressing CLIC4-GFP and RFP-tagged proteins were generated using lentiviral transduction. Lentiviral constructs encoding PLC-PH-RFP and MLC2-RFP, along with packaging vectors psPAX2 and pCMV-VSV-G, were used for the production of lentiviral particles. The psPAX2 plasmid was obtained from Didier Trono (Addgene plasmid #12260; http://n2t.net/addgene:12260; RRID:Addgene_12260), and pCMV-VSV-G was a gift from Bob Weinberg (Addgene plasmid #8454; http://n2t.net/addgene:8454; RRID:Addgene_8454). These plasmids facilitated the packaging and transduction of lentiviruses into the target cells.

HEK293T cells were used for lentiviral packaging. To prepare the lentiviral transfection mixture, 1000 ng of the transfer plasmid, 1000 ng of psPAX2, and 100 ng of

pCMV-VSV-G were combined with 20 µl of Opti-MEM (Thermo Fisher Scientific, 31985062) per well of a six-well plate. Separately, 93 µl of Opti-MEM was mixed with 7 µl of FuGENE transfection reagent (Promega, E2311) and incubated at room temperature for 5 minutes. The plasmid mixture was then added dropwise to the transfection reagent, incubated for 30 minutes, and evenly distributed into the culture media of HEK293T cells. Following 24 hours of incubation, the transfection media was replaced with fresh growth media.

Conditioned media containing lentiviral particles were collected at two-time points, 48 hours and 72 hours post-transfection. The collected viral supernatants were pooled, filtered through a 0.45 µm syringe filter to remove cellular debris, and aliquoted into 1 ml fractions. These aliquots were stored at -80°C for subsequent use. Residual HEK293T cells were discarded using bleach sterilization to ensure safety and sterility.

After lentivirus preparation, viral transduction was performed. HeLa S3 cells expressing CLIC4-GFP were seeded into six-well plates at 20% confluency. On the first day, media containing 8 µg/ml protamine sulfate (P4020, Sigma-Aldrich) was added to each well, followed by the dropwise addition of 500 µl of viral supernatant. The next day, the viral media was replaced with fresh growth media. A second round of transduction was performed on the third day, and on the fourth day, RFP signals were checked under a fluorescence microscope. When RFP expression was observed, the growth media was replaced with antibiotic selection media containing 1.5 µg/ml puromycin. Over the following two to three days, cells that did not receive viral particles died, while successfully transduced cells survived. After two passages, the surviving cells were frozen and stored in liquid nitrogen for future experiments. The generated stable cell lines were validated using fluorescence microscopy to confirm the expression of CLIC4-GFP and RFP-tagged proteins.

3.2.4. Plasmid Transfection and Drug Treatment

For plasmid transfection, Lipofectamine TM 2000 (Invitrogen, 11668027) was used following the manufacturer's instructions. Cells were seeded into a 24-well plate at 40% confluency. The next day, 500 ng of plasmid DNA was diluted in 50 µl of Opti-MEM, while 1 µl of Lipofectamine TM 2000 was diluted in a separate 50 µl of Opti-MEM. The

diluted solutions were combined in a 1.5 ml eppendorf tube and incubated for 15 minutes at room temperature. Meanwhile, the cell culture medium was replaced with DMEM lacking FBS and antibiotics. The transfection mixture was then added dropwise to the cells. Imaging experiments were conducted 48 hours post-transfection.

To inhibit palmitoylation, cells were incubated with 200 µM 2BP (Sigma-Aldrich, 21604) and DMSO overnight [91]. Treated cells were fixed, immunostained for CLIC4, and imaged in the confocal microscope.

3.2.5. Protein Pull-down with Lipid-Coated Beads

HeLa S3 and HeLa Kyoto cells were seeded in 15 cm plates and synchronized to mitosis using monopolar synchronization. Mitotic cells were pelleted and lysed in 450 µl of binding buffer containing 10 mM HEPES (pH 7.4), 150 mM NaCl, 0.25% Nonidet P-40, and protease inhibitors (1 mM PMSF, 50 mM NaF, 10 mM Na_3VO_4). The lysate was homogenized using a sonicator, followed by centrifugation at 4000 g for 20 minutes to remove debris. The supernatant was transferred to a fresh tube, and protein concentration was determined using the Bradford assay. Equal amounts of whole-cell lysate protein were used for each condition. The lysates were precleared by incubation with 30 µl of control beads for 1 hour. Subsequently, 4 mg of whole-cell lysate protein was incubated with 60 µl of bead slurry coated with $PI(3,5)P_2$ (Echelon, P-B035A), $PI(4,5)P_2$ (Echelon, P-B045A), or control beads. HeLa S3 cell lysates were incubated with the beads overnight, whereas HeLa Kyoto cell lysates were incubated for 4 hours. Following incubation, the samples were centrifuged at 2.5 g for 2 minutes at 4°C and washed three times with binding buffer to remove unbound proteins. The bound proteins were eluted by resuspending the bead samples in 2x sample buffer containing 100 mM DTT and boiling at 90°C for 10 minutes. Eluted proteins were analyzed by Western blot to evaluate protein-lipid interactions.

3.2.6. Microscopy and Analysis

For imaging fixed samples, confocal microscopy was performed using Leica DMi8/SP8 TCS-DLS laser scanning confocal microscopes (LAS-X Software). The HC PL APO 63×/1.40 Oil CS2 objective was utilized for high-resolution imaging on the Leica DMi8/SP8 TCS-DLS system.

Fluorescence imaging was carried out with a Leica DMi8 widefield microscope, equipped with HC PL FL L 20×/0.40 CORR and HC PL APO 63×/1.40–0.60 OIL objectives, providing the necessary resolution and flexibility for observing cellular processes. Image quantification, including intensity measurements and spatial analysis, was conducted using ImageJ software, ensuring accuracy and reproducibility in data analysis.

For membrane enrichment analysis in mitotic cells, the outer surface of the membrane was defined, and fluorescence intensity along with the area was measured. Subsequently, the outer region of interest (ROI) was scaled down by a factor of 0.75 and designated as the inner ROI. Fluorescence intensity and area were measured again for this inner ROI.

To determine membrane enrichment, the intensity of the inner ROI was subtracted from the outer ROI, and the same subtraction was performed for their respective areas. The resulting intensity value was divided by the corresponding area to calculate the membrane mean intensity. Similarly, the inner mean intensity was obtained by dividing the inner intensity by the inner area. Finally, the membrane mean intensity was divided by the inner mean intensity to quantify the membrane enrichment of the protein.

3.2.7. Live cell imaging of Membrane Blebs

Stable HeLa S3 cell lines expressing CLIC4-GFP and Ezrin-RFP/LifeAct-RFP/MLC2-RFP were generated. To isolate the cells expressing GFP and RFP in higher level in the population, the dual-color cells are sorted using Bio-Rad S3e Cell Sorter. After the sorting, the cells were seeded into the glass-bottom ibidi plates and synchronized to interphase. The cells were released from the interphase by replacing the thymidine-containing media with growth media. Then, the mitosis cells were imaged real-time using Zeiss Lattice Lightsheet 7 with the close cabinet that provides 37 °C temperature and 5% CO2. The images were taken single z-stack with 0.4 second intervals. For the analysis of the protein arrival time, the individual blebs were used to generate the kymographs of GFP and RFP signals through time in ImageJ software. The straight line was drawn through the bleb and “Multi-kymograph” plug-in was used to generate kymographs. By analyzing the plot profile of each time point on the kymographs, the time points when the

proteins are enriched on the membrane were determined. The arrival time of RFP proteins was compared to the time points of CLIC4-GFP. This imaging procedure was applied to other cell lines and CLIC4 GFP will be visualized with Ezrin-RFP, Lifeact-RFP, and MLC2-RFP proteins at the bleb membrane.

3.2.8. siRNA treatment

HeLa S3 cells were seeded at 20% confluency into 24-well plates containing coverslips for immunofluorescence staining and 6-well plates for Western blot analysis. On the following day, prior to transfection, cells were starved in DMEM without FBS and antibiotics. For each well to be transfected, the desired RNAi duplex (control, Ezrin, or Anillin) and 1.5 µl Lipofectamine RNAiMAX (13778075, Thermo Fisher) were separately diluted in 50 µl Opti-MEM. The two solutions were combined and incubated for 15 minutes at room temperature. After incubation, 100 µl of the transfection mixture was added to each well, resulting in a final siRNA concentration of 20 nM for the respective siRNAs. Transfection media was replaced with growth media after 5 hours of incubation. On the third day, a second round of siRNA transfection was performed using the same protocol. By the fifth day, cells were ready for either immunofluorescence staining or Western blot analysis, depending on the experimental requirement.

3.2.9. Generation of Giant Plasma Membrane Vesicles (GPMVs)

Giant plasma membrane vesicles (GPMVs) were prepared using HeLa cells seeded into 35-mm cell culture dishes or glass-bottom plates, depending on the experimental requirements. On the first day, cells were seeded at approximately 30% confluency and cultured under appropriate conditions. By the second day, cells typically reached 70% confluency and were ready for vesicle generation. To induce GPMV formation, cells were washed once with HBSS buffer, followed by the addition of 300 µl of freshly prepared GPMV buffer. Two types of GPMV buffers were used depending on the experiment: (1) HBSS buffer containing 2 mM NEM, or (2) HBSS buffer containing 25 mM PFA and 2 mM DTT. After the addition of GPMV buffer, cells were incubated at 37°C for 3 hours. GPMV formation was confirmed by observing free-floating, dark, spherical vesicles under a ×20 objective using a Zeiss LSM 780 confocal microscope. Once vesicles were identified, the supernatant containing GPMVs was carefully collected and transferred into

microcentrifuge tubes to avoid contamination with cellular debris. They were transferred to glass bottom plates for imaging. The vesicles were visualized using laser-scanning confocal microscopy Zeiss LSM 980 equipped with 20× water-immersion objective lens.

3.2.10. Post-Translational Modification (PTM) Proteomics

To investigate the post-translational modifications (PTMs) of CLIC4, HeLa S3 cells stably expressing CLIC4-GFP were synchronized at interphase, mitosis, and cytokinesis. Cells were pelleted at these stages and lysed in a buffer containing 10 mM Tris-Cl (pH 7.5), 150 mM NaCl, 0.5 mM EDTA, 0.5% NP-40, 0.09% NaN_3, and protease and phosphatase inhibitor cocktails. The cell lysates were centrifuged for protein extraction and the supernatant was incubated with GFP-Trap resin (ChromoTek GFP-Trap Agarose) to isolate CLIC4-GFP.

After binding, the GFP-Trap resin was washed thoroughly, and the bound proteins were eluted with 0.2 M glycine (pH 2.5). The elutes were neutralized immediately using 1 M Tris base (pH 10.4). The efficiency of CLIC4-GFP enrichment and elution was verified by Western blot analysis of small-scale samples from total cell lysates and elutes.

Eluted CLIC4-GFP proteins were digested with trypsin to produce peptide mixtures for mass spectrometry analysis. The peptide samples were analyzed using nano-liquid chromatography coupled to Q-Exactive Orbitrap mass spectrometry. For each experimental condition, two biological replicates were processed, with three technical replicates analyzed per biological repeat to ensure robust data acquisition.

Proteome Discoverer 2.3 software was used for data processing and analysis. CLIC4 protein was identified with an average sequence coverage of approximately 85% across all samples.

**PTM Proteomics was performed by Ceyda Seren Ceylan.*

3.2.11. Palmitoylation Assay Using Click Chemistry

3.2.11.1. Preparation of Membrane Lysates

Each pellet was resuspended in 1 mL of lysis buffer (PBS, pH 7.4, supplemented with 1 mM PMSF and 1 mM HDSF) on ice. The samples were sonicated on ice for three

cycles of 10 seconds at 70% amplitude with 50% power, followed by incubation on ice for 1 hour. The lysates were then diluted with 5 mL PBS and centrifuged at 100,000 × g for 1 hour at 4°C using a 90-TI rotor. The supernatant was collected into a fresh tube, while the pellet was resuspended in 1.5 mL PBS containing 2% SDS and vortexed thoroughly.

3.2.11.2. Click Chemistry

Click chemistry was performed to label proteins with biotin-azide. A 50 mM TCEP solution in PBS was prepared and the pH of the TCEP solution was neutralized using 10 N KOH and verified using pH indicator paper. For each sample, a 1.5 mL reaction mixture was prepared containing 30 µL of 50 mM CuSO4, 30 µL of 50 mM TCEP, 90 µL of 1.67 mM TBTA, and 7.5 µL of 100 mM biotin-azide. The reaction was vortexed and incubated at 37°C for 30 minutes, followed by another vortex and an additional 30 minutes of incubation.

3.2.11.3. Methanol/Chloroform Precipitation

Proteins were precipitated from a 1 mL sample volume using a methanol/chloroform method. Four volumes (6 mL) of methanol were added to the sample, and vortexed, followed by 1.5 volumes (2.25 mL) of chloroform. The sample was vortexed again and 3 volumes (4.5 mL) of water were added, resulting in a cloudy mixture. The mixture was centrifuged at 4,000 × g for 20 minutes at room temperature to form a protein layer at the interface. The top layer was carefully removed, leaving a small volume behind. To wash the precipitate, 3 volumes (4.5 mL) of methanol were added, vortexed, and centrifuged at 4,000 × g for 10 minutes. This wash step was repeated, and residual methanol was carefully removed without disturbing the protein pellet.

3.2.11.4. Streptavidin Incubation and On-Bead Digestion

The protein pellet was solubilized in 1 mL of 6 M urea in PBS containing 2% SDS and divided into two 500 µL samples. Hydroxylamine treatment was performed on one sample by adding 26.3 µL of 50% hydroxylamine solution to achieve a final concentration of 2.5%. Aliquots of input material (10 µL, 2%) were saved for analysis. Streptavidin beads were preconditioned by washing twice with PBS and once with 0.1% SDS in PBS.

The samples were diluted 20-fold with PBS to a total volume of 10 mL, incubated with the beads overnight at room temperature, and aliquots of unbound material were collected. Beads were washed four times with PBS before elution.

For elution, an SDS-Laemmli buffer containing 50 mM TCEP and 500 nM biotin was prepared by adding 60 µL of biotin stock (5 µM) to 600 µL buffer. Elution was performed by adding 200 µL of this solution to the beads and boiling at 98°C for 10 minutes with shaking at 1,000 rpm. The eluted proteins were collected, and samples were prepared for downstream analyses.

**This protocol was performed by Gamze Nur Yapıcı.*

Table 3. The list of antibodies used for Western Blot (WB) and Immunofluorescence Staining (IF) with their host, brand, lot number and dilution information in Chapter 3.

Antibody Name	Host	Brand	Product No	Dilution	Application
Alpha Tubulin (DM1A)	Mouse	Cell Signaling Technology	3873S	1:2000 and 1:1000	WB and IF
Anilin	Rabbit	Abcam	ab99352	1:500 and 1:200	WB and IF
Ezrin	Rabbit	Cell Signaling Technology	3145S	1:500	WB and IF
Myosin IIb (D8H8) XP(R)	Rabbit	Cell Signaling Technology	3726S	1:500	WB
P-ezrin ERM	Rabbit	Cell Signaling Technology	3726S	1:400	WB and IF
Profilin-1	Rabbit	Cell Signaling Technology	3237	1:1000	WB and IF
phospho-myosin light chain (S19)	Mouse	Cell Signaling Technology	3675S	1:500 and 1:200	WB and IF
phospho-myosin light chain 2 (thr18/ser19)	Rabbit	Cell Signaling Technology	3674	1:500 and 1:200	WB and IF

CLIC4	Mouse	Santa Cruz	Sc-135739	1:500 and 1:100	WB and IF
Dia2 (C-15)	Goat	Santa Cruz	Sc-10889	1:200	WB and IF
Integrin Beta1 (12G10)	Mouse	Abcam	Ab30394	1:500	IF
Alexa Fluor 488	Mouse	Invitrogen	A21202	1:1000	IF
Alexa Fluor 488	Rabbit	Invitrogen	A21206	1:1000	IF
Alexa Fluor 555	Mouse	Invitrogen	4409S	1:1000	IF
Alexa Fluor 555	Rabbit	Cell Signaling Technology	4413S	1:1000	IF
HRP-conjugated secondary antibody	Rabbit	Cell Signaling Technology	7074S	1:2000	WB
HRP-conjugated secondary antibody	Mouse	Cell Signaling Technology	70765	1:2000	WB

3.3. RESULTS

3.3.1. Molecular Analysis of CLIC4's Translocation to the Plasma Membrane during Cell Division

3.3.1.1. Membrane Binding of CLIC4 through phosphoinositol binding

Phosphoinositols are critical membrane phospholipids that regulate various cellular processes, including vesicular trafficking and cell division, by modulating membrane dynamics. Among them, $PI(4,5)P_2$ is highly enriched in the plasma membrane and plays a crucial role in cytokinesis by mediating adhesion between the contractile ring and the plasma membrane [25, 92]. At the cleavage furrow, $PI(4,5)P_2$ serves as a binding site for proteins such as ezrin and anillin, which interact with CLIC4. Ezrin binds $PI(4,5)P_2$ at the plasma membrane and, upon phosphorylation, anchors the cortical actomyosin network [93]. Anillin, via its PH domain, stabilizes the contractile ring by binding $PI(4,5)P_2$ at the cleavage furrow [62]. Another key phosphoinositol, PI3P, is a marker for early endosomes and is converted into $PI(3,5)P_2$ in late endosomes, where it regulates endosomal membrane trafficking [94]. CLIC4's association with endosomal compartments enriched in PI3P and $PI(3,5)P_2$ suggests its potential role in endosomal membrane regulation [61]. These findings emphasize the importance of exploring CLIC4's interactions with $PI(4,5)P_2$ and $PI(3,5)P_2$ and their roles in CLIC4's membrane localization during cell division.

To investigate the interaction of CLIC4 with $PI(4,5)P_2$ and $PI(3,5)P_2$, lipid-binding assays were performed using HeLa Kyoto cells synchronized to mitosis. Cell lysates were incubated with lipid-coated beads designed to capture proteins that specifically bind $PI(4,5)P_2$ or $PI(3,5)P_2$. Western blot analysis of the eluted proteins revealed that a greater amount of CLIC4 protein was bound to $PI(3,5)P_2$ than $PI(4,5)P_2$, with the control showing the least binding (Figure 21).

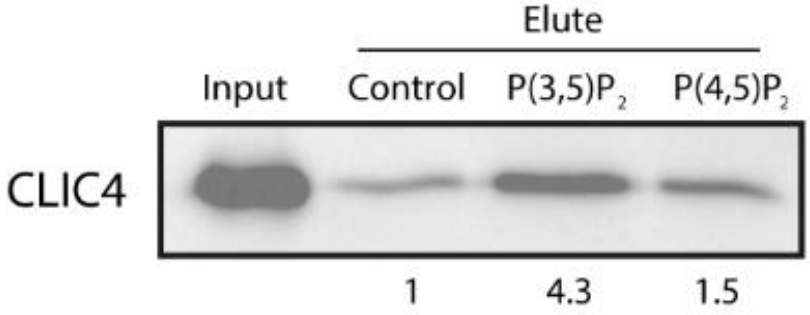

Figure 21. The examination of proteins that were pulled down from mitotic HeLa S3 cell lysates using control, PI(3,5)P_2-coated and PI(4,5)P_2-coated beads with Western blot analysis.

The mitotic cell lysates (input), and elute proteins were resolved with 10% SDS-PAGE, followed by incubation with CLIC4 antibody. Band intensities were normalized to control.

To further examine the spatial relationship between CLIC4 and PI(4,5)P_2 during cell division, fluorescence imaging was conducted using HeLa S3 cells expressing CLIC4-GFP and PLCδ1PH-RFP (PLC-PH-RFP), a PI(4,5)P_2 biosensor which binds PI(4,5)P_2 at the plasma membrane, translocates to the cytosol upon PI(4,5)P_2 hydrolysis, and associates again with the membrane when PI(4,5)P2 is resynthesized [95]. This dynamic behavior, coupled with fluorescence tagging, allows precise monitoring of PI(4,5)P_2 localization. Imaging revealed colocalization of CLIC4 and PI(4,5)P_2 at the plasma membrane during mitosis, with pronounced enrichment at the cleavage furrow during cytokinesis (Figure 22).

The stronger interaction of CLIC4 with PI(3,5)P_2 suggests a potential role for CLIC4 in regulating endosomal homeostasis [4], as PI(3,5)P_2 is predominantly localized to endosomal compartments [4]. Brightfield microscopy was used to investigate the impact of CLIC4 depletion on endosomal function. In interphase cells lacking CLIC4, enlarged vesicles were observed, indicating disrupted endosomal regulation. This phenotype aligns with CLIC4's interaction with PI(3,5)P_2, supporting its role in maintaining endosomal homeostasis [61] (Figure 23).

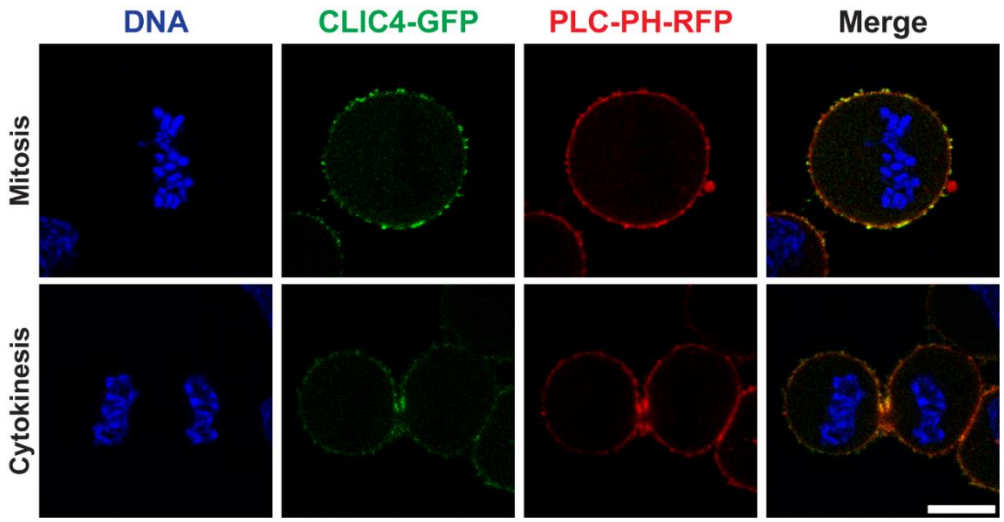

Figure 22. CLIC4 colocalized with PI(4,5)P2 during cell division.

The localization of CLIC4-GFP (green) and PLC-PH-RFP (biosensor of PI(4,5)P2, red) during mitosis and cytokinesis. DNA staining (Hoescht) is blue. Images were taken in confocal microscopy, scale bar, 10 μm.

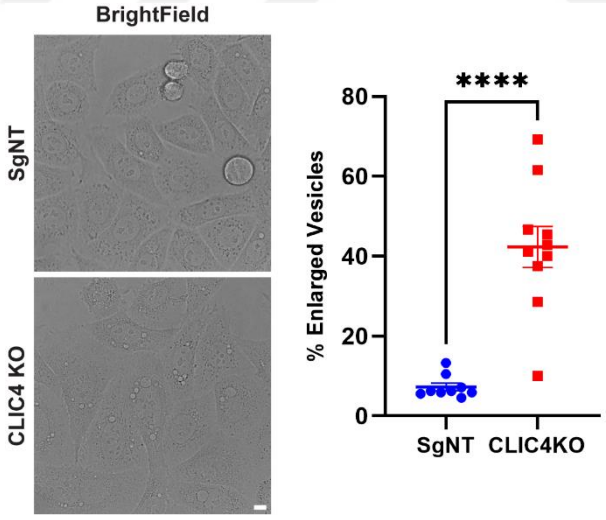

Figure 23. The absence of CLIC4 in HeLa S3 cells caused enlarged vesicles.

Statistical significance was determined using a two-tailed unpaired t-test (*P<0.05; ****P<0.0001). Images were taken in widefield microscopy, scale bar, 10 μm.

3.3.1.2. Membrane Binding of CLIC4 through post-translational modifications

Post-translational modifications (PTMs) are covalent alterations of proteins, involving the addition or removal of chemical groups such as acetyl, phosphoryl, or methyl groups. These modifications can influence protein-protein interactions, folding, stability, and localization by altering the protein's charge, conformation, or hydrophobicity [96]. Given their broad functional implications, understanding the PTMs of CLIC4 during cell division is critical for elucidating the mechanisms underlying its cell division-specific translocation to the plasma membrane.

PTM proteomics identified nine distinct modifications on CLIC4, including seven acetylations and two phosphorylations. Phosphorylation at serine 4 (S4) was consistently observed throughout the cell cycle, while phosphorylation at serine 108 (S108) was specific to mitosis and cytokinesis. Of the seven lysine acetylations, four (K11, K15, K90, and K212) were detected across all cell cycle stages. Interestingly, acetylations at lysines 150 (K150) and 238 (K238) were unique to cytokinesis. Acetylation at lysine 177 (K177), however, was observed in both interphase and cytokinesis, indicating it is not exclusive to cell division (Figure 24).

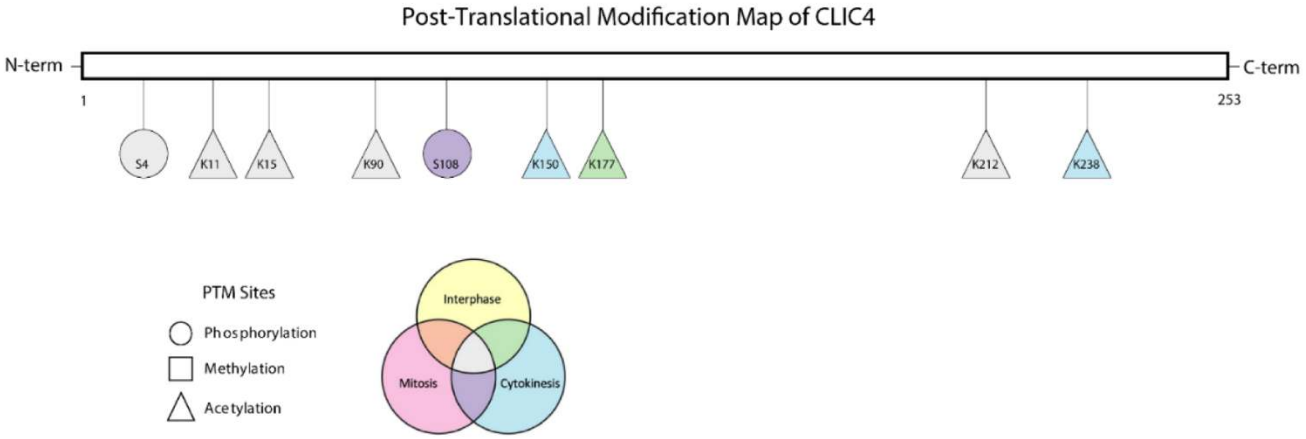

Figure 24. CLIC4 has several post-translational modifications in cell cycle dependent manner.

CLIC4, a 253-amino-acid-long protein, is eluted from interphase, mitosis, and cytokinesis cells. The Venn diagram illustrates its protein modifications across interphase (yellow), mitosis (pink), and cytokinesis (blue), with overlapping regions indicating shared modifications. Phosphorylation is represented by circles, while acetylation is depicted as triangles.

The phosphorylation of CLIC4 at S108 is notable because it is observed only during mitosis and cytokinesis, aligning with its translocation to the plasma membrane. Previous studies have shown that CDK5, a kinase activated by oxidative stress, phosphorylates CLIC4 at S108, promoting its stability and accumulation in N2A cells [97, 98]. Although CDK5 is predominantly involved in cytoskeleton regulation, membrane transport, and cell migration in neuronal cells, it shares 62% sequence homology with CDK1 and CDK2, key regulators of cell division [99]. This raises the possibility that CDK5-like kinases involved in cell division could phosphorylate CLIC4 at S108, influencing its membrane localization during mitosis and cytokinesis.

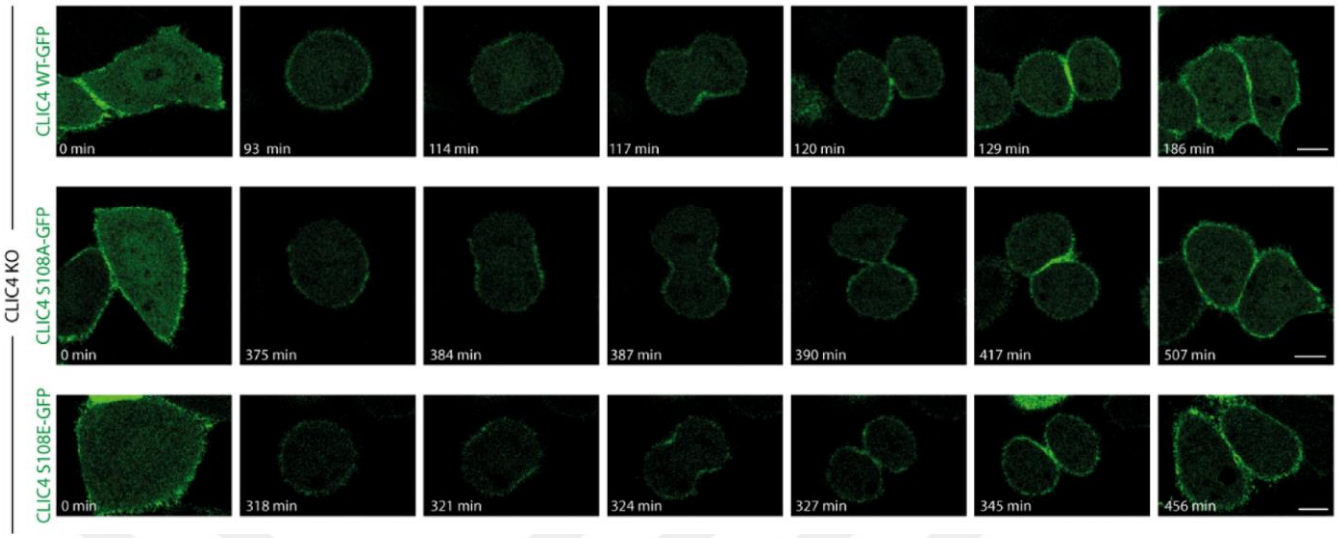

Figure 25. Phospho-mutant (CLIC4-S108A-GFP), and phospho-mimetic (CLIC4-S108E-GFP) in CLIC4 knock-out cells localized similar to CLIC4-WT-GFP during cell division.

Frames representing the phases of cell division are shown from the captured images in 3 minutes time interval using confocal microscopy. Images represent single z-sections. Scale bars, 10 μm.

To examine the functional relevance of S108 phosphorylation in the plasma membrane localization of CLIC4 during cell division, the S108 residue was mutated to alanine and glutamic acid via site-directed mutagenesis, generating phospho-mutant (S108A) and phospho-mimetic (S108E) forms of CLIC4. These constructs, along with wild-type CLIC4-GFP (CLIC4-WT-GFP) as a control, were transiently transfected into CLIC4 knock-out cells. Live-cell imaging using a Leica DMI8 SP8 confocal microscope was used to observe the localization of CLIC4 during cell division. The results revealed that both the phospho-mutant and phospho-mimetic forms of CLIC4 localized to the mitotic cell surface and accumulated at the cleavage furrow like in wild-type CLIC4 (Figure 25). This suggests that phosphorylation at S108 does not influence the plasma membrane localization of CLIC4 during cell division.

Model membrane systems are essential tools for investigating protein-membrane interactions, addressing challenges arising from biological membranes' complex nature.

Unlike protein-protein interactions, which can be examined using specific biochemical tools like antibodies, protein-lipid interactions lack such precise targeting strategies [100-102]. As a result, model membrane systems have emerged as a powerful tool for investigating these interactions by mimicking the physical and molecular characteristics of cellular membranes [101, 103]. Among the various model membrane systems, Giant Plasma Membrane Vesicles (GPMVs) offer a unique advantage by retaining the lipid and protein diversity of native membranes while being free of cytoskeletal and organelle components [103]. GPMVs are derived directly from the plasma membrane, retaining its lipid and protein diversity while excluding cytoskeletal and organelle components. These vesicles separate into distinct liquid phases, mirroring native membrane behavior and enabling the study of proteins in physiologically relevant environments [103]. By using GPMVs, we examined CLIC4's localization at membrane lipid domains, providing insights into its dynamic plasma membrane association during cytokinesis.

To examine CLIC4's localization at the plasma membrane using model membrane systems, we generated GPMVs using two different treatments: PFA-DTT and NEM [104]. DTT is known to cleave S-linked fatty acids, thereby disrupting protein palmitoylation and preventing palmitoylated proteins from associating with the plasma membrane in GPMVs [105]. In our experiments, CLIC4 was observed at the plasma membrane of GPMVs generated with NEM, but not in those formed with PFA-DTT. This result suggests that CLIC4's localization at the plasma membrane may depend on its palmitoylation (Figure 26).

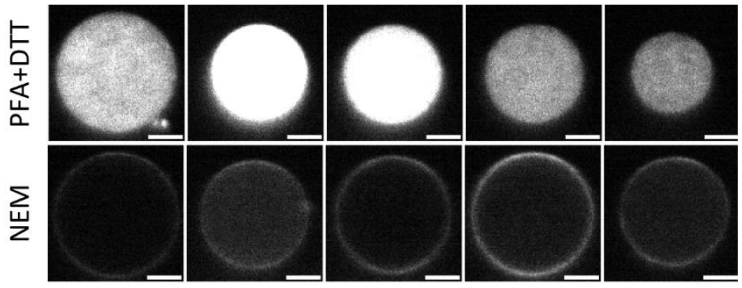

Figure 26. CLIC4-GFP is localized to the several GPMV's membrane which are generated using NEM.

GPMVs were generated using 25 mM PFA and 2 mM DTT (top) or 2 mM NEM (bottom). Images were taken using confocal microscopy and represent single z-sections. Scale bars, 5 μm.

To investigate the role of palmitoylation in CLIC4's localization at the plasma membrane, we treated HeLa S3 cells with 2-bromopalmitate (2BP), a widely used inhibitor that blocks the addition of palmitate to proteins [106]. Immunostaining of 2BP-treated mitotic cells showed a significant decrease in enrichment of CLIC4 at the mitotic cell surface (Figure 27), indicating that palmitoylation is important for its surface enrichment during mitosis.

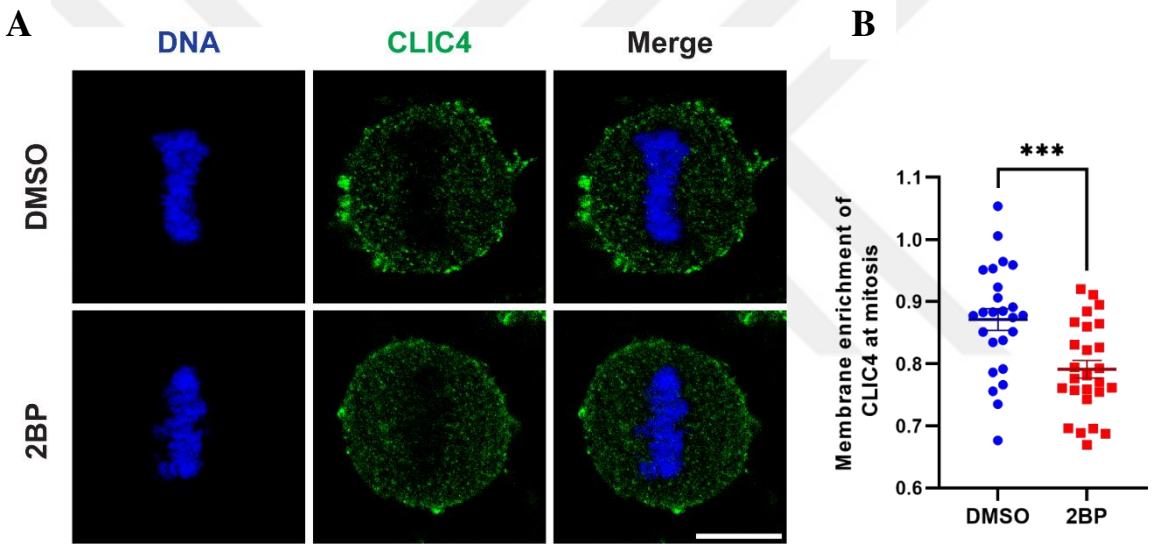

Figure 27. CLIC4 localization at the mitotic cell surface decreased after 2BP treatment.

A. CLIC4 (green) localization during mitosis in control (DMSO) (top) and palmitoylation inhibitor (2BP, 200uM)-treated (bottom) cells. DNA (DAPI) in blue. Scale bar: 10 μm. **B.** Quantification of the plasma membrane (PM) enrichment of CLIC4 in the control (n= 25) and 200uM 2BP-treated (n=26) mitotic cells. Error bars show the s.d. ns, not significant; **P<0.01; ***P<0.001.

To validate the palmitoylation of CLIC4, a click chemistry-based assay was performed using 17-ODYA and palmitic acid for metabolic labeling of palmitoylated

proteins [107]. 17-ODYA, a bioorthogonal probe compatible with biotin-azide, enabled specific labeling, while palmitic acid served as a negative control as it cannot react with biotin-azide [107]. Following mitotic synchronization and cell lysis, 17-ODYA-labeled proteins were exchanged with biotin via click chemistry, while palmitic acid-labeled proteins remained unlabeled. Streptavidin beads were then used to enrich biotin-bound proteins, which were subsequently analyzed by Western blotting. The results demonstrated the presence of CLIC4 in elute from 17-ODYA-labeled samples, but not in the palmitic acid control, confirming that CLIC4 undergoes palmitoylation during mitosis (Figure 28).

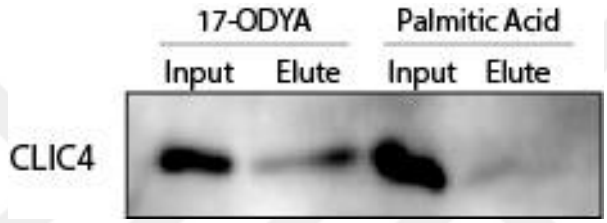

Figure 28. Palmitoylation of CLIC4 protein is confirmed using the click chemistry based palmitoylation assay.

3.3.2. The Role of CLIC4 in Polar Membrane Blebbing During Cytokinesis

Blebbing at the poles of dividing cells plays a critical role in relieving intracellular tension generated by the constriction of the actomyosin ring [77]. The absence of both CLIC1 and CLIC4 leads to abnormal polar blebbing during cytokinesis due to the detachment of the cortical actomyosin network from the plasma membrane. Localization of CLIC1 and CLIC4 to polar membrane blebs further underscores their importance in regulating bleb dynamics [62].

3.3.2.1. The Hierarchical Assembly of CLIC4 and Cortical Proteins at Membrane Blebs

To investigate the temporal dynamics of CLIC4 relative to key bleb-associated proteins, including actin, ezrin, and myosin light chain (MLC), live-cell imaging was

performed using Zeiss lattice light-sheet microscopy (LLSM). This technique provides high spatiotemporal resolution with minimal phototoxicity, making it ideal for imaging dynamic processes like blebbing during cytokinesis [108]. HeLa S3 cells co-expressing CLIC4-GFP and RFP-tagged marker proteins were imaged during cytokinesis, and kymographs were generated to analyze protein arrival times at the plasma membrane.

In cells expressing Lifeact-RFP (an actin marker) and CLIC4-GFP, membrane blebs at the polar cortex were visualized during cytokinesis (Figure 29A). Kymograph analysis of 52 blebs from eight cells revealed that actin assembles at the bleb rim approximately 5 seconds before CLIC4 (Figures 29C and D). Representative images showed that actin primarily localized to the bleb rim during the expansion phase, with CLIC4 gradually enriching in a similar pattern (Figure 29B). These findings suggest that both actin and CLIC4 contribute to the expansion phase by stabilizing the bleb membrane.

Ezrin, a membrane-cytoskeleton linker protein, plays a critical role in regulating the bleb life cycle. Imaging of HeLa S3 cells co-expressing ezrin-RFP and CLIC4-GFP revealed colocalization of the two proteins at the cleavage furrow and polar membrane blebs during cytokinesis (Figure 30A). Kymograph analysis of 32 blebs from six cells demonstrated that enrichment of CLIC4 at the plasma membrane precedes ezrin's localization (Figure 30D). Time-lapse microscopy showed that ezrin initially localizes at the bleb neck during initiation and then progressively redistributes along the bleb rim. Its intensity increases from the neck to the apex of the bleb during expansion (Figure 30B). These observations suggest that CLIC4 supports membrane stabilization early in the bleb life cycle, while ezrin contributes to later stages of expansion (Figure 30C).

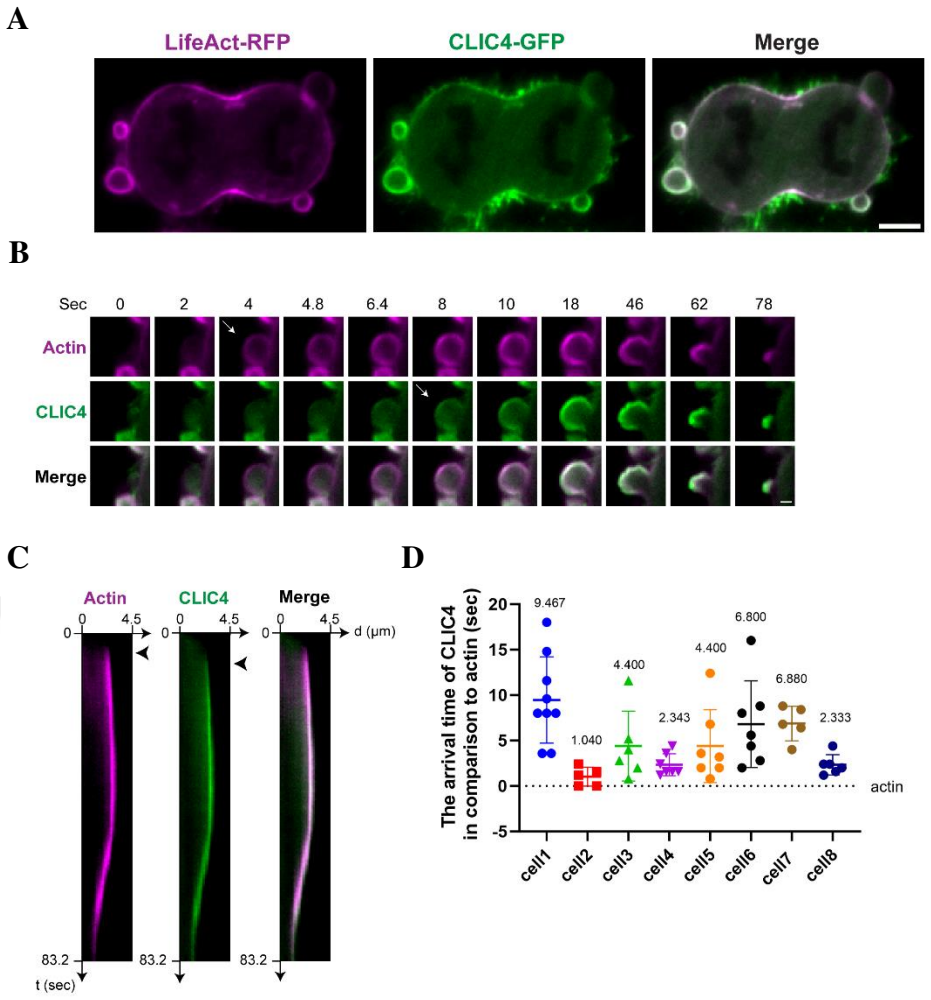

Figure 29. Actin is assembled before the localization of CLIC4 on the membrane bleb.

A. The representative images of LifeAct-RFP (magenta) and CLIC4-GFP (green) expressing cell during cytokinesis. Lattice light-sheet microscopy was used to acquire a single plane time-series at 0.4 second intervals. Scale bar, 10 μm. **B.** Time-lapse of individual bleb life cycle to visualize the appearance of F-actin and CLIC4. White arrows indicate the first observed frame with membrane localization of each protein. Scale bar, 1 μm. **C**. Kymographs depicting the dynamic localization of F-actin and CLIC4 over time. The horizontal axis represents bleb initiation, expansion, and retraction phases. The vertical axis represents time. Black arrows indicate the time point when each protein localizes to the membrane bleb. **D**. Quantitative analysis of CLIC4's arrival time relative to F-actin in 8 cytokinetic cells and 52 individual polar blebs. Data are presented as mean ± SD (error bars).

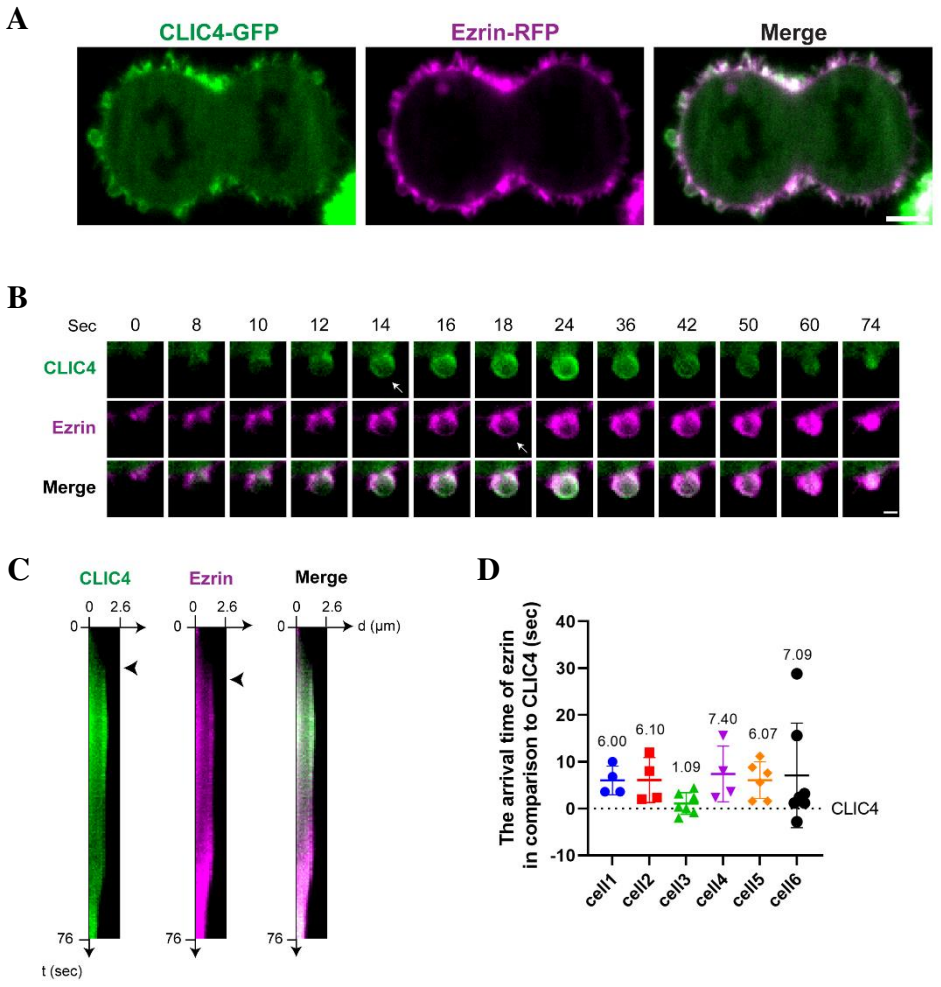

Figure 30. Ezrin is recruited to the bleb cortex after CLIC4's binding on the membrane.

A. The representative images of CLIC4-GFP (green) and ezrin-RFP (magenta) expressing cell during cytokinesis. Lattice light-sheet microscopy was used to acquire a single plane time-series at 0.4 second intervals. Scale bar, 10 μm. **B.** Time-lapse of individual bleb life cycle to visualize the appearance of CLIC4 and ezrin. White arrows indicate the first observed frame with membrane localization of each protein. Scale bar, 1 μm. **C.** Kymographs depicting the dynamic localization of CLIC4 and ezrin over time. The horizontal axis represents bleb initiation, expansion, and retraction phases. The vertical axis represents time. Black arrows indicate the time point when each protein localizes to the membrane bleb. **D.** Quantitative analysis of ezrin's arrival time relative to CLIC4 in

6 cytokinetic cells and 32 individual polar blebs. Data are presented as mean ± SD (error bars).

Myosin, an actin-binding motor protein, generates the contractility necessary for bleb retraction [109]. Imaging of HeLa S3 cells co-expressing CLIC4-GFP and MLC2-RFP revealed that myosin localizes to polar blebs during cytokinesis (Figure 31A) , but its recruitment occurs significantly later than CLIC4 (Figure 31B). Analysis of 30 blebs from six cells showed that myosin is recruited approximately 12 seconds after CLIC4 localization (Figure 31D). Time-lapse images illustrated increasing myosin intensity during retraction, indicating its essential role in bleb shrinkage and closure (Figure 31B). Kymograph analysis confirmed that while CLIC4 localizes during the expansion phase, myosin recruitment is restricted to the retraction phase (Figure 31C).

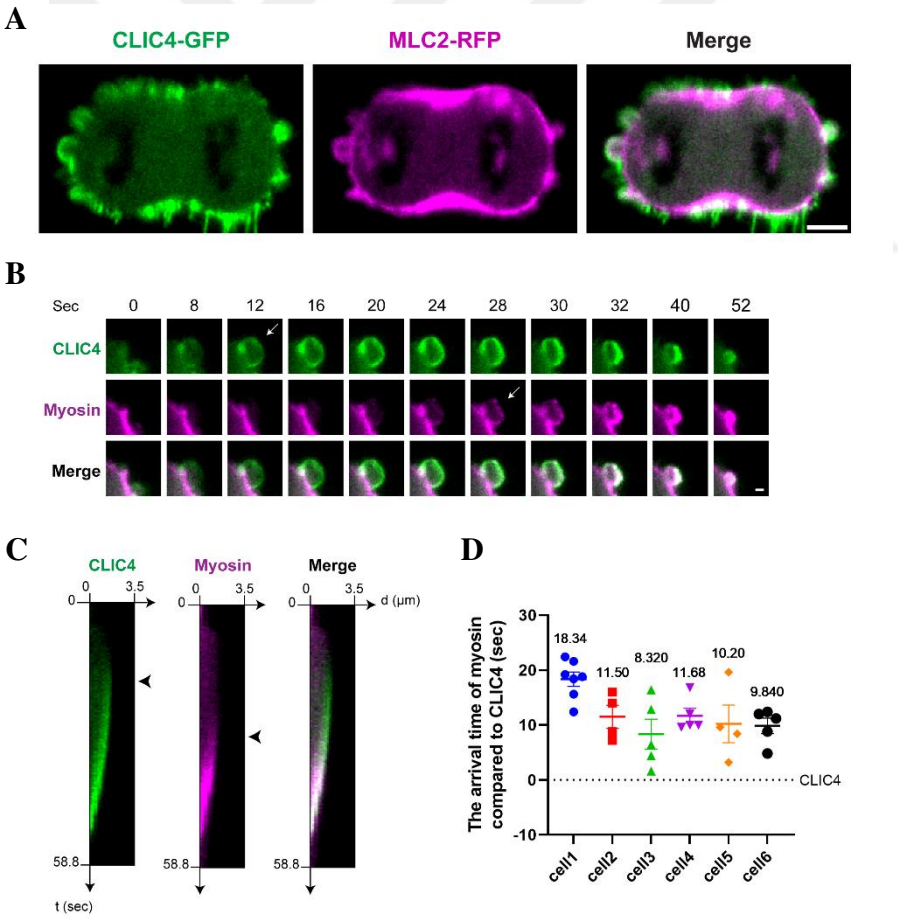

Figure 31. Myosin localizes on the bleb rim during the retraction after the accumulation of CLIC4.

A. The representative images of CLIC4-GFP (green) and MLC2-RFP (magenta) expressing cell during cytokinesis. Lattice light-sheet microscopy was used to acquire a single plane time-series at 0.4 second intervals. Scale bar, 10 μm. **B.** Time-lapse of individual bleb life cycle to visualize the appearance of CLIC4 and myosin. White arrows indicate the first observed frame with membrane localization of each protein. Scale bar, 1 μm. **C.** Kymographs depicting the dynamic localization of CLIC4 and myosin over time. The horizontal axis represents bleb initiation, expansion, and retraction phases. The vertical axis represents time. Black arrows indicate the time point when each protein localizes to the membrane bleb. **D**. Quantitative analysis of myosin's arrival time relative to CLIC4 in 6 cytokinetic cells and 30 individual polar blebs. Data are presented as mean ± SD (error bars).

3.3.2.2. The Regulation of Bleb Size During Cytokinesis

The size of membrane blebs is tightly regulated to maintain cellular integrity and stability during cytokinesis [77]. The maximum size of the blebs which is the largest area that bleb expand is depending on the duration time of expansion phase [79]. Therefore, bleb dynamics were analyzed in terms of total lifespan, expansion, and retraction times in HeLa S3 cells co-expressing CLIC4-GFP and RFP-tagged marker proteins. Across three cell lines, the average bleb lifespan was approximately 50 seconds. The expansion times were measured from bleb initiation to the point of maximum size and interestingly, cells co-expressing CLIC4-GFP and ezrin-RFP exhibited longer expansion times compared to other cell lines, while retraction times were shortest in these cells. (Figure 32).

To explore the effect of protein arrival timing on bleb size, the maximum bleb area was analyzed relative to the timing of protein assembly to the membrane bleb. In CLIC4-GFP Lifeact-RFP cells, actin consistently arrived at the bleb rim before the bleb reached its maximum size, but no correlation was found between actin arrival time and bleb size (Figure 33). Similarly, in CLIC4-GFP ezrin-RFP cells, ezrin arrival occurred either simultaneously with or after the bleb reached its maximum size, with no significant impact on bleb dimensions (Figure 34). In contrast, CLIC4-GFP MLC2-RFP cells showed a clear correlation between myosin arrival timing and bleb size: delayed myosin recruitment led to larger blebs (Figure 35), consistent with previous reports linking myosin activation to bleb size regulation [110].

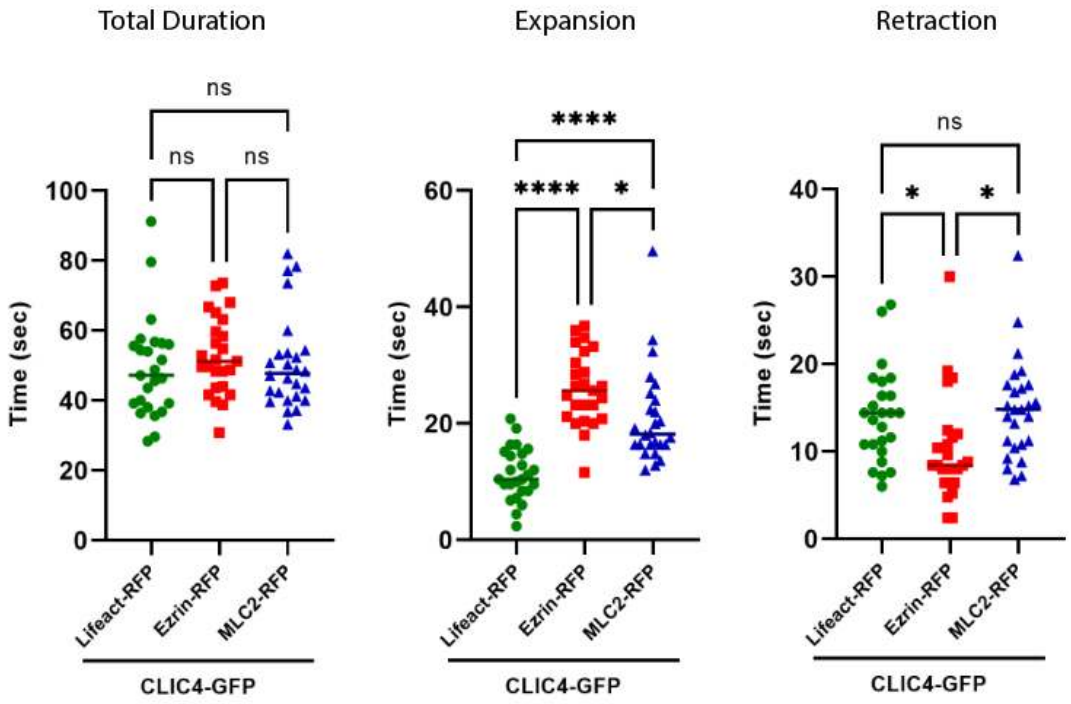

Figure 32. Time of blebs' total duration, expansion and retraction phases were measured from CLIC4-GFP expressing LifeAct-RFP/Ezrin-RFP/MLC2-RFP cells.

CLIC4-GFP; LifeAct-RFP n= 25 cells, Ezrin-RFP n=25 cells, MLC2-RFP cells n=26 cells. The statistical significance was determined using a one-way ANOVA Tukey's multiple comparison (ns: non-significant, *P<0.05; ****P<0.0001).

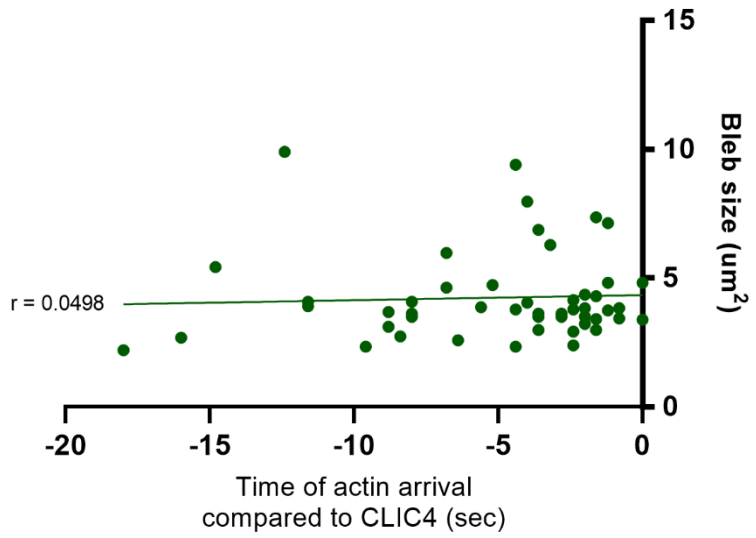

Figure 33. Maximum bleb size is not correlated with time of actin arrival compared to CLIC4 arrival (t=0).

CLIC4-GFP; LifeAct-RFP n= 52 cells, Pearson correlation was performed. Bleb size indicates maximum dimension reached by the bleb during its expansion phase.

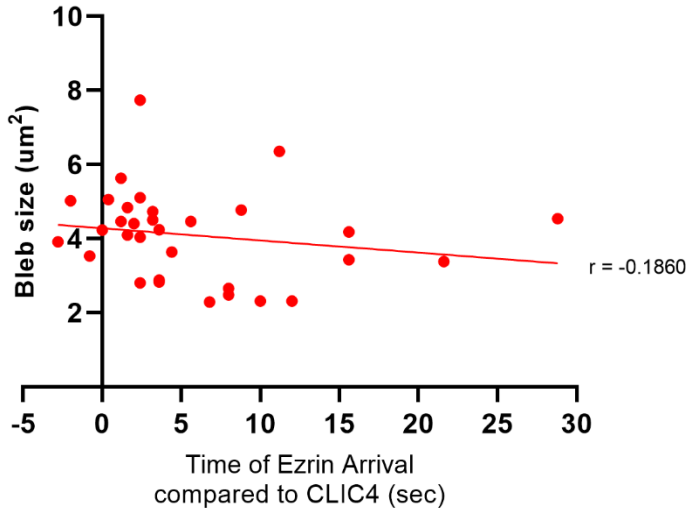

Figure 34. Maximum bleb size is not correlated with time of ezrin arrival compared to CLIC4 arrival (t=0).

CLIC4-GFP; ezrin-RFP n= 32 cells, Pearson correlation was performed. Bleb size indicates maximum dimension reached by the bleb during its expansion phase.

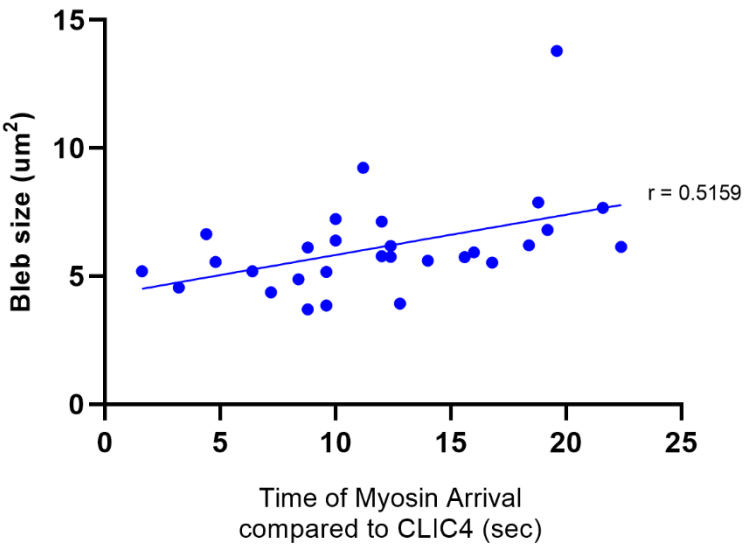

Figure 35. Maximum bleb size has positive correlation with time of myosin arrival compared to CLIC4 arrival (t=0).

CLIC4-GFP; MLC2-RFP n= 32 cells, Pearson correlation was performed. Bleb size indicates maximum dimension reached by the bleb during its expansion phase.

3.3.2.3. Insights into CLIC4's Role in Bleb Dynamics

Live-cell lattice light-sheet microscopy revealed a hierarchical order of protein recruitment to polar membrane blebs during cytokinesis, with actin assembling first, followed by CLIC4, ezrin, and finally myosin (Figure 36A). This sequential localization highlights distinct roles for each protein in different phases of the bleb life cycle. During expansion, actin, CLIC4, and ezrin stabilize the membrane and support bleb growth, while myosin drives contraction during the retraction phase (Figure 36B).

Our findings indicate that while CLIC4, actin, and ezrin influence the expansion phase of membrane blebs, their arrival times have minimal impact on bleb size. In contrast, delayed recruitment of myosin leads to increased bleb dimensions, underscoring its critical role in regulating the retraction phase and maintaining bleb size. These

observations provide new insights into the dynamic interplay between cortical proteins and CLIC4 during cytokinesis.

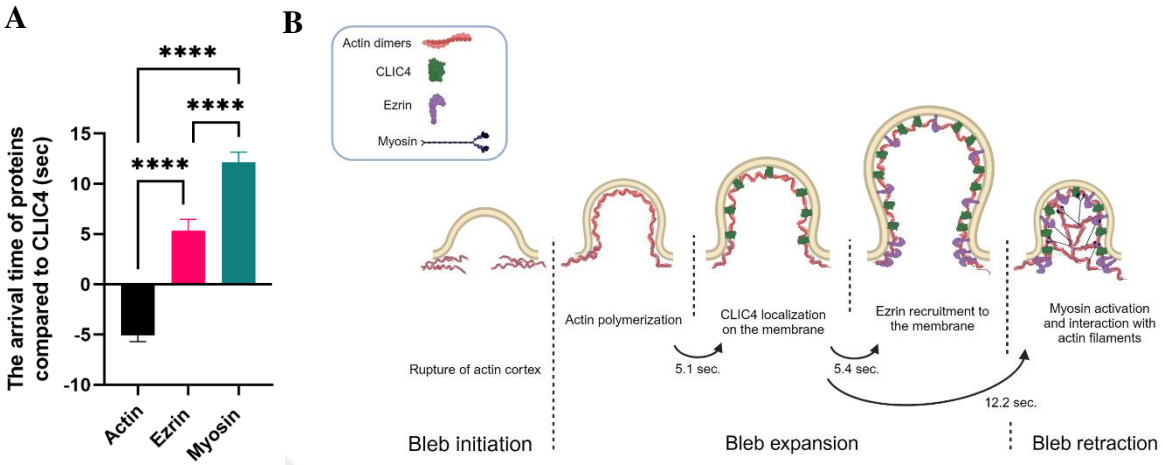

Figure 36. The relative arrival times of actin, ezrin, and myosin at the membrane bleb compared to CLIC4.

A. Graphical Analysis of protein arrival time compared to CLIC4 (t = 0 s) are presented. Error bars represent the standard error of the mean (SEM). Asterisks denote statistically significant differences in arrival times between the proteins (One-way ANOVA, ****p<0.001). **B.** A model describing the bleb life cycle including the bleb initiation, expansion, and retraction. Disruption of the actin cortex initiates blebbing, followed by actin polymerization within the protrusion. CLIC4 localizes to the expanding membrane, followed by ezrin recruitment to the bleb cortex. Subsequently, increased actin filament assembly and myosin recruitment to the membrane bleb generate contractility, leading to bleb retraction.

3.3.3. Investigating the Role of CLIC proteins in Cytoskeletal Regulation during cytokinesis

3.3.3.1. CLIC4 and Its Interactions with Anillin and Ezrin

CLIC4 plays a critical role in cytokinesis through interactions with key cytoskeletal proteins such as anillin and ezrin. Notably, the absence of CLIC1 and CLIC4 results in reduced phosphorylated ERM (pERM) localization at the cleavage furrow [62]. To further investigate these interactions, siRNA treatments targeting anillin and ezrin were performed. Interestingly, anillin depletion did not affect the localization of CLIC4 to the

cleavage furrow during cytokinesis (Figure 37). Similarly, siEzrin-treated cells showed no differences in CLIC4 localization compared to controls (Figure 38). These results indicate that CLIC4 localization to the cleavage furrow occurs independently of both anillin and ezrin. However, the decreased pERM levels observed in CLIC4KO cells highlight the role of CLIC4 in regulating pERM localization at the cleavage furrow (Figure 39).

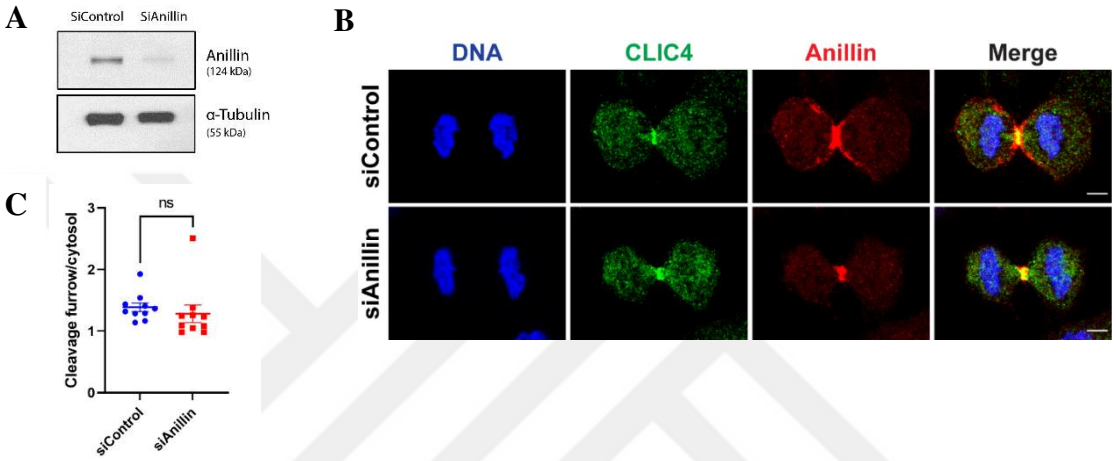

Figure 37. Anillin depletion with siRNA treatment does not affect CLIC4 localization at cleavage furrow.

A. The anillin depletion with siRNA were confirmed using Western Blot. **B.** Representative images of siControl and siAnillin treated cells during cytokinesis stained with CLIC4 antibody (green), anillin antibody (red) and Hoechst for DNA (blue). CLIC4 intensities were measured from 3 different ROI's at cleavage furrow and cytosol, then average CLIC4 intensities form cleavage furrow and cytosol ratio was calculated to show the cleavage furrow enrichment. Scale bar: 10 μm. **C.** The graph of CLIC4 intensity ratio at cleavage furrow to cytosol. Student t-test was performed. Error bars show the s.d. ns, not significant.

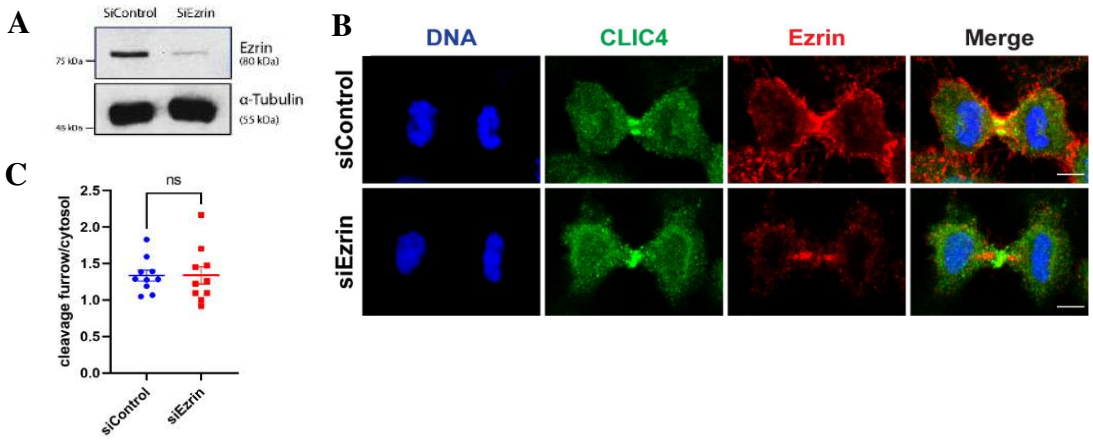

Figure 38. Depletion of ezrin with siRNA treatment does not affect the localization of CLIC4 at the cleavage furrow.

A. The ezrin depletion with siRNA was confirmed using Western Blot. **B.** Representative images of siControl and siEzrin treated cells during cytokinesis stained with CLIC4 antibody (green), ezrin antibody (red) and Hoechst for DNA (blue). CLIC4 intensities were measured from 3 different ROI's at cleavage furrow and cytosol, then average CLIC4 intensities form cleavage furrow and cytosol ratio was calculated to show the cleavage furrow enrichment. Scale bar: 10 µm. **C.** The graph of CLIC4 intensity ratio at cleavage furrow to cytosol. Student t-test was performed. Error bars show the s.d. ns, not significant.

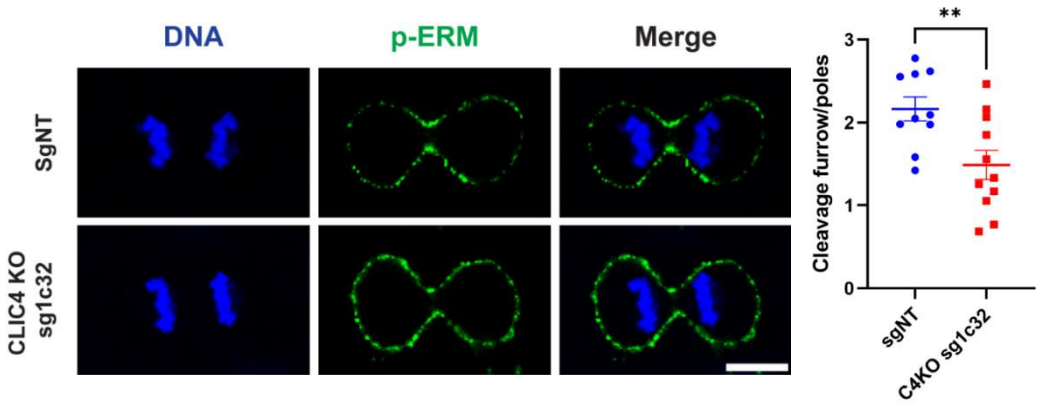

Figure 39. pERM intensity at the cleavage furrow were reduced in CLIC4KO cells.

Representative images of SgNT (non-targeted guide RNA) and CLIC4KO (sg1c32 line) cells during cytokinesis. CLIC4 intensities were estimated from cleavage furrow and cytosol, then ratio was calculated to show the cleavage furrow enrichment. Error bars show the s.d. ns, not significant; **P<0.01. Scale bar: 10 µm.

3.3.3.2. Profilin-1 and mDia2 Dynamics in CLIC1/4-Deficient Cells

Profilin-1, a G-actin-binding protein, promotes ATP-actin dimer formation and facilitates F-actin polymerization and elongation through interactions with formins, including mDia2 [13]. Among the formin family, mDia2 is critical for actomyosin ring formation and cytokinesis [111]. CLIC4 interacts directly with profilin-1 as part of the RhoA-mDia2 signaling pathway, which assembles the cortical actin network during cell division [71].

To investigate profilin-1 and mDia2 regulation in the absence of CLIC1 and CLIC4, control and CLIC1/4 double knockout (DKO) cells were synchronized at interphase, mitosis, and cytokinesis. Western blot analysis revealed no significant differences in the protein levels of profilin-1 or mDia2 between control and CLIC1/4 DKO cells across all cell cycle stages. Immunofluorescence staining of profilin-1 and mDia2 at the single-cell level similarly showed no differences in their localization patterns between control and CLIC1/CLIC4-deficient cells. These findings suggest that the absence of CLIC1 and CLIC4 does not directly influence profilin-1 or mDia2 protein levels or localization during cell division.

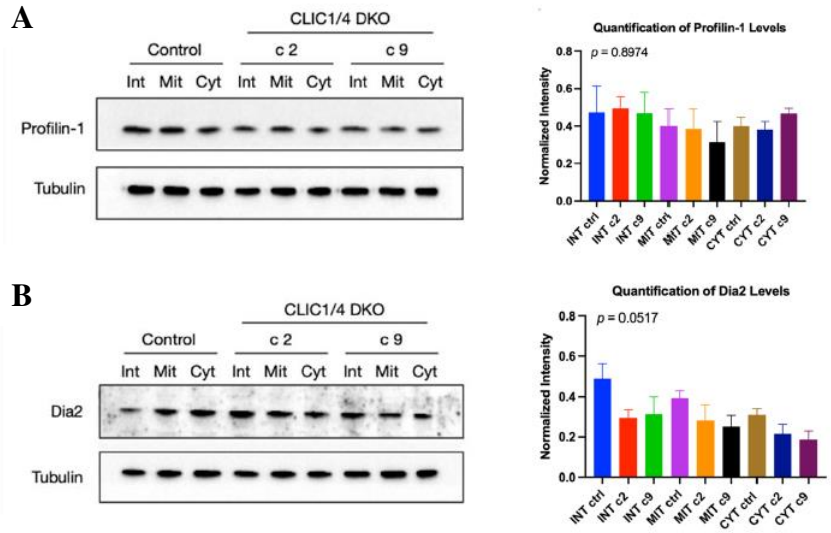

Figure 40. Western blot analysis was performed to examine the expression levels of Profilin-1 and Dia2 proteins in control and CLIC1/4 DKO cells in during cell division.

Western membranes were blotted with antibodies against Profilin-1 (A), Dia2 (B), and Tubulin. Tubulin was used as a loading control. Signal quantification was conducted using Image Lab software (Bio-Rad). "Ctrl" represents the control group, while "c2" and "c9" correspond to two separate non-CLIC colonies. INT: Interphase, MIT: Mitosis, CYT: Cytokinesis.

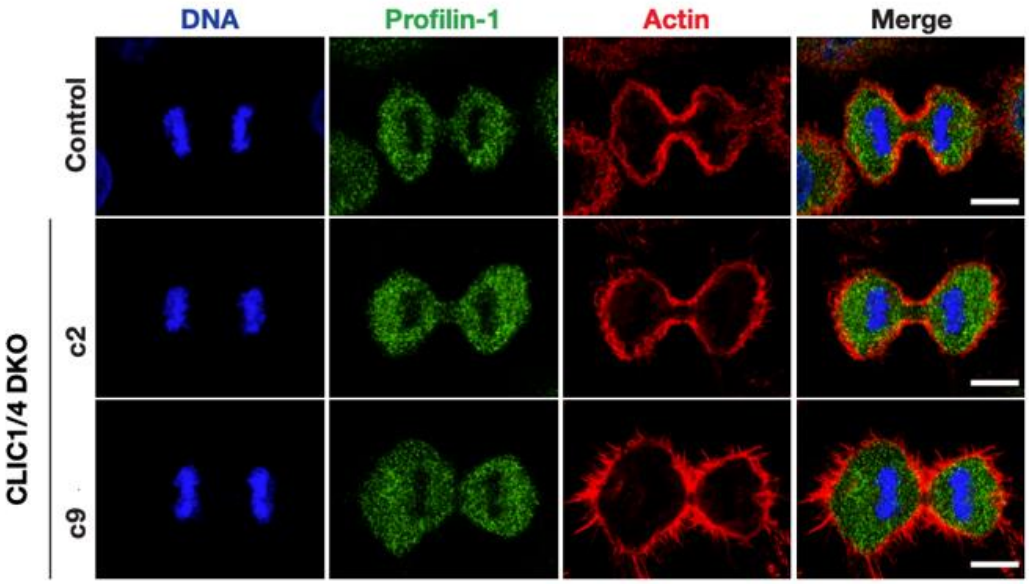

Figure 41. Localization of endogenous Profilin-1 in CLIC1/4 DKO and control cells during cytokinesis.

Fixed HeLa S3 cells in the cytokinesis phase were stained with Profilin-1 antibody (green), Phalloidin-555 (red), and Hoechst (blue). Scale bar: 10 μm.

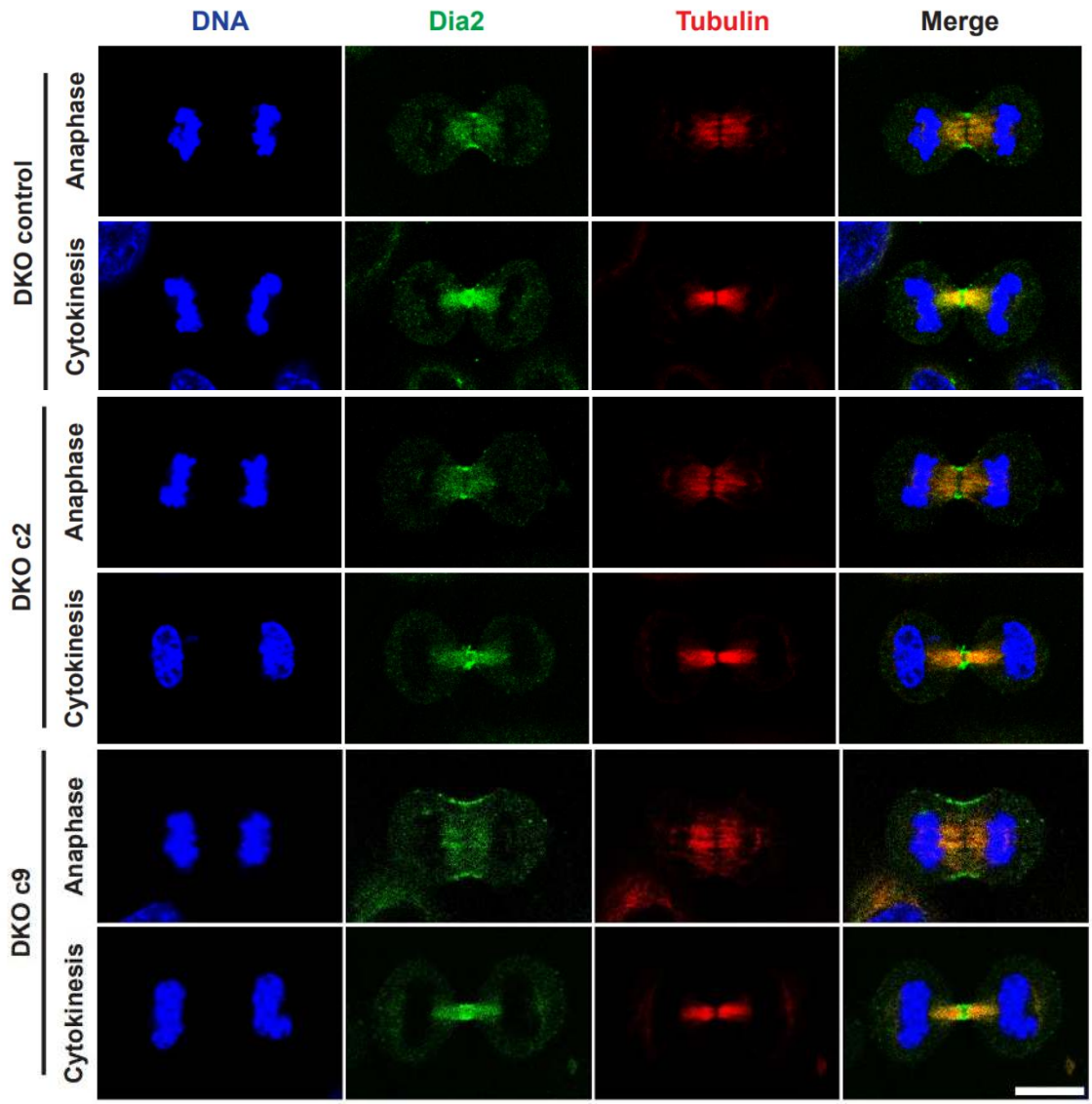

Figure 42. Localization of endogenous Dia2 in CLIC1/4 DKO and control cells during cytokinesis.

TCA-fixed HeLa S3 cells were stained with Dia2 antibody (green), tubulin antibody (red), and Hoechst (blue). Scale bar: 10 μm.

3.3.3.3. Non-Muscle Myosin II Dynamics in CLIC1/4-Deficient Cells

Non-muscle myosin II (NMII) is essential for contractile ring formation and constriction at the cleavage furrow during cytokinesis [14, 112]. Phosphorylation of the regulatory light chain (MLC) at Serine 19 facilitates NMII interaction with actin, initiating actomyosin complex formation and contraction, while dual phosphorylation at Serine 19 and Threonine 18 enhances myosin filament assembly [87]. Given CLIC4's

role in the cortical actin network [71], the phosphorylation state and protein levels of NMII were analyzed in CLIC1/4-deficient cells.

Western blot analysis of synchronized CLIC1/4 DKO cells at interphase, mitosis, and cytokinesis revealed no differences in total myosin IIB levels compared to controls. Similarly, phospho-myosin (S19) levels followed a comparable pattern in both groups, with low expression at interphase, an increase during mitosis, and a decrease during cytokinesis. Immunofluorescence staining of di-phosphorylated myosin (T18/S19) confirmed its localization at the centrosomes and cleavage furrow but showed no differences in localization between control and CLIC1/4 DKO cells. Quantification of phospho-myosin (S19) signal at the cleavage furrow further corroborated these findings, with no significant differences detected between the two groups. These results indicate that the absence of CLIC1 and CLIC4 does not significantly affect NMII protein levels, phosphorylation states, or localization during cytokinesis.

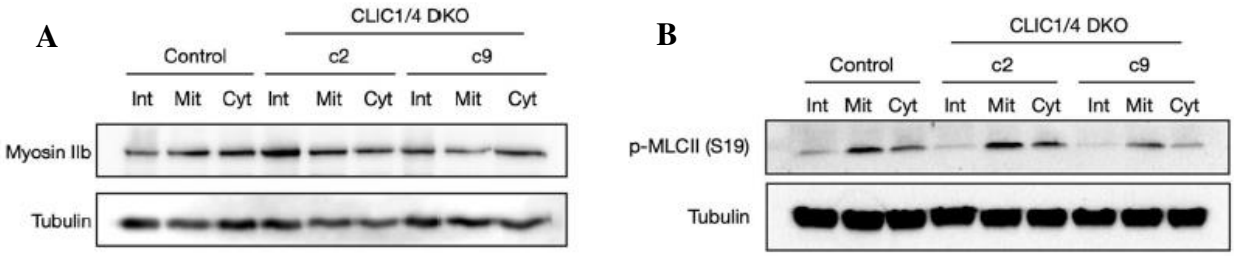

Figure 43. Western blot analysis of myosin IIb and p-myosin levels in control and CLIC1/4 DKO cells across different cell cycle phases.

Western blot membranes were probed with antibodies against myosin IIb (A), p-myosin (S19) (B) and tubulin, with tubulin used as a loading control. Int: Interphase, Mit: Mitosis, Cyt: Cytokinesis.

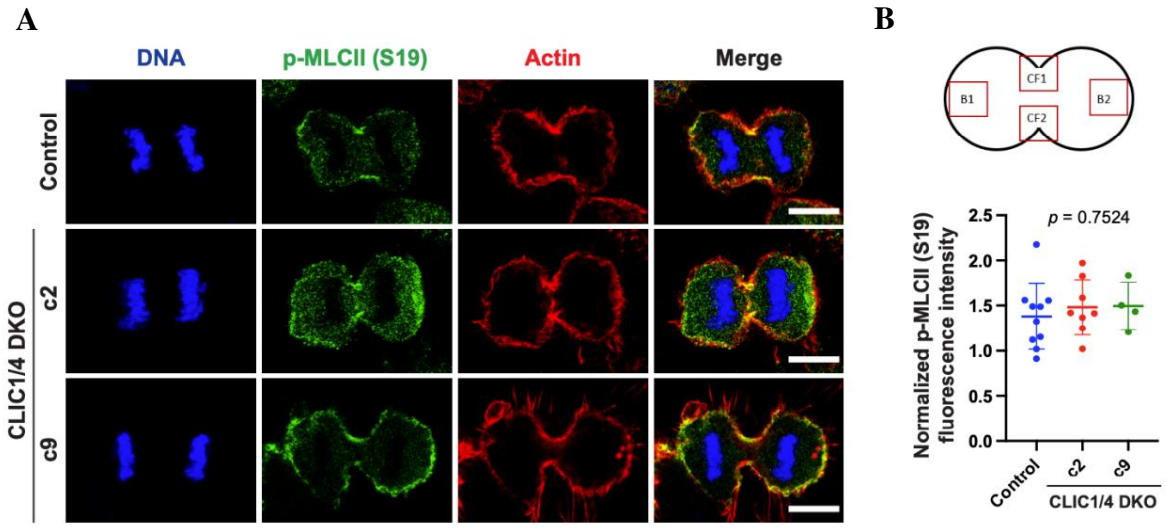

Figure 44. Comparison of phospho-MLCII (S19) levels in CLIC1/4 DKO and control cells during cytokinesis.

A. Fixed CLIC1/4 DKO and control HeLa S3 cells in the cytokinesis were stained with phospho-MLCII (S19) antibody (green), Phalloidin-555 (red), and Hoechst (blue). Scale bar: 10 µm. **B.** Normalized phosphorylation signal was calculated by comparing the average signal intensity at selected cleavage furrow regions (CF1 and CF2) to the background signal from equivalent-sized regions within the cell (B1 and B2). Bars represent the mean normalized signal with standard deviation across cells. Statistical analysis was performed using one-way ANOVA.

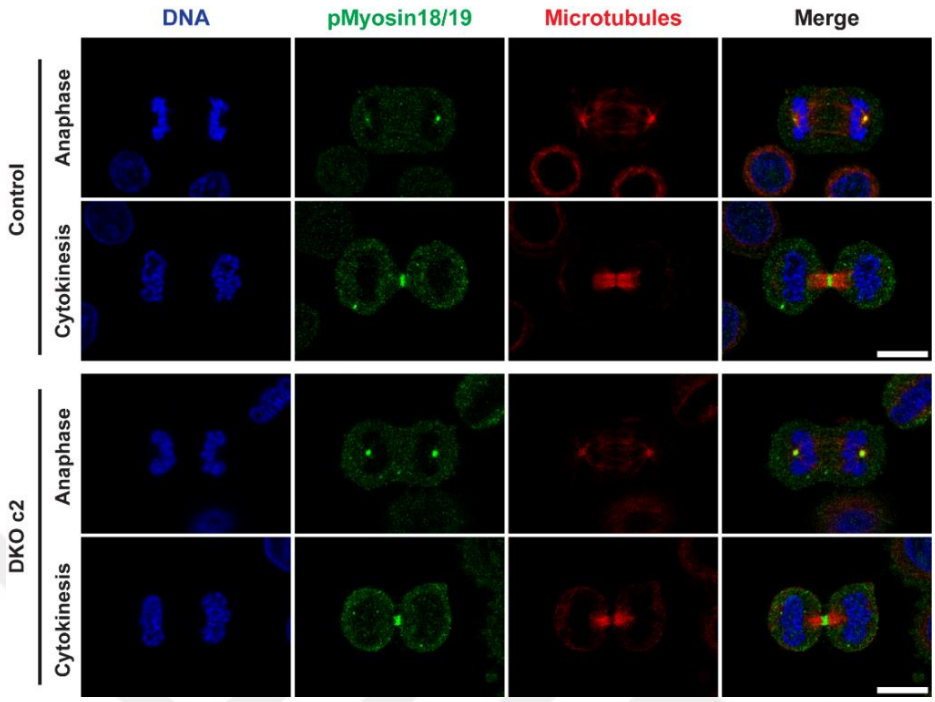

Figure 45. Phospho-MLCII (T18/S19) localization in CLIC1/4 DKO and control cells during cytokinesis.

Fixed CLIC1/4 DKO and control HeLa S3 cells in the cytokinesis were stained with phospho-MLCII (T18/S19) antibody (green), tubulin antibody (red), and Hoechst (blue). Scale bars: 10 μm.

3.3.3.4. Integrin Dynamics in CLIC1/4-Deficient Cells

Integrins are crucial for substrate adhesion, spindle orientation, and daughter cell separation during mitosis and cytokinesis. Mitotic-specific adhesion sites enriched in β1- and αvβ5-integrins provide stability and positional memory, supporting proper spindle orientation and accurate cell division even in the absence of classical adhesion components like talin and actin. Substrate stiffness further influences integrin assembly and maturation, linking extracellular matrix rigidity to successful mitotic progression [113].

Control and CLIC1/4 DKO cells were imaged during interphase, mitosis, and cytokinesis to examine integrin dynamics during cell division. No differences in integrin localization patterns were observed between the two groups, suggesting that the absence

of CLIC1 and CLIC4 does not impact integrin-mediated adhesion or dynamics during the cell cycle.

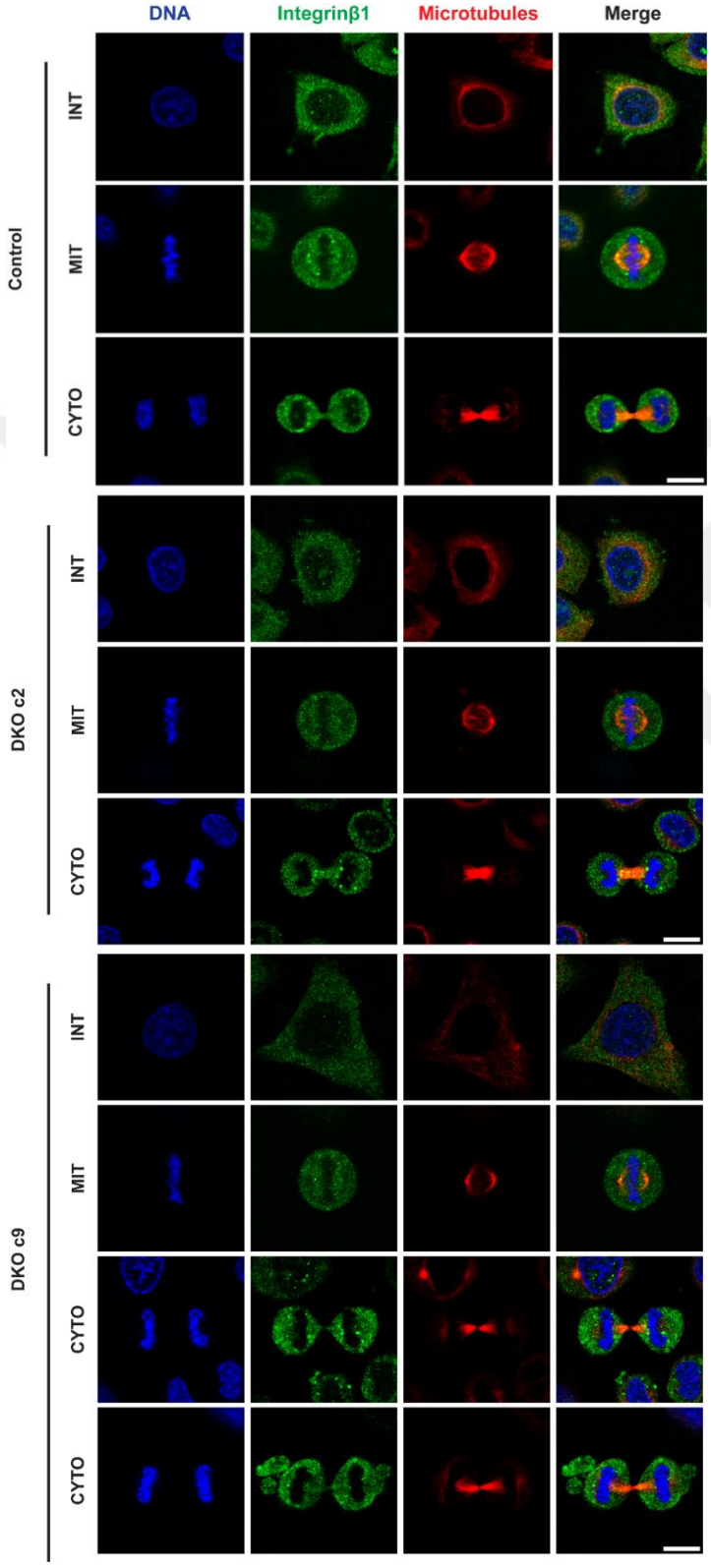

Figure 46. Integrin localization in control and CLIC1/4 DKO cells in interphase, mitosis and cytokinesis.

Fixed CLIC1/4 DKO and control HeLa S3 cells in the interphase, mitosis and cytokinesis were stained with Integrin beta-1 antibody (green), tubulin antibody (red), and Hoechst (blue). Scale bars: 10 μm.

3.4. DISCUSSION AND CONCLUSION

This study provides an extensive characterization of CLIC4 protein during cell division. It highlights its critical role in the regulation of membrane dynamics and cytoskeletal stability during cell division.

In this study, we demonstrated that CLIC4 localizes to the plasma membrane during mitosis in palmitoylation-dependent manner. While earlier proteomics studies identified CLIC4 within mammalian palmitoylomes [50, 114-116], there was no validation experiments for CLIC4 and the absence of predicted palmitoylation sites left it unclear whether CLIC4 undergoes direct or indirect palmitoylation [117]. Our results address this uncertainty, showing that inhibiting palmitoylation significantly diminishes CLIC4's surface localization during mitosis. Despite the significant reduction, CLIC4 does not completely disappear from the membrane when the palmitoylation is inhibited. This indicates that the palmitoylation is not the only mechanism for membrane localization of CLIC4. Moreover, a study identified six conserved residues in CLIC4, including Cys35 and Phe37, which align with key enzymatic and glutathione-binding sites in GST-omega 1 [3]. Mutating these residues disrupts CLIC4's response to RhoA activation, preventing its membrane association, indicating that factors beyond palmitoylation contribute to its plasma membrane localization. Additionally, click chemistry experiments using 17-ODYA labeling confirmed that CLIC4 undergoes palmitoylation during mitosis. However, it remains unclear whether palmitoylation directly affects CLIC4's function in cell division, as our study primarily highlights its impact on localization. Further investigations are necessary to determine whether CLIC4's role in cytokinesis depends on this modification.

The specific cysteine residue involved in CLIC4 palmitoylation remains unknown, though previous studies suggest that Cys35 is crucial for its plasma membrane localization upon RhoA activation [3]. Consistent with this, we observed that the C35A mutant failed to translocate to the membrane in our previous study [62], making it a strong candidate for further investigation. Additionally, identifying the ZDHHC palmitoyltransferase responsible for CLIC4's palmitoylation will be critical to fully

understanding the upstream regulation of this process. These findings set the stage for future research to elucidate how dynamic lipid modifications influence CLIC4's localization and function, providing a broader understanding of its role in cytokinesis.

The ability of CLIC proteins, including CLIC4, to associate with lipid bilayers or plasma membrane lipids can be inferred from previous studies. Surface plasmon resonance (SPR) experiments have shown that human and invertebrate CLIC proteins, such as CLIC1, CLIC4, Exc-4, and DmCLIC, bind to artificial lipid bilayers in a concentration-dependent manner [58, 118]. This membrane association is enhanced under acidic pH and oxidizing conditions, which are known to induce structural transitions in CLIC1, including the exposure of hydrophobic regions [60, 63]. Although CLIC4 lacks the disulfide bond-forming residues that mediate these changes in CLIC1, it is plausible that CLIC4 undergoes a distinct conformational adjustment that facilitates its lipid-binding ability. Our findings suggest that CLIC4 is associated with specific lipids, including phosphoinositols, in the plasma membrane. The observed colocalization of CLIC4 with $PI(4,5)P_2$ at the cleavage furrow, along with its immunoprecipitation with $PI(3,5)P_2$ and $PI(4,5)P_2$, further supports its lipid-binding capability. The acidic head groups of phosphoinositols might interact with hydrophobic or positively charged regions on CLIC4 that become exposed under specific cellular conditions, such as during oxidative stress or at low pH. This interaction could stabilize CLIC4 at the plasma membrane during cytokinesis, where lipid composition is dynamically regulated.

Lipids are not merely structural components of membranes but also play active roles in signaling and membrane dynamics during cell division [119]. Phosphoinositides, such as PI(3,5)P2 and PI(4,5)P2, are particularly critical for coordinating actin dynamics, membrane curvature, and the recruitment of cytoskeletal regulators to specific membrane domains [94]. CLIC4's interaction with these phosphoinositides suggests that it may act as a lipid adaptor, integrating lipid signaling with cytoskeletal regulation at the cleavage furrow. This role is further supported by its palmitoylation, a lipid modification that enhances its membrane association, indicating a potential synergy between direct lipid binding and lipid modifications in regulating its localization and function. This dual mechanism aligns with the behavior of other cell division proteins, such as Rho GTPases and ERM family members, which rely on lipid modifications or lipid-binding domains

for membrane targeting and activity [114, 120, 121] . Together, these findings highlight the importance of lipids in regulating CLIC4's function and suggest that its ability to integrate lipid signaling with cytoskeletal dynamics is critical for maintaining membrane integrity and cortical stability during cytokinesis.

CLIC4 and ezrin appear to coordinate their roles in regulating membrane-cortex dynamics during cytokinesis and bleb life cycle. In our previous study, ezrin was identified as interaction partner of CLIC4 [62]. Notably, the depletion of CLIC4 was found to reduce ezrin phosphorylation at the cleavage furrow, highlighting CLIC4's role in promoting ezrin activation during cytokinesis. Both CLIC4 and ezrin localize to cortical blebs during the retraction phase, suggesting a functional partnership in maintaining cortical tension. CLIC4 may facilitate ezrin recruitment and stabilization at the cortex, while ezrin's actin-membrane bridging activity could, in turn, enhance CLIC4's association with dynamically remodeling regions. In the absence of CLIC1 and CLIC4, abnormal blebbing is observed at the polar cortex during cell division, likely due to disrupted CLIC4-ezrin interactions leading to cortical instability. To better understand this phenomenon, further investigation is needed to analyze the characteristics of these abnormal blebs and determine whether there is a delay in ezrin or myosin recruitment. Additionally, clarifying whether CLIC4 directly regulates ezrin phosphorylation or acts through upstream pathways such as RhoA signaling will provide deeper insights into their role in cytokinesis and membrane-cortex dynamics.

Collectively, our study demonstrates that CLIC4 interacts with phosphoinositols, including $PI(3,5)P_2$ and $PI(4,5)P_2$, and localizes to the plasma membrane during mitosis in a palmitoylation-dependent manner (Figure 47). Live-cell imaging revealed CLIC4's sequential recruitment to membrane blebs, contributing to the stabilization of the expansion phase in coordination with actin and ezrin. Although the absence of CLIC1 and CLIC4 does not affect the localization or levels of key cytoskeletal regulators such as myosin II, mDia2, or profilin-1, the observed reduction in phosphorylated ERM proteins at the cleavage furrow highlights a unique role for CLIC proteins in regulating cortical dynamics via ezrin activation. These insights not only expand our understanding of CLIC4's contribution to cell division but also highlight its potential as a critical player in maintaining membrane integrity and cortical stability during dynamic cellular

processes. Future studies investigating the upstream regulation of CLIC4 localization and its interactions with other membrane-associated proteins will further illuminate its biological significance in cell division and beyond.

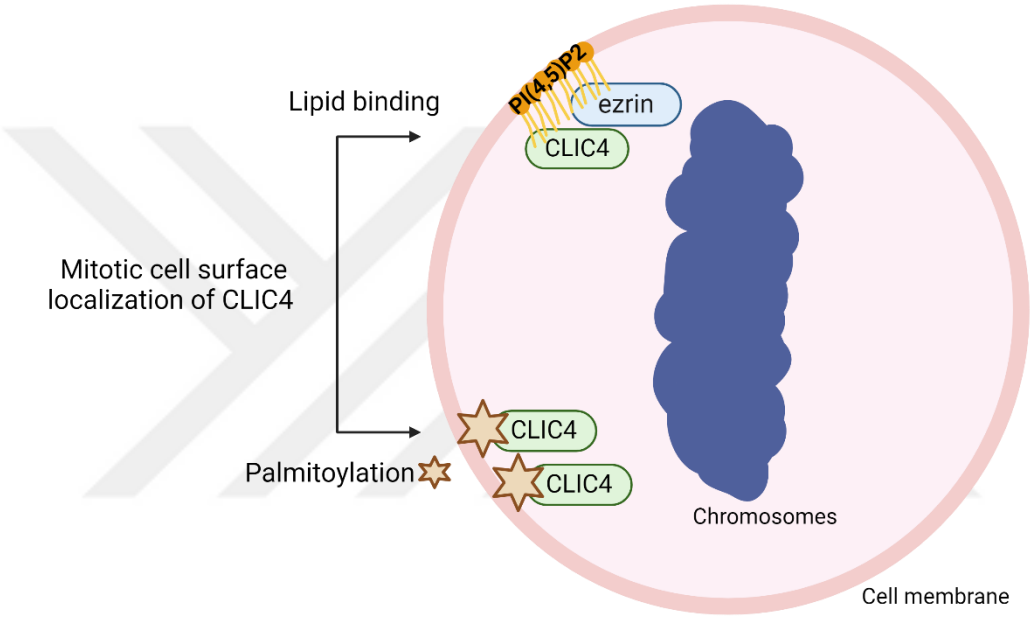

Figure 47. The proposed mechanisms for CLIC4's membrane localization during mitosis. (BioRender.com)

BIBLIOGRAPHY

1. Özlü, N., et al., *Quantitative comparison of a human cancer cell surface proteome between interphase and mitosis.* Embo j, 2015. **34**(2): p. 251-65.
2. Zhang, S. and X. Fu, *The Clinical Significance and Biological Function of PCDH7 in Cervical Cancer.* Cancer Manag Res, 2021. **13**: p. 3841-3847.
3. Ponsioen, B., et al., *Spatiotemporal regulation of chloride intracellular channel protein CLIC4 by RhoA.* Mol Biol Cell, 2009. **20**(22): p. 4664-72.
4. Hasegawa, J., B.S. Strunk, and L.S. Weisman, *PI5P and PI(3,5)P(2): Minor, but Essential Phosphoinositides.* Cell Struct Funct, 2017. **42**(1): p. 49-60.
5. Scholey, J.M., I. Brust-Mascher, and A. Mogilner, *Cell division.* Nature, 2003. **422**(6933): p. 746-52.
6. Wang, Z., *Cell Cycle Progression and Synchronization: An Overview.* Methods Mol Biol, 2022. **2579**: p. 3-23.
7. Lancaster, O.M. and B. Baum, *Shaping up to divide: coordinating actin and microtubule cytoskeletal remodelling during mitosis.* Semin Cell Dev Biol, 2014. **34**: p. 109-15.
8. Vermeulen, K., D.R. Van Bockstaele, and Z.N. Berneman, *The cell cycle: a review of regulation, deregulation and therapeutic targets in cancer.* Cell Prolif, 2003. **36**(3): p. 131-49.
9. Jones, M.J. and M.C. Jones, *Cell cycle control by cell-matrix interactions.* Curr Opin Cell Biol, 2024. **86**: p. 102288.
10. Bournaka, S., et al., *The cell cycle revisited: DNA replication past S phase preserves genome integrity.* Semin Cancer Biol, 2024. **99**: p. 45-55.
11. Norbury, C. and P. Nurse, *Animal cell cycles and their control.* Annu Rev Biochem, 1992. **61**: p. 441-70.
12. Rizzelli, F., et al., *The crosstalk between microtubules, actin and membranes shapes cell division.* Open Biology, 2020. **10**(3): p. 190314.
13. Chesarone, M.A., A.G. DuPage, and B.L. Goode, *Unleashing formins to remodel the actin and microtubule cytoskeletons.* Nature Reviews Molecular Cell Biology, 2010. **11**(1): p. 62-74.
14. Cheffings, Thomas H., Nigel J. Burroughs, and Mohan K. Balasubramanian, *Actomyosin Ring Formation and Tension Generation in Eukaryotic Cytokinesis.* Current Biology, 2016. **26**(15): p. R719-R737.
15. Lancaster, O.M., et al., *Mitotic rounding alters cell geometry to ensure efficient bipolar spindle formation.* Dev Cell, 2013. **25**(3): p. 270-83.
16. Ramkumar, N. and B. Baum, *Coupling changes in cell shape to chromosome segregation.* Nature Reviews Molecular Cell Biology, 2016. **17**(8): p. 511-521.
17. Bovellan, M., et al., *Cellular Control of Cortical Actin Nucleation.* Current Biology, 2014. **24**(14): p. 1628-1635.
18. Salbreux, G., G. Charras, and E. Paluch, *Actin cortex mechanics and cellular morphogenesis.* Trends Cell Biol, 2012. **22**(10): p. 536-45.
19. Kosako, H., et al., *Rho-kinase/ROCK is involved in cytokinesis through the phosphorylation of myosin light chain and not ezrin/radixin/moesin proteins at the cleavage furrow.* Oncogene, 2000. **19**(52): p. 6059-6064.
20. Yüce, O., A. Piekny, and M. Glotzer, *An ECT2-centralspindlin complex regulates the localization and function of RhoA.* J Cell Biol, 2005. **170**(4): p. 571-82.
21. Carreno, S., et al., *Moesin and its activating kinase Slik are required for cortical stability and microtubule organization in mitotic cells.* J Cell Biol, 2008. **180**(4): p. 739-46.

22. Machicoane, M., et al., *SLK-dependent activation of ERMs controls LGN–NuMA localization and spindle orientation*. Journal of Cell Biology, 2014. **205**(6): p. 791-799.
23. Clucas, J. and F. Valderrama, *ERM proteins in cancer progression*. Journal of Cell Science, 2014. **127**: p. 267 - 275.
24. Nguyen, L. and D. Robinson, *The Unusual Suspects in Cytokinesis: Fitting the Pieces Together*. Frontiers in Cell and Developmental Biology, 2020. **8**.
25. Field, C.M., et al., *Characterization of anillin mutants reveals essential roles in septin localization and plasma membrane integrity*. Development, 2005. **132**(12): p. 2849-60.
26. Green, R.A., E. Paluch, and K. Oegema, *Cytokinesis in animal cells*. Annu Rev Cell Dev Biol, 2012. **28**: p. 29-58.
27. Liu, J., et al., *Cleavage Furrow Organization Requires PIP2-Mediated Recruitment of Anillin*. Current Biology, 2012. **22**(1): p. 64-69.
28. Field, C.M. and B.M. Alberts, *Anillin, a contractile ring protein that cycles from the nucleus to the cell cortex*. J Cell Biol, 1995. **131**(1): p. 165-78.
29. Frenette, P.S. *RhoA Recruits Ect2 and Anillin to the Cortex where they interact to Maintain Furrow Ingression during Cytokinesis*. 2011.
30. Liu, J., et al., *Cleavage Furrow Organization Requires PIP₂-Mediated Recruitment of Anillin*. Current Biology, 2012. **22**(1): p. 64-69.
31. Addi, C., et al., *The Flemmingsome reveals an ESCRT-to-membrane coupling via ALIX/syntenin/syndecan-4 required for completion of cytokinesis*. Nature Communications, 2020. **11**(1): p. 1941.
32. Andrade, V., et al., *Caveolae promote successful abscission by controlling intercellular bridge tension during cytokinesis*. bioRxiv, 2022: p. 2022.01.04.474800.
33. Hu, C.-K., M. Coughlin, and T.J. Mitchison, *Midbody assembly and its regulation during cytokinesis*. Molecular Biology of the Cell, 2012. **23**(6): p. 1024-1034.
34. Nollet, F., P. Kools, and F. van Roy, *Phylogenetic analysis of the cadherin superfamily allows identification of six major subfamilies besides several solitary members*. J Mol Biol, 2000. **299**(3): p. 551-72.
35. Morishita, H. and T. Yagi, *Protocadherin family: diversity, structure, and function*. Curr Opin Cell Biol, 2007. **19**(5): p. 584-92.
36. Boggon, T.J., et al., *C-cadherin ectodomain structure and implications for cell adhesion mechanisms*. Science, 2002. **296**(5571): p. 1308-13.
37. Sano, K., et al., *Protocadherins: a large family of cadherin-related molecules in central nervous system*. The EMBO Journal, 1993. **12**(6): p. 2249-2256.
38. Chen, W.V. and T. Maniatis, *Clustered protocadherins*. Development, 2013. **140**(16): p. 3297-302.
39. Yoshida, K., *Fibroblast cell shape and adhesion in vitro is altered by overexpression of the 7a and 7b isoforms of protocadherin 7, but not the 7c isoform*. Cell Mol Biol Lett, 2003. **8**(3): p. 735-41.
40. Yoshida, K., et al., *Cloning, expression analysis, and chromosomal localization of BH-protocadherin (PCDH7), a novel member of the cadherin superfamily*. Genomics, 1998. **49**(3): p. 458-61.
41. Chen, H.F., et al., *Protocadherin 7 inhibits cell migration and invasion through E-cadherin in gastric cancer*. Tumour Biol, 2017. **39**(4): p. 1010428317697551.
42. Zhou, X., et al., *PROTOCADHERIN 7 Acts through SET and PP2A to Potentiate MAPK Signaling by EGFR and KRAS during Lung Tumorigenesis*. Cancer Res, 2017. **77**(1): p. 187-197.
43. Roux, K.J., et al., *A promiscuous biotin ligase fusion protein identifies proximal and interacting proteins in mammalian cells*. Journal of Cell Biology, 2012. **196**(6): p. 801-810.
44. Ozkan Kucuk, N.E., et al., *Cell cycle-dependent palmitoylation of*

protocadherin 7 by ZDHHC5 promotes successful cytokinesis. Journal of Cell Science, 2023.
45. Blaskovic, S., M. Blanc, and F.G. van der Goot, *What does S-palmitoylation do to membrane proteins?* Febs j, 2013. **280**(12): p. 2766-74.
46. Linder, M.E. and R.J. Deschenes, *Palmitoylation: policing protein stability and traffic*. Nature Reviews Molecular Cell Biology, 2007. **8**(1): p. 74-84.
47. Woodley, K.T. and M.O. Collins, *Regulation and function of the palmitoyl-acyltransferase ZDHHC5*. The FEBS Journal, 2021. **288**(23): p. 6623-6634.
48. Smotrys, J.E. and M.E. Linder, *Palmitoylation of intracellular signaling proteins: regulation and function*. Annu Rev Biochem, 2004. **73**: p. 559-87.
49. Main, A. and W. Fuller, *Protein S-Palmitoylation: advances and challenges in studying a therapeutically important lipid modification*. The FEBS Journal, 2022. **289**(4): p. 861-882.
50. Söderberg, O., et al., *Direct observation of individual endogenous protein complexes in situ by proximity ligation*. Nature Methods, 2006. **3**(12): p. 995-1000.
51. Wan, J., et al., *Palmitoylated proteins: purification and identification*. Nat Protoc, 2007. **2**(7): p. 1573-84.
52. Thilly, W.G., *Chapter 25 Maintenance of Perpetual Synchrony in HeLa S3 Culture: Theoretical and Empirical Approaches*, in *Methods in Cell Biology*, D.M. Prescott, Editor. 1976, Academic Press. p. 273-285.
53. Piekny, A.J. and M. Glotzer, *Anillin is a scaffold protein that links RhoA, actin, and myosin during cytokinesis*. Curr Biol, 2008. **18**(1): p. 30-6.
54. Söderberg, O., et al., *Characterizing proteins and their interactions in cells and tissues using the in situ proximity ligation assay*. Methods, 2008. **45**(3): p. 227-32.
55. Suh, K.S., et al., *CLIC4, an intracellular chloride channel protein, is a novel molecular target for cancer therapy*. J Investig Dermatol Symp Proc, 2005. **10**(2): p. 105-9.
56. Littler, D.R., et al., *The enigma of the CLIC proteins: Ion channels, redox proteins, enzymes, scaffolding proteins?* FEBS Letters, 2010. **584**(10): p. 2093-2101.
57. Gururaja Rao, S., N.J. Patel, and H. Singh, *Intracellular Chloride Channels: Novel Biomarkers in Diseases*. Frontiers in Physiology, 2020. **11**.
58. Jiang, L., et al., *CLIC proteins, ezrin, radixin, moesin and the coupling of membranes to the actin cytoskeleton: a smoking gun?* Biochim Biophys Acta, 2014. **1838**(2): p. 643-57.
59. Hare, J.E., et al., *Interaction of Human Chloride Intracellular Channel Protein 1 (CLIC1) with Lipid Bilayers: A Fluorescence Study*. Biochemistry, 2016. **55**(27): p. 3825-3833.
60. Warton, K., et al., *Recombinant CLIC1 (NCC27) assembles in lipid bilayers via a pH-dependent two-state process to form chloride ion channels with identical characteristics to those observed in Chinese hamster ovary cells expressing CLIC1*. J Biol Chem, 2002. **277**(29): p. 26003-11.
61. Hsu, K.-S., et al., *CLIC4 regulates late endosomal trafficking and matrix degradation activity of MMP14 at focal adhesions in RPE cells*. Scientific Reports, 2019. **9**(1): p. 12247.
62. Uretmen Kagiali, Z.C., et al., *CLIC4 and CLIC1 bridge plasma membrane and cortical actin network for a successful cytokinesis*. Life Science Alliance, 2020. **3**(2): p. e201900558.
63. Goodchild, S.C., et al., *Oxidation promotes insertion of the CLIC1 chloride intracellular channel into the membrane*. European Biophysics Journal, 2009. **39**(1): p. 129-138.
64. Singh, H., *Two decades with dimorphic Chloride Intracellular Channels (CLICs)*. FEBS Letters, 2010. **584**(10): p. 2112-2121.
65. Manori, B., et al., *Chloride intracellular channel (CLIC) proteins function as*

fusogens. Nat Commun, 2024. **15**(1): p. 2085.
66. Ferofontov, A., et al., *Conserved cysteine dioxidation enhances membrane interaction of human Cl– intracellular channel 5*. The FASEB Journal, 2020. **34**(8): p. 9925-9940.
67. Littler, D.R., et al., *Crystal structure of the soluble form of the redox-regulated chloride ion channel protein CLIC4*. The FEBS Journal, 2005. **272**(19): p. 4996-5007.
68. Al Khamici, H., et al., *Members of the chloride intracellular ion channel protein family demonstrate glutaredoxin-like enzymatic activity*. PLoS One, 2015. **10**(1): p. e115699.
69. Harrop, S.J., et al., *Crystal structure of a soluble form of the intracellular chloride ion channel CLIC1 (NCC27) at 1.4-A resolution*. J Biol Chem, 2001. **276**(48): p. 44993-5000.
70. Chou, S.-Y., et al., *CLIC4 regulates apical exocytosis and renal tube luminogenesis through retromer- and actin-mediated endocytic trafficking*. Nature Communications, 2016. **7**(1): p. 10412.
71. Argenzio, E., et al., *Profilin binding couples chloride intracellular channel protein CLIC4 to RhoA-mDia2 signaling and filopodium formation*. J Biol Chem, 2018. **293**(50): p. 19161-19176.
72. Charras , G.T., et al., *Reassembly of contractile actin cortex in cell blebs*. Journal of Cell Biology, 2006. **175**(3): p. 477-490.
73. Charras, G.T., et al., *Life and times of a cellular bleb*. Biophys J, 2008. **94**(5): p. 1836-53.
74. Fishkind, D.J., L.G. Cao, and Y.L. Wang, *Microinjection of the catalytic fragment of myosin light chain kinase into dividing cells: effects on mitosis and cytokinesis*. J Cell Biol, 1991. **114**(5): p. 967-75.
75. Trinkaus, J.P., *Surface activity and locomotion of Fundulus deep cells during blastula and gastrula stages*. Dev Biol, 1973. **30**(1): p. 69-103.
76. Mills, J.C., et al., *Apoptotic membrane blebbing is regulated by myosin light chain phosphorylation*. J Cell Biol, 1998. **140**(3): p. 627-36.
77. Sedzinski, J., et al., *Polar actomyosin contractility destabilizes the position of the cytokinetic furrow*. Nature, 2011. **476**(7361): p. 462-466.
78. Erickson, C.A. and J.P. Trinkaus, *Microvilli and blebs as sources of reserve surface membrane during cell spreading*. Experimental Cell Research, 1976. **99**(2): p. 375-384.
79. Tinevez, J.Y., et al., *Role of cortical tension in bleb growth*. Proc Natl Acad Sci U S A, 2009. **106**(44): p. 18581-6.
80. Lorentzen, A., et al., *An ezrin-rich, rigid uropod-like structure directs movement of amoeboid blebbing cells*. Journal of Cell Science, 2011. **124**(8): p. 1256-1267.
81. Sao, K., et al., *Myosin II governs intracellular pressure and traction by distinct tropomyosin-dependent mechanisms*. Molecular Biology of the Cell, 2019. **30**(10): p. 1170-1181.
82. Maugis, B., et al., *Dynamic instability of the intracellular pressure drives bleb-based motility*. J Cell Sci, 2010. **123**(Pt 22): p. 3884-92.
83. Julian, L. and M.F. Olson, *Apoptotic membrane dynamics in health and disease*. Cell Health and Cytoskeleton, 2015. **7**(null): p. 133-142.
84. Aoki, K., et al., *A RhoA and Rnd3 cycle regulates actin reassembly during membrane blebbing*. Proceedings of the National Academy of Sciences, 2016. **113**(13): p. E1863-E1871.
85. Barry, D.J., et al., *Open source software for quantification of cell migration, protrusions, and fluorescence intensities*. Journal of Cell Biology, 2015. **209**(1): p. 163-180.
86. Wang, X., et al., *Effects of the Laplace pressure on the cells during cytokinesis*. iScience, 2021. **24**(9): p. 102945.
87. Matsumura, F., *Regulation of myosin II during cytokinesis in higher*

eukaryotes. Trends in Cell Biology, 2005. **15**(7): p. 371-377.
88. Amano, M., M. Nakayama, and K. Kaibuchi, *Rho-kinase/ROCK: A key regulator of the cytoskeleton and cell polarity*. Cytoskeleton (Hoboken), 2010. **67**(9): p. 545-54.
89. Argenzio, E., et al., *Profilin binding couples chloride intracellular channel protein CLIC4 to RhoA–mDia2 signaling and filopodium formation*. Journal of Biological Chemistry, 2018. **293**(50): p. 19161-19176.
90. Bartolini, F., et al., *The formin mDia2 stabilizes microtubules independently of its actin nucleation activity*. The Journal of cell biology, 2008. **181**(3): p. 523-536.
91. Webb, Y., L. Hermida-Matsumoto, and M.D. Resh, *Inhibition of Protein Palmitoylation, Raft Localization, and T Cell Signaling by 2-Bromopalmitate and Polyunsaturated Fatty Acids**. Journal of Biological Chemistry, 2000. **275**(1): p. 261-270.
92. Emoto, K., et al., *Local change in phospholipid composition at the cleavage furrow is essential for completion of cytokinesis*. J Biol Chem, 2005. **280**(45): p. 37901-7.
93. Fievet, B.T., et al., *Phosphoinositide binding and phosphorylation act sequentially in the activation mechanism of ezrin*. J Cell Biol, 2004. **164**(5): p. 653-9.
94. Posor, Y., W. Jang, and V. Haucke, *Phosphoinositides as membrane organizers*. Nature Reviews Molecular Cell Biology, 2022. **23**(12): p. 797-816.
95. van der Wal, J., et al., *Monitoring agonist-induced phospholipase C activation in live cells by fluorescence resonance energy transfer*. J Biol Chem, 2001. **276**(18): p. 15337-44.
96. Ramazi, S. and J. Zahiri, *Post-translational modifications in proteins: resources, tools and prediction methods*. Database, 2021. **2021**.
97. Dhariwala, F.A. and M.S. Rajadhyaksha, *An Unusual Member of the Cdk Family: Cdk5*. Cellular and Molecular Neurobiology, 2008. **28**(3): p. 351-369.
98. Guo, D., et al., *Cyclin-dependent kinase 5-mediated phosphorylation of chloride intracellular channel 4 promotes oxidative stress-induced neuronal death*. Cell Death Dis, 2018. **9**(10): p. 951.
99. Sharma, S. and P. Sicinski, *A kinase of many talents: non-neuronal functions of CDK5 in development and disease*. Open Biology, 2020. **10**(1): p. 190287.
100. Cespedes, P.F., et al., *Model membrane systems to reconstitute immune cell signaling*. FEBS J, 2021. **288**(4): p. 1070-1090.
101. Sezgin, E. and P. Schwille, *Model membrane platforms to study protein-membrane interactions*. Molecular Membrane Biology, 2012. **29**(5): p. 144-154.
102. Céspedes, P.F., et al., *T-cell trans-synaptic vesicles are distinct and carry greater effector content than constitutive extracellular vesicles*. Nature Communications, 2022. **13**(1): p. 3460.
103. Gerstle, Z., R. Desai, and S.L. Veatch, *Giant Plasma Membrane Vesicles: An Experimental Tool for Probing the Effects of Drugs and Other Conditions on Membrane Domain Stability*. Methods Enzymol, 2018. **603**: p. 129-150.
104. Sezgin, E., et al., *Elucidating membrane structure and protein behavior using giant plasma membrane vesicles*. Nat Protoc, 2012. **7**(6): p. 1042-51.
105. Levental, I., et al., *Palmitoylation regulates raft affinity for the majority of integral raft proteins*. Proceedings of the National Academy of Sciences, 2010. **107**(51): p. 22050-22054.
106. Davda, D., et al., *Profiling targets of the irreversible palmitoylation inhibitor 2-bromopalmitate*. ACS Chem Biol, 2013. **8**(9): p. 1912-7.
107. Martin, B.R. and B.F. Cravatt, *Large-scale profiling of protein palmitoylation in mammalian cells*. Nat Methods, 2009. **6**(2): p. 135-8.
108. Chen, B.-C., et al., *Lattice light-sheet microscopy: Imaging molecules to embryos at high spatiotemporal resolution*. Science, 2014. **346**(6208): p. 1257998.

109. Taneja, N. and D.T. Burnette, *Myosin IIA drives membrane bleb retraction*. Mol Biol Cell, 2019. **30**(9): p. 1051-1059.
110. Taneja, N., S.M. Baillargeon, and D.T. Burnette, *Myosin light chain kinase-driven myosin II turnover regulates actin cortex contractility during mitosis*. Mol Biol Cell, 2021. **32**(20): p. br3.
111. Watanabe, S., et al., *mDia2 induces the actin scaffold for the contractile ring and stabilizes its position during cytokinesis in NIH 3T3 cells*. Mol Biol Cell, 2008. **19**(5): p. 2328-38.
112. Sellers, J.R., *Myosins: a diverse superfamily*. Biochimica et Biophysica Acta (BBA) - Molecular Cell Research, 2000. **1496**(1): p. 3-22.
113. Huber, M., et al., *In mitosis integrins reduce adhesion to extracellular matrix and strengthen adhesion to adjacent cells*. Nature Communications, 2023. **14**(1): p. 2143.
114. Mariscal, J., et al., *Comprehensive palmitoyl-proteomic analysis identifies distinct protein signatures for large and small cancer-derived extracellular vesicles*. J Extracell Vesicles, 2020. **9**(1): p. 1764192.
115. Won, S.J. and B.R. Martin, *Temporal Profiling Establishes a Dynamic S-Palmitoylation Cycle*. ACS Chem Biol, 2018. **13**(6): p. 1560-1568.
116. Serwa, R.A., et al., *Systems Analysis of Protein Fatty Acylation in Herpes Simplex Virus-Infected Cells Using Chemical Proteomics*. Chem Biol, 2015. **22**(8): p. 1008-17.
117. Shipston, M.J., *Ion channel regulation by protein S-acylation*. J Gen Physiol, 2014. **143**(6): p. 659-78.
118. Hossain, K.R., et al., *Cholesterol Promotes Interaction of the Protein CLIC1 with Phospholipid Monolayers at the Air–Water Interface*. Membranes, 2016. **6**(1): p. 15.
119. Carlton, J.G., H. Jones, and U.S. Eggert, *Membrane and organelle dynamics during cell division*. Nature Reviews Molecular Cell Biology, 2020. **21**(3): p. 151-166.
120. Pradhan, A.J., et al., *Protein acylation by saturated very long chain fatty acids and endocytosis are involved in necroptosis*. Cell Chem Biol, 2021. **28**(9): p. 1298-1309.e7.
121. Roberts, P.J., et al., *Rho Family GTPase modification and dependence on CAAX motif-signaled posttranslational modification*. J Biol Chem, 2008. **283**(37): p. 25150-25163.